




12-2016

DEVELOPMENT OF INSTRUMENTATION AND CONTROL SYSTEMS FOR AN INTEGRAL LARGE SCALE PRESSURIZED WATER REACTOR

Matthew Rowland Morrow Lish
University of Tennessee, Knoxville, mlish@vols.utk.edu

Follow this and additional works at: https://trace.tennessee.edu/utk_graddiss

 Part of the [Controls and Control Theory Commons](#), [Nuclear Engineering Commons](#), and the [Systems Engineering Commons](#)

Recommended Citation

Lish, Matthew Rowland Morrow, "DEVELOPMENT OF INSTRUMENTATION AND CONTROL SYSTEMS FOR AN INTEGRAL LARGE SCALE PRESSURIZED WATER REACTOR. " PhD diss., University of Tennessee, 2016. https://trace.tennessee.edu/utk_graddiss/4146

This Dissertation is brought to you for free and open access by the Graduate School at TRACE: Tennessee Research and Creative Exchange. It has been accepted for inclusion in Doctoral Dissertations by an authorized administrator of TRACE: Tennessee Research and Creative Exchange. For more information, please contact trace@utk.edu.

To the Graduate Council:

I am submitting herewith a dissertation written by Matthew Rowland Morrow Lish entitled "DEVELOPMENT OF INSTRUMENTATION AND CONTROL SYSTEMS FOR AN INTEGRAL LARGE SCALE PRESSURIZED WATER REACTOR." I have examined the final electronic copy of this dissertation for form and content and recommend that it be accepted in partial fulfillment of the requirements for the degree of Doctor of Philosophy, with a major in Nuclear Engineering.

Belle R. Upadhyaya, Major Professor

We have read this dissertation and recommend its acceptance:

Jamie B. Coble, Arthur E. Ruggles, James L. Simonton

Accepted for the Council:

Carolyn R. Hodges

Vice Provost and Dean of the Graduate School

(Original signatures are on file with official student records.)

**DEVELOPMENT OF INSTRUMENTATION AND
CONTROL SYSTEMS FOR AN INTEGRAL LARGE
SCALE PRESSURIZED WATER REACTOR**

**A Dissertation Presented for the
Doctor of Philosophy
Degree**

The University of Tennessee, Knoxville

**Matthew Rowland Morrow Lish
December 2016**

Copyright © 2016 by Matthew Rowland Morrow Lish
All rights reserved.

Acknowledgments

I would like to thank my parents for teaching me to think critically, and always supporting and encouraging my endeavors. I would like to thank my advisor, Dr. Belle Upadhyaya, for his countless hours of advising, feedback, and encouragement throughout my graduate studies, shaping me into a better researcher, a better writer, and a better scientist. I am also thankful for his efforts in securing the funding which allowed me to pursue my graduate education through grants and graduate research and teaching assistantships. I am grateful to the entire faculty of the Department of Nuclear Engineering at the University of Tennessee for their teaching and expertise throughout my graduate studies. In particular, I would like to thank Dr. Jamie Coble, Dr. Arthur Ruggles, and Dr. James Simonton, doctoral committee members, without whose feedback and insight, this dissertation would not be possible. My research, this dissertation, and my capabilities as an investigator have benefitted greatly from their expertise. I would like to acknowledge the help given by Dr. J. Wesley Hines, Nuclear Engineering Department Head. Lastly, I would like to thank the U.S. Department of Energy's Nuclear Energy University Programs for providing the grant funding for the work upon which this dissertation is based.

Abstract

Small and large scale integral light water reactors are being developed to supply electrical power and to meet the needs of process heat, primarily for water desalination. This dissertation research focuses on the instrumentation and control of a large integral inherently safe light water reactor (designated as I²S-LWR) which is being designed as part of a grant by the U.S. Department of Energy Integrated Research Project (IRP). This 969 MWe integral pressurized water reactor (PWR) incorporates as many passive safety features as possible while maintaining competitive costs with current light water reactors. In support of this work, the University of Tennessee has been engaged in research to solve the instrumentation and control challenges posed by such a reactor design. This dissertation is a contribution to this effort. The objectives of this dissertation are to establish the feasibility and conceptual development of instrumentation strategies and control approaches for the I²S-LWR, with consideration to the state of the art of the field.

The objectives of this work are accomplished by the completion of the following tasks:

- Assessment of instrumentation needs and technology gaps associated with the instrumentation of the I²S-LWR for process monitoring and control purposes.
- Development of dynamic models of a large integral PWR core, micro-channel heat exchangers (MCHX) that are contained within the reactor pressure vessel, and steam flashing drums located external to the containment building.
- Development and demonstration of control strategies for reactor power regulation, steam flashing drum pressure regulation, and flashing drum water level regulation for steady state and load-following conditions.
- Simulation, detection, and diagnosis of process anomalies in the I²S-LWR model.

This dissertation is innovative and significant in that it reports the first instrumentation and control study of nuclear steam supply by integral pressurized water reactor coupled to an isenthalpic expansion vessel for steam generation. Further, this dissertation addresses the instrumentation and control challenges associated with integral reactors, as well as improvements to inherent safety possible in the instrumentation and control design of integral reactors. The results of analysis and simulation demonstrate the successful development of dynamic modeling, control strategies, and instrumentation for a large integral PWR.

Table of Contents

1	INTRODUCTION, BACKGROUND, AND OBJECTIVES	1
1.1	Introduction	1
1.2	Increasing Energy Demands Worldwide.....	4
1.3	Increasing Water Demands Worldwide	6
1.4	Transitioning to Nuclear Base Load Generation.....	8
1.5	The Integral Inherently Safe Light Water Reactor (I ² S-LWR)	10
1.6	Objective of the Dissertation and Original Contributions.....	13
2	PROCESS INSTRUMENTATION OF I²S-LWR	15
2.1	Safety Systems	15
2.1.1	Reactor Variable Overpower	17
2.1.2	High Logarithmic Power Level	17
2.1.3	High Local Power Density	17
2.1.4	Low Departure from Nucleate Boiling Ratio (DNBR)	18
2.1.5	High/Low Pressurizer Pressure	18
2.1.6	High/Low Steam Generator Water Level.....	18
2.1.7	High/Low Steam Generator Pressure	18
2.1.8	High Containment Pressure	19
2.1.9	Low Reactor Coolant Flow.....	19
2.2	Ex-core Nuclear Instrumentation	19
2.2.1	Typical PWR Nuclear Instrumentation	21
2.3	Instrumentation of In-Vessel Systems.....	30
2.3.1	In-core Instrumentation	30
2.3.2	Pressurizer Instrumentation	32
2.3.3	DHRS Instrumentation	34
2.3.4	CRDM/RCCA Instrumentation	36

2.3.5 Primary Coolant Inventory Monitoring	36
2.3.6 Primary Coolant Temperature Instrumentation	37
2.3.7 Primary Coolant Flow Measurement.....	38
2.3.8 Cable Routing	44
2.4 Secondary Side Instrumentation.....	46
2.5 Accident Monitoring	49
3 DYNAMIC MODELING OF THE I²S-LWR PRIMARY AND SECONDARY SYSTEMS.....	52
3.1 Reactor Core Model	55
3.1.1 Modeling Approach	55
3.1.2 Parameters for Reactor Core Model	58
3.2 Micro-channel Heat Exchanger (MCHX) Model.....	61
3.2.1 Modeling Approach	61
3.2.2 Parameters for MCHX Model	63
3.3 Steam Flashing Drum Model	64
3.3.1 Modeling Approach	64
3.3.2 Parameters for Flashing Drum Model	71
3.4 Testing Models for Stability.....	71
3.4.1 Reactivity Insertion.....	71
3.4.2 Feedwater and Steam Flow Reductions.....	74
4 DEVELOPMENT OF CONTROL SYSTEMS.....	84
4.1 Control Measurements and Control Actions	84
4.1.1 Reactor Power Control	84
4.1.2 Flashing Drum Steam Flow Control.....	85
4.1.3 Flashing Drum Feedwater Flow Control	85
4.2 Steady State Control.....	86
4.2.1 Controller Stability	86

4.2.2	Transient Control	88
4.3	Control during Load Changes	98
4.3.1	Control Strategies for Load Following	98
4.3.2	Simulating and Controlling Load Changes in I ² S-LWR	100
4.4	Resilient Control Considerations for the I ² S-LWR	103
5	ANOMALY DETECTION AND ISOLATION	108
5.1	Auto-Associative Kernel Regression Data Based Modeling	108
5.2	Sequential Probability Ratio Test	109
5.3	Simulated Anomalies	111
5.3.1	Sensor Drift	111
5.3.2	Coolant Flow Rate Reduction	119
5.3.3	Heat Exchanger Fouling	119
6	SUMMARY, CONCLUSIONS, AND RECOMMENDATIONS	
	FOR FUTURE WORK	127
6.1	Summary	128
6.2	Conclusions	131
6.3	Recommendation for Future Work	131
	REFERENCES	133
	VITA	141

List of Tables

Table 2-1. Sensor selection for Reactor Safety Systems [US NRC, 1983; US NRC, 2010; Arizona Public Service Company, 2007].	20
Table 2-2. Comparison of SPND emitter elements for use in FID assemblies [Heibel and Kistler, 2009].	31
Table 3-1. Reactor core and primary coolant loop parameters.	59
Table 3-2. Micro-channel primary heat exchanger modeling parameters.	64
Table 3-3. Flashing drum simulation parameters.	72
Table 4-1: Total reactor scrams fitting criteria by cause [Quinn, et al, 2012].	106

List of Figures

Figure 1-1. Projected global energy demand through 2040 (quadrillion Btu) [U.S. EIA, 2013]. ..	5
Figure 1-2. Projected national water withdrawal as a percentage of total available water. Source: United Nations Environment Program [United Nations Environmental Program]).....	7
Figure 1-3. Projected global water scarcity, by nation, in 2025. Note many areas not affected by physical water scarcity are affected by economic water scarcity. Source: International Water Management Institute [IWMI, 2000]......	7
Figure 1-4. Integral Inherently Safe Light Water Reactor schematic. Not to scale. Note decay heat exchanger (DHX), primary heat exchanger (PHX), steam flashing drum. Not pictured systems include integral control rod drive mechanisms and pressurizer heaters and sprayers [Petrovic, 2014].	12
Figure 2-1: Radial locations of instrumentation channels in the Arkansas Nuclear One – Unit 2, a CE design. Upper case letters refer to Figure 2-2 and Figure 2-3 [Arkansas Power & Light Co., 1978].	22
Figure 2-2: Location of the uncompensated ion chambers within the reactor cavity of the Arkansas Nuclear One – Unit 2 CE plant [Arkansas Power & Light Co., 1978].....	23
Figure 2-3. Instrumentation channel locations for cross-sections A and B [Arkansas Power & Light Co., 1978].....	24
Figure 2-4. Instrumentation channel locations for cross-sections C and D [Arkansas Power & Light Co., 1978].....	25
Figure 2-5: Thermal neutron flux profile of the I ² S-LWR reactor design concept at full power and with various concentrations of dissolved boron [Petrovic and Flashpoehler, 2015]. The innermost shaded region is the reactor core from centerline to outer radius (tan). Outside of that region is the neutron reflector and core barrel (light and dark grey), followed by the downcomer (blue), RPV (dark grey), reactor cavity (white), and biological containment (light grey, outermost).....	27
Figure 2-6. Flux ranges of detectors in a standard Westinghouse PWR [WEC, 1984]......	28
Figure 2-7. Westinghouse ITTA In-core detector assembly [Heibel and Kistler, 2009].....	31
Figure 2-8: Proposed detector configuration for I ² S-LWR.....	33
Figure 2-9. DHRS heat exchanger and associated instrumentation (Figure from [Mommott, et al, 2014], annotation by author).....	35

Figure 2-10. Side profile of conceptual application of ultrasonic flow meter in the down-comer of I ² S-LWR for measurement of non-fully developed flow rate of primary coolant. The red and green paths indicate pulses going against and with the flow, respectively [Upadhyaya, et al, NET 2015].	40
Figure 2-11: Proposed cable routing for in-core detectors and rod control cluster assemblies....	45
Figure 2-12. Instrumentation for the secondary coolant loop and steam flashing drum of I ² S-LWR [Upadhyaya, et al, 2015].	47
Figure 3-1. Nodalization of point kinetics and heat transfer from nuclear fuel to primary coolant in the core.	56
Figure 3-2. Nodal model of counter-flow micro-channel heat exchanger in I ² S-LWR. Each node models half the length of the micro-channels for each coolant.	62
Figure 3-3. Nodal representation of steam flashing drum model.	68
Figure 3-4. Drum inlet enthalpy functional fit comparison. The parabolic fit shows an improvement in the R ² value.	68
Figure 3-5. Drum saturated liquid enthalpy as a function of pressure. Deviations are apparent in the linear fit at the ends and in the middle. The parabolic fit shows an improvement in the R ² value.	69
Figure 3-6. Drum saturated vapor enthalpy as a function of pressure. The most significant difference between the linear and parabolic functional fits is in the vapor data. The parabolic fit is rounded to one from the sixth decimal place.	70
Figure 3-7. Fractional power response to +10 cent reactivity insertion.	72
Figure 3-8. Fuel temperature response to a +10-cent reactivity insertion.	73
Figure 3-9. Core exit and hot leg temperature responses to a +10-cent reactivity insertion.	75
Figure 3-10. Heat exchanger secondary outlet response to +10cent reactivity insertion.	75
Figure 3-11. Fraction of inlet flow vaporized in flashing drum response to +10 cent reactivity insertion. Vaporization fraction achieves similar value at increased operating pressure and inlet temperature as prior to perturbation.	76
Figure 3-12. Flashing drum uncontrolled pressure response to +10 cent reactivity insertion.	76
Figure 3-13. Flashing drum uncontrolled level response to +10 cent reactivity insertion.	77
Figure 3-14. Heat exchanger secondary inlet response to +10 cent reactivity insertion.	77

Figure 3-15. Response of the secondary coolant MCHX inlet temperature for a 5% decrease in the feed flow rate at 500 seconds followed by a 5% reduction in steam flow rate at 600 seconds.	79
Figure 3-16. Primary coolant cold leg temperature response for a 5% decrease in the feed flow rate at 500 seconds followed by a 5% reduction in steam flow rate at 600 seconds.	79
Figure 3-17. Response of the fractional reactor power for a 5% decrease in the feed flow rate at 500 seconds followed by a 5% reduction in steam flow rate at 600 seconds.	80
Figure 3-18. Response of the fuel temperature for a 5% decrease in the feed flow rate at 500 seconds followed by a 5% reduction in steam flow rate at 600 seconds.	80
Figure 3-19. Response of the primary coolant core exit temperature for a 5% decrease in the feed flow rate at 500 seconds followed by a 5% reduction in steam flow rate at 600 seconds.	81
Figure 3-20. Response of the MCHX water exit temperature for a 5% decrease in the feed flow rate at 500 seconds followed by a 5% reduction in steam flow rate at 600 seconds.	81
Figure 3-21. Response of the flashing drum water level for a 5% decrease in the feed flow rate at 500 seconds followed by a 5% reduction in steam flow rate at 600 seconds.	82
Figure 3-22. Response of the flashing drum steam pressure for a 5% decrease in the feed flow rate at 500 seconds followed by a 5% reduction in steam flow rate at 600 seconds.	82
Figure 3-23. Response of the nuclear core total reactivity (sum of feedback effects) level for a 5% decrease in the feed flow rate at 500 seconds followed by a 5% reduction in steam flow rate at 600 seconds.	83
Figure 3-24. Response of the flashing drum vaporization fraction for a 5% decrease in the feed flow rate at 500 seconds followed by a 5% reduction in steam flow rate at 600 seconds.	83
Figure 4-1. Average primary coolant temperature controlled by external reactivity insertion for I ² S-LWR with constant feedwater and steam flow rates.	89
Figure 4-2. Drum level controlled by feedwater flow rate for I ² S-LWR with constant external reactivity and steam flowrate.	90
Figure 4-3. Steam pressure controlled by steam flowrate for I ² S-LWR with constant external reactivity and feedwater flowrate.	91
Figure 4-4. Average primary coolant temperature based reactivity control plus drum level based feedwater flowrate control for I ² S-LWR with constant steam flowrate.	92

Figure 4-5. Average primary coolant temperature based reactivity control plus steam pressure based steam flowrate control for I ² S-LWR with constant feedwater flowrate. This approach is clearly unstable.	93
Figure 4-6. Steam pressure based steam flowrate control plus drum level based feedwater flowrate control for I ² S-LWR with constant external reactivity.	94
Figure 4-7. Control of I ² S-LWR with controllers operating on external reactivity, steam flowrate and feedwater flowrate.	95
Figure 4-8. Controlled system response to +10-cent reactivity perturbation. System returns to previous condition.	96
Figure 4-9. Controlled system response to 5% decrease in feedwater flow rate. System returns to previous condition.	97
Figure 4-10. Coolant temperature variation with power level for constant average primary coolant temperature based control.	99
Figure 4-11. Coolant temperature variation with power level for constant primary coolant hot leg temperature based control.	99
Figure 4-12. Selected variables under load following conditions performed by programmed average primary coolant temperature reactivity control. Controlled parameters of the flashing drum are maintained. Note behavior of coolant temperatures. Rather than maintaining a constant primary cold leg temperature, constant feedwater temperature causes all coolant temperatures to converge at lower value than primary cold leg temperature.	102
Figure 4-13. Reactor control by average primary coolant temperature program ranging from average temperature at full power (114.25°C) to flashing drum operating temperature (286.6°C). Power is varied between full power and 20% of full power at a rate of 1% per minute.	104
Figure 5-1. SPRT decision-making of the existence of a fault in the hot leg sensor drift data. .	113
Figure 5-2. Fault isolation by comparison of SPRT results for each variable in sensor fault data set.	114
Figure 5-3. Fault hypothesis of drifting sensor among four redundant sensors. At a drift rate of 1%, or 3.3°C per month, the SPRT flags the error by about 17 days into the test, or about 1.9°C of drift.	115
Figure 5-4. Fault hypothesis of non-drifting sensor number 2. If the test persists long enough, without the removal of the drifting sensor from the model, the SPRT eventually determines that	

the stable sensors are also erroneous. In practice, a drifting sensor is removed from the AAKR model when the drift is detected, allowing for continued, but less robust, monitoring of the remaining sensors.....	116
Figure 5-5. Fault hypothesis of non-drifting sensor number 2. If the test persists long enough, without the removal of the drifting sensor from the model, the SPRT eventually determines that the stable sensors are also erroneous. In practice, a drifting sensor is removed from the AAKR model when the drift is detected, allowing for continued, but less robust, monitoring of the remaining sensors.....	117
Figure 5-6. Fault hypothesis of non-drifting sensor number 2. If the test persists long enough, without the removal of the drifting sensor from the model, the SPRT eventually determines that the stable sensors are also erroneous. In practice, a drifting sensor is removed from the AAKR model when the drift is detected, allowing for continued, but less robust, monitoring of the remaining sensors.....	118
Figure 5-7. SPRT decision-making of the existence of a fault in the pump (motor) malfunction flow fault data.	120
Figure 5-8. Fault isolation by comparison of SPRT results for each variable in flow fault.	121
Figure 5-9. Anomaly diagnosis of presence of fault in the fractional reactor core power signal by SPRT under a simulated heat exchanger fouling scenario. After 8,008 observations, corresponding to 5.97% fouling, the ratio test settles on the faulted hypothesis.....	122
Figure 5-10. Anomaly diagnosis of presence of fault in the hot leg temperature signal by SPRT under a simulated heat exchanger fouling scenario. After 25,960 observations, corresponding to 22.16% fouling, the ratio test settles on the faulted hypothesis. This makes sense when it is considered that the effect of the heat exchanger fouling on hot leg temperature is minimized by the coolant passing through the core, where it picks up a lot of energy.	123
Figure 5-11. Anomaly diagnosis of presence of fault in the cold leg temperature signal by SPRT under a simulated heat exchanger fouling scenario. After 3,234 observations, corresponding to 1.78% fouling, the ratio test settles on the faulted hypothesis. This makes sense when it is considered that the effect of the heat exchanger fouling is most immediately reflected in less energy lost by the primary coolant, increasing the temperature of the secondary coolant as compared to the training data. This shows that the cold leg temperature signal is an important signal to monitor for heat exchanger performance.....	124

Figure 5-12. Anomaly diagnosis of presence of fault in the MCHX inlet temperature signal by SPRT under a simulated heat exchanger fouling scenario. After 5,884 observations, corresponding to 4.07% fouling, the ratio test settles on the faulted hypothesis.....	125
Figure 5-13. Anomaly diagnosis of presence of fault in the MCHX outlet temperature signal by SPRT under a simulated heat exchanger fouling scenario. After 6,896 observations, corresponding to 5.01% fouling, the ratio test settles on the faulted hypothesis.....	126

List of Acronyms

AAKR – Auto-associative kernel regression
BOP – Balance of plant
CE – Combustion Engineering
CRDM – Control rod drive mechanism
DBA – Design basis accident
DEC – Design extension conditions
DCD – Design control document
DHRS – Decay heat removal system
DHX – Decay heat exchanger
DNBR – Departure from nucleate boiling ratio
DOE – Department of Energy
EIA – Energy Information Agency
FID – Fixed in-core detector
FSAR – Final safety analysis report
FSER – Final safety evaluation report
IAEA – International Atomic Energy Agency
IEO – International Energy Outlook
I²S-LWR – Integral Inherently Safe Light Water Reactor
IITA – In-core instrument thimble assembly
INL – Idaho National Laboratory
IRIS – International Reactor Innovative and Secure
IRP – Integrated research projects
LB LOCA – Large break loss of coolant accident
LMTD – Log-mean temperature difference
LOCA – Loss of flow accident
LOFA – Loss of flow accident
LWR – Light water reactor
MCHX – Micro-channel heat exchanger
NEI – Nuclear Energy Institute
NEUP – Nuclear Energy University Programs

NRC – Nuclear Regulatory Commission
NSSS – Nuclear steam supply system
ODE – Ordinary differential equation
OECD – Organization for Economic Cooperation and Development
PCS – Power conversion system
PHX – Primary heat exchanger
PID – Proportional integral differential (controller)
PPL – Plant parameter list
PWR – Pressurized water reactor
RCCA – Rod control cluster assembly
RCP – Reactor coolant pump
RMSE – Root mean square error
RPI – Rod position indicator
RPS – Reactor protection system
RPV – Reactor pressure vessel
RTD – Resistance temperature detector
SB LOCA – Small break loss of coolant accident
SiC – Silicon carbide
SMR – Small modular reactor
SNR – Signal-to-noise ratio
SPND – Self powered neutron detector
SPRT – Sequential probability ratio test
TC – Thermocouple
TPLS – Thermal prove level sensor
UTSG – U-tube steam generator
WEC – Westinghouse Electric Company
WHO – World Health Organization

1 INTRODUCTION, BACKGROUND, AND OBJECTIVES

1.1 Introduction

Sometimes there are groundbreaking discoveries in science and engineering that push forward human understanding and technology in dramatic ways. In between those moments of transformation, scientists and engineers make the incremental advances that create the technologies which solve the problems of the future and generally transfer the burden of labor from human to machine. In order to solve the problems of the future, it is necessary to have some justifiable predictions about the future. One such prediction is that the number of people on the planet will increase. This is an easy prediction to justify, because it has always been so. With the exclusion of periods of war, natural disaster, or disease, human population has increased to the carrying capacity of our technology for producing the building blocks of human life. Another obvious characteristic of the world is that it, and the resources on it, are finite. There is only so much of any given element on the planet.

These two premises form a basic model. Humans expand, and consume resources doing so, and resources are fundamentally finite. Thus, eventually, resources must be generated in a manner that has a net neutral impact on the global ecosystem. In advanced civilization, the two most important resources are energy and water. Energy is used to power the machines that carry the burden of labor. While fresh water is indisputably the most critical resource for the basic survival of humans, it is far more integral to advanced civilization than merely sustaining the drinking requirements of a population. Water is critical to all the industries that sustain and advance civilization, too. It is used in resource acquisition industries such as agriculture, mining, and electricity production, as well as resource application industries such as manufacturing, research and development, and food and beverage. The demand for water and energy continues to drive advances in technology in both efficiency and production of both critical resources. The need for water and energy is highest in developing economies where the lack of these resources retards development [Africa Progress Panel, 2015; Brown and Lall, 2006]. In economic terms, demand for a resource is not defined as the population needs of the resource, but rather as the populations purchasing power for that resource. When there is plenty of economic demand, the market for that resource is driven to fill this demand, which drives down the per unit price of the resource [Cowen and Tabarrok, 2013]. This is why the cost of water and power is generally cheaper in developed

nations. As resources become scarce, prices tend to go up, yet cheap energy and water is critical for economies to develop and maintain themselves.

Another consequence of under developed economies is the political instability that generally accompanies economic instability. Economic and political instability promote conflict and threaten global stability. Thus it is in the interest of the entire human population to eradicate economic instability through developing economies in under developed regions that support stable civilization. However, currently existing economic instability makes the deployment of nuclear technology precarious in such environments due to the increased risk of proliferation of nuclear material to malicious agents.

All of this presents a significant gap in established technology for delivering reliable, sustainable energy and water to support the growth of stable economies in less developed parts of the world. A malicious or subverted insider poses a threat to a secure facility that is difficult to predict and quantify. Therefore, it is beneficial to minimize the number of people who must have access to a secure facility, and to minimize the ways in which such persons could sabotage the facility. Automation of the operation of the facility is one practical way to accomplish these goals. So we can conceive of a largely automated plant producing both electrical energy and desalinated, potable water. If such a plant were powered by one or more nuclear cores of low-enriched fuel, with a tightly monitored material stream, it could conceivably be deployed anywhere, regardless of local stability, while presenting much lower proliferation risk than would deploying current fission power plant technology alongside an electrically powered water desalination facility.

Relying predominantly on a nuclear powered core for electricity means that the plant must follow the daily and seasonal load changes. This is called load following. In countries where nuclear power makes up a smaller fraction of the total electrical supply, it is economically advantageous to run the nuclear power plants at full power continuously, and accommodate the changes in load using other sources connected across the electrical distribution grid. This is because the economics of nuclear power plants are relatively independent of the cost of the uranium that makes up the fuel. Even if these costs double, it would not have a large effect on the cost of generating nuclear power [Kaplan, 2008]. Thus operating at low power level or high power level costs about the same but generates dramatically different revenue from that operation. Operating a plant at low power condition is generally not profitable. In the United States, where nuclear power is responsible for about 20% of electricity generation, nuclear power plants try to

operate at maximum output as much as possible, to maximize the economics of plant operation. In countries such as France, where nuclear power is responsible for about 75% of electricity generation, considerably more load following is demanded of nuclear power plants. They are successful at daily changes of up to 75% of rated power [Lokhov, 2011]. So, while it is technically feasible to load follow nuclear cores, it remains economically and energetically inefficient to sustain low power operation.

Co-generation plants offer a solution to this inefficiency. Instead of changing the nuclear reactor core power level with fluctuations in grid demand, the premise would be to fluctuate the fraction of the core power delivered to the electricity generating turbine, while keeping the core power level constant. The fraction not delivered to the turbine would be delivered to the co-generation application. In this case, desalination of sea water for industrial and human consumption is the cogeneration application. So the power level of the nuclear core remains constant, and the fraction of that energy delivered to the generation of each revenue stream is modified to accommodate the changes in the demand for the product that varies most rapidly, electricity.

Filling this technological void requires addressing many smaller technology gaps. One of which is how to power a facility that produces both electricity and potable water. The U.S. Department of Energy's Nuclear Energy University Program's Integrated Research Projects (DOE NEUP IRP) program is currently funding the first phase of development of a large scale, integral nuclear power plant targeted at fulfilling a wide range of improvements over existing third generation nuclear plants, while maintaining economic competitiveness with existing designs. This reactor is named the Integral Inherently Safe Light Water Reactor, or I²S-LWR. The general idea is to combine the inherent safety benefits of the integrated primary coolant loop design found in candidate small modular reactors with the proven economics of the existing fleet of large scale nuclear reactors. This reactor concept also makes a compelling candidate for the power source of an automated co-generation facility. Integral reactors, and the I²S-LWR in particular, pose interesting challenges to the instrumentation and control of such plants, particularly when the ultimate goal of automated operation is considered. This dissertation will establish the design concept for the instrumentation and control strategies for this large scale integral PWR.

1.2 Increasing Energy Demands Worldwide

The U.S. Energy Information Administration (EIA), an independent statistics and analysis agency within the U.S. Department of Energy (DOE), publishes an annual document called the International Energy Outlook (IEO), which presents the EIA's assessment of the global energy markets and projections for the future. However, the report does not evaluate the same markets every year. Some issues focus on some markets while other issues offer comprehensive global analyses. The IEO for 2013 presents the most recent EIA projections for global energy consumption.

In the IEO 2013, the EIA projects a 56 percent increase in global annual energy consumption between 2010 and 2040 [U.S. EIA, 2013]. That comes to about 88 million gigawatt-hours (GWh), or 11,155 power plants operating at 1 gigawatt electric (GWe) with a capacity factor of 90 percent. That is the amount of new capacity that has to be produced by 2040. Their projections indicate that the majority of this growth will be in developing countries that are not part of the Organization for Economic Cooperation and Development (OECD). The OECD is an organization with the mission “to promote policies that will improve the economic and social well-being of people around the world” [OECD]. The OECD is made up mostly of the western developed countries in North America and Western Europe, and their allies around the world, including Greece, Turkey, Japan, South Korea, Australia, New Zealand, Chile, Mexico, and Israel. The largest non-OECD economies are China, India and Brazil, all of which are in the top ten largest economies in the world, with China being the second largest. Non-OECD countries, in aggregate, will experience a 90 percent increase in energy consumption as compared to 17 percent in OECD countries. Figure 1-1 shows the historical and projected global energy consumption between 1990 and 2040, by decade, and delineated by OECD and non-OECD countries.

The driving force in sustained increased energy consumption is long term economic growth. China and India have averaged 10.4 percent per year and 6.4 percent per year economic growth rate, respectively, between 1990 and 2010, and remain among the fastest growing economies in the world [U.S. EIA, 2013]. Developing economies drive increased consumption of energy, and tend to have the least stable infrastructures and regulatory environments. A stable infrastructure, particularly electricity, is critical to a developing economy and can significantly curtail it, as seen by rolling blackouts that periodically leave millions of people without electricity in India, forcing some businesses to close their doors and others to have unpredictable production schedules.

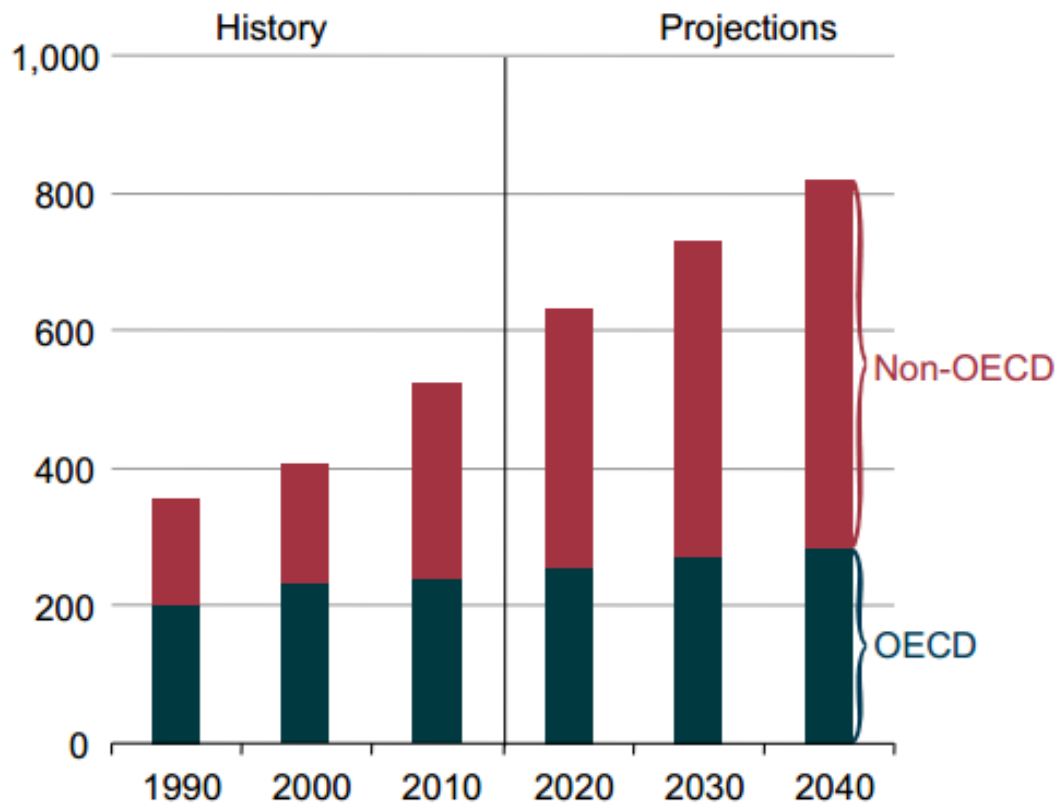


Figure 1-1. Projected global energy demand through 2040 (quadrillion Btu) [U.S. EIA, 2013].

The lack of stable infrastructure and robust regulations increases the onus on power plant designers to design plants that further improve safety and resilience to accidents when considering nuclear powered electricity generation in developing countries, where it has the greatest potential to be used for new generation capacity.

1.3 Increasing Water Demands Worldwide

Water is the foundation of life on our planet. Currently, one in ten people on the planet lack access to clean water, and one in three lack access to a toilet [WHO, 2015]. That is roughly twice the population of the United States without access to clean water. In low and middle income countries, one third of healthcare facilities operate without a reliable source of clean water. One third of schools around the world also lack clean water and adequate sanitation. This situation is, on the whole, not expected to improve. Figure 1-2 and Figure 1-3 show how the consumption of water is expected to change globally by 2025. Figure 1-2 shows the water withdrawn from natural sources as a percentage of total available water. Figure 1-3 shows physical and economic scarcity of water across the globe, divided by nation. Together, these figures demonstrate that even developed nations that are not projected to experience water scarcity by 2025 are still using more water than the environment can replenish, which leads to the conclusion that they will experience water scarcity in the future beyond 2025. Further, the number and location of countries that will experience physical or economic water scarcity by 2025 does not bode well for economic and physical security the world over.

When rivers, lakes and aquifers run dry, and without considering the ecological side effects of drinking such water sources dry, the ocean becomes the only remaining source of water. This water is not potable, as the salinity of the ocean is incompatible with the digestive tracts of land based mammals like humans. Our cells lack the ability to extract water from solutions that have a higher ion content than the fluid inside the cells. Simply put, we can't drink the ocean water without dramatically reducing the salt content. Such a process is called desalination, and there are several techniques for doing so. If the desalination process is to be used to aid in load following the electrical demands of the grid, then the desalination process must be able to rapidly change its process rate.

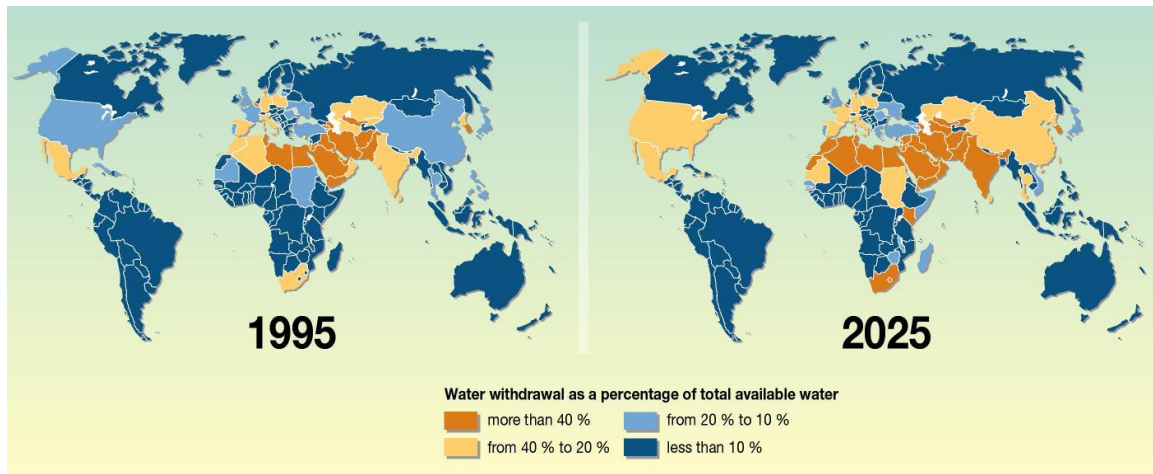


Figure 1-2. Projected national water withdrawal as a percentage of total available water. Source: United Nations Environment Program [United Nations Environmental Program]).

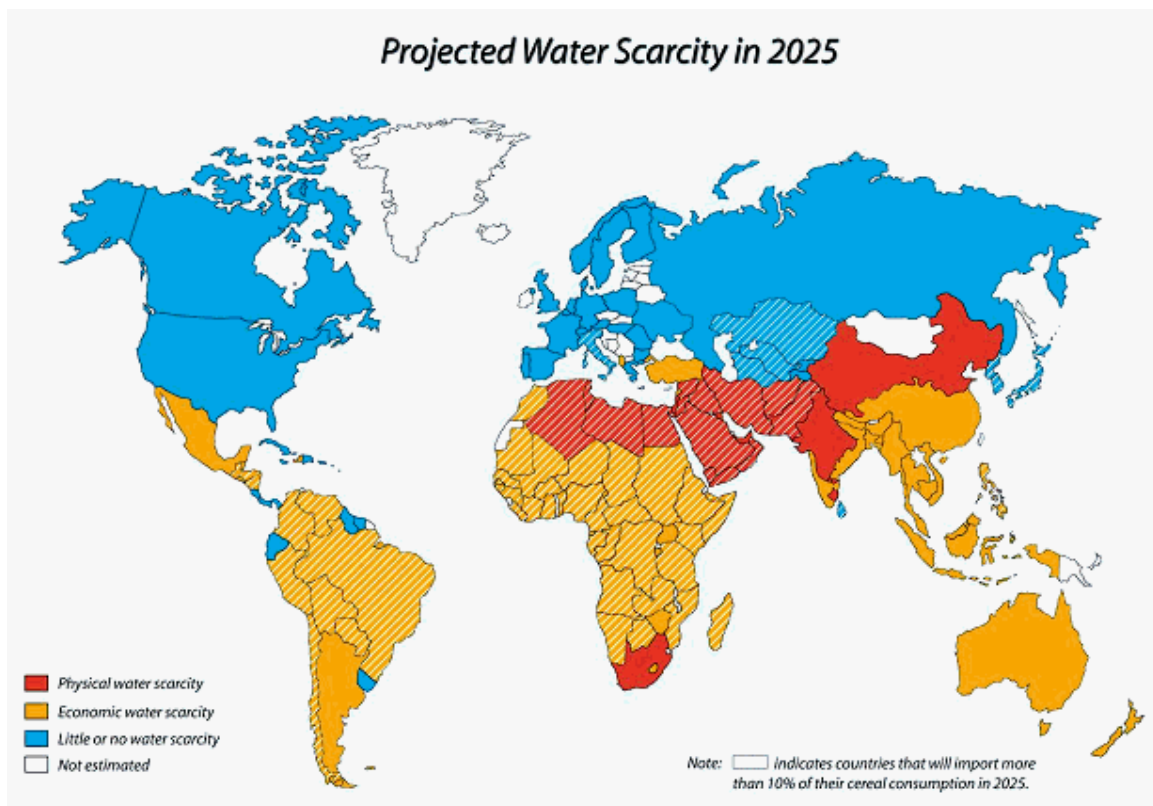


Figure 1-3. Projected global water scarcity, by nation, in 2025. Note many areas not affected by physical water scarcity are affected by economic water scarcity. Source: International Water Management Institute [IWMI, 2000].

This can be accomplished either by portioning coolant between the electric turbines and a process-heat based desalination process, or by maintaining constant turbine output, and portioning the electrical output of the turbine between the grid and an electrically driven desalination process. Regardless of the chosen approach, the desalination technology must be carefully matched to the reactor and power conversion system in order to accommodate load following operation where the nuclear powered electrical plant must accommodate all changes in grid demand.

1.4 Transitioning to Nuclear Base Load Generation

India and China both have new nuclear power plants under construction with plans for more, yet they do not have plants to significantly increase the fraction of total energy production from nuclear power. They continue to rely upon coal as the largest single source of electricity production, as does the United States. The global climate science community overwhelmingly accepts the theorized processes of anthropogenic climate change [Cook, et al, 2016, Cook, et al, 2013; Anderegg, 2010; Doran and Zimmerman, 2009; Oreskes, 2004], yet U.S. domestic policy has not yet taken adequate strides to mitigate these processes. Coal is responsible for about 77% percent of the carbon dioxide (CO₂) emitted from electricity generation and only about 39% of the electricity produced. Nuclear power is responsible for about 20% of the electricity generated in the U.S. and does not have direct CO₂ emissions. To replace the electricity generated by coal would require roughly tripling the electricity generated by nuclear from about 797 billion kilowatt-hours (kWh) to 2,391 billion kWh. A 1 GWe nuclear reactor operating at full power, with a capacity factor equal to the U.S. average of 91.7%, generates about 8.04 billion kWh every year. To take over the roughly 1,594 billion kWh currently generated annually by coal would require an additional 199 nuclear reactors. That's two new reactors at every operating nuclear power plant in the country. However, many existing nuclear sites cannot feasibly add new reactors because of the limits of the local environment for ultimate heat rejection, available land use, or other factors [World Nuclear Association, 2016].

The choice of replacing coal plants with nuclear plants is necessitated by the fact that there is no other technology capable of replacing the load generated by coal without also contributing large amounts of CO₂ and other greenhouse gases to the atmosphere, exacerbating the climate problems we already face. However, selling the public on building nearly 200 new nuclear reactors, not to mention finding the capital investment for that many multi-billion dollar projects, is no small feat.

Adding two 1,117 MWe Westinghouse AP1000 reactors to the V.C. Summer Nuclear Generating Station in South Carolina will cost owners approximately \$10 billion. Duke Energy's construction of its new Lee plant, also with two AP1000 reactors, is estimated to cost \$11 billion, excluding financing costs and inflation. However, financing costs can nearly double total costs, as estimated by Florida Power and Light in planning the addition of two units to the Turkey Point site. The estimated costs range without financing for the addition of two AP1000 reactors is between \$6.9 billion and \$10.1 billion, while the estimate range including financing costs is between \$12.9 billion and \$18 billion. Building new plants is costlier than adding units to existing plants because new plants require more site preparation work and infrastructure development. Costs also vary significantly geographically due to local and state regulations and site specific engineering requirements. If we use a conservative estimate of \$10 billion in average total costs per reactor, 200 new reactors would cost approximately two trillion dollars [World Nuclear Association, 2016].

Despite the need, there are significant sources of resistance to replacing coal and combustible fuel sources with nuclear power, aside from just the industries that are built on combustible fuels. The Nuclear Energy Institute (NEI) commissions semi-annual public opinion surveys about public views toward nuclear power in the U.S. A recent poll found that 86% of the general public favors license renewal for existing plants that meet regulations, 77% of respondents agree that utilities should prepare now and build new nuclear capacity in the next decade, if needed, and 83% of the public believe it is important for U.S. nuclear companies to lead in international energy markets. However, only 62% of respondents agreed that the U.S. should definitely build more nuclear power plants in the future [Bisconti, 2015a]. Further, a separate survey of people who live near nuclear power plants, referred to as 'plant neighbors' express even stronger support than the general public for nuclear power, with 50% of nuclear neighbors strongly favoring the electricity source as compared to 27% of the general population, and a total of 83% generally favoring (somewhat favoring + strongly favoring) as compared to 68% of the general population generally favoring nuclear power [Bisconti, 2015b]. Despite these responses, the question not asked was whether people felt that nuclear generating capacity should be increased enough to take over base load generation.

1.5 The Integral Inherently Safe Light Water Reactor (I²S-LWR)

The I²S-LWR is a novel Pressurized Water Reactor (PWR) concept being developed by a multi-institutional team led by Georgia Institute of Technology, under the DOE NEUP IRP. The I²S-LWR aims to deliver 969 MWe power output, comparable to other large scale LWRs, while simultaneously delivering improved safety over other Generation III+ LWRs. This reactor concept aims to achieve these goals by incorporating inherent safety features in the design.

The first and most significant of these features is an integral design of the primary coolant flow path. The primary coolant does not leave the reactor pressure vessel in order to exchange energy with the secondary coolant. This eliminates the need for large pipes to carry the primary coolant between the pressure vessel and the heat exchanger, and in so doing removes the possibility of a large break loss of coolant accident (LB LOCA). There are still small diameter water lines which exit the pressure vessel as part of the pressurizer and chemical volume control systems. This reactor concept achieves confinement of the primary coolant by a technique novel to LWRs, liquid to liquid heat exchange without boiling between primary and secondary coolant. In the preliminary scoping phase of the reactor project, the possibility of using a once-through, helical coil type primary heat exchanger was evaluated. Such an exchanger would have produced superheated steam from feedwater, as is proposed in multiple small modular reactor (SMR) designs such as the NuScale SMR [Reyes and Lorenzini, 2012], B&W mPower [Halfinger and Haggerty, 2012], and the International Reactor Innovative and Secure (IRIS) design [Carelli, et al, 2004]. It was determined that to use such a method of steam generation for a 3,000 MWth reactor would require a heat exchanger either so tall as to require a pressure vessel too large to reasonably manufacture, or so complicated that it would be too expensive and not able to pass maintenance and inspection requirements. Consequently, the use of liquid to liquid heat exchange in a microchannel heat exchanger was selected [Kromer, et al, 2016].

Another system integrated inside the reactor pressure vessel (RPV) is the reactivity control system, consisting of control and safety rods, rod position measurement devices, and rod drive mechanisms, which move the rods in and out of the fuel assemblies. The rods are grouped in clusters, and the position measurement devices and drive mechanism are combined in units called rod control cluster assemblies (RCCAs). In a traditional PWR, the RCCAs are located outside the RPV, and the control rods penetrate the RPV in order to access the fuel assemblies in the reactor core. In the event of mechanical failure of a drive mechanism, the difference in pressure between

the reactor coolant and the environment outside the pressure vessel can eject a rod or cluster of rods out of the core, introducing a large positive addition of reactivity to the fuel. This can cause fuel damage and even catastrophic damage to the reactor and the plant, resulting in loss of life, property, and release of radiological material to the public environment. By confining the control rods and RCCAs to the inside of the pressure vessel, the I²S-LWR eliminates the possibility of a rod ejection accident. Without the pressure differential across the RPV, there is no motive force to eject a rod from the core, even if the RCCA suffers mechanical failure. In fact, if mechanical failure or loss of power to the RCCA occurs, gravity will drive the affected control rods to fully insert into the core, rather than be ejected from it.

The I²S-LWR also features a fully passive decay heat removal system (DHRS) designed to provide indefinite core cooling as long as the core remains submerged in coolant. A schematic of the integral layout of the I²S-LWR is presented in Figure 1-4 [Petrovic, 2014].

Prohibiting reactor pressure vessel penetrations at elevations below four feet above the top of the reactor core prevents the possibility of a small-break LOCA (SB LOCA) leading to core uncover. In fact, with three out of four natural circulation DHRS units in operation, only pressure vessel failure can cause core uncover. This is achieved by reducing the volume of the containment building and operating the containment building at higher than atmospheric pressure, causing the system to achieve pressure equilibrium between the inside and outside of the RPV in the event of a SB LOCA. This prevents the core from becoming uncovered by coolant evaporation.

Another system novel to commercial nuclear power is the use of a steam flashing drum for generating the steam which powers the turbines of the power conversion system (PCS). In a steam flashing drum, high pressure, high temperature, but subcooled water enters through an accelerating nozzle into a drum which is at a lower pressure, saturated condition. In the drum there are both liquid and vapor forms of water, but no other fluids. When the inlet stream is presented to the lower pressure condition, it undergoes a process called isenthalpic expansion. The energy of the stream does not change, but the portioning of that energy within the stream changes. The majority of the inlet stream remains liquid, but at a lower temperature and pressure, specifically, the operating pressure of the drum and the corresponding saturation temperature. A fraction of the inlet stream is rapidly vaporized, hence the terminology “flash vaporization.” The vaporized water is in equilibrium with the liquid water, at saturation condition.

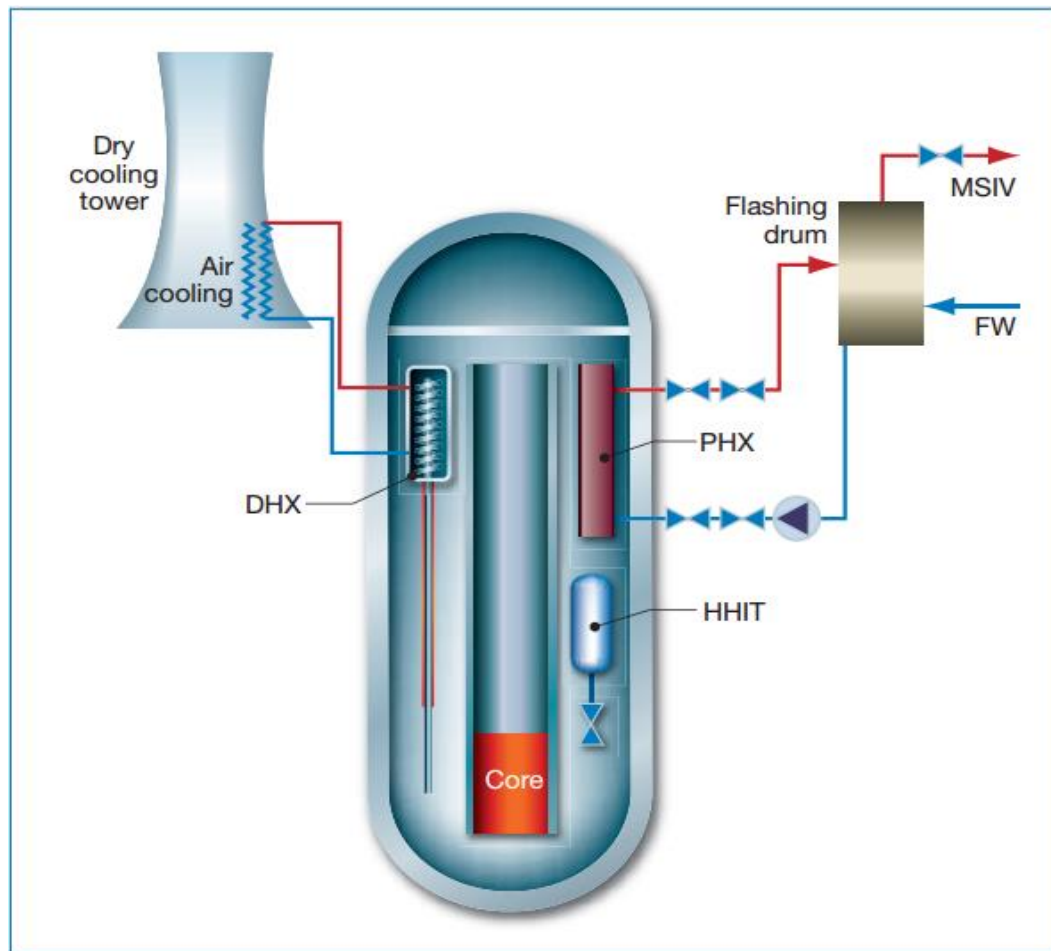


Figure 1-4. Integral Inherently Safe Light Water Reactor schematic. Not to scale. Note decay heat exchanger (DHX), primary heat exchanger (PHX), steam flashing drum. Not pictured systems include integral control rod drive mechanisms and pressurizer heaters and sprayers [Petrovic, 2014].

The energy to overcome the large enthalpy of vaporization of water, breaking the non-covalent hydrogen bonding which gives water its unique properties, is the energy lost by the majority of the inlet stream while reducing in energy from the inlet stream pressure and temperature to the saturated liquid enthalpy. Design considerations for the flashing drum as well as the PCS are discussed in a paper by collaborators Matthew Memmott of Brigham Young University and Annalisa Manera of the University of Michigan [Memmott and Manera, 2015].

This process produces saturated steam, so there will be entrained droplets of liquid water in the vapor flow, which must be removed with moisture separators and steam dryers in the same manner as used in traditional shell and tube steam generators.

Though not a part of the original design proposal for the I²S-LWR, black start capability should be included in the implementation of these plants, particularly for use as isolated power systems. Black start capability is the ability to bring all systems on-line and begin generating electricity without the use of off-site power. This can be accomplished by having a small gas powered turbine generator on site with sufficient fuel in storage to shut the plant down, operate during refueling, and bring the plant back online.

1.6 Objective of the Dissertation and Original Contributions

The purpose of this dissertation is to identify and, as much as possible, solve the instrumentation and control challenges posed by the I²S-LWR and other integral reactors. Integral reactors present the potential for significant improvements in passive plant safety, accident resilience and mitigation, and capital cost reduction if produced in large numbers, taking advantage of economies of production scale. They also pose a lot of challenges to adequately monitoring the processes to ensure mitigating actions are taken quickly enough to prevent adverse or unforeseen events from resulting in radiological release, which can be catastrophic to people and the environment. The I²S-LWR aims to engineer as many features that inherently ensure passive safety in a large scale nuclear reactor as possible, and this work aims to provide a comprehensive strategy for the instrumentation and control (I&C) of such a reactor.

The following tasks will be completed to achieve the objective of this dissertation:

- Dynamic modeling and simulation of reactor core, microchannel heat exchanger, and steam flashing drum in MATLAB/Simulink environment.
- Reasonable estimation of parameters not defined elsewhere by the design team to

support this modeling.

- Control strategy development and testing for integrated models of reactor system during full range of operating conditions, with emphasis on load following.
- Instrumentation strategies for in-vessel systems including reactor vessel (neutron flux, flow, level, and temperature measurements), control rod drive mechanisms (A.K.A. rod control cluster assemblies), primary coolant pressurizer, primary heat exchangers, passive decay heat removal heat exchangers.
- Instrumentation strategies for ex-vessel components of the nuclear steam supply system (NSSS) including steam flashing drum and secondary coolant loop, passive decay heat removal systems, safety related nuclear instrumentation system (power monitors), reactor coolant pumps.
- Signal and power cabling routing and exit strategies for in vessel equipment and instrumentation, with consideration to the radiation environment and signal noise introduced by utilizing long runs of cable.
- Simulation of various anomaly scenarios for development and evaluation of monitoring and diagnostic strategies for large scale integral reactors.
- Development of monitoring and diagnostic strategies for the modeled systems.

In this dissertation, the following original contributions to the field of nuclear reactor systems I&C are made:

- Instrumentation strategies for large scale integral PWRs and their accompanying radiation environments.
- Dynamic modeling of isenthalpic expansion vessel for nuclear steam supply systems coupled to an integral PWR.
- Control strategies for such systems, demonstrated in the dynamic model, for low to full power operation.

2 PROCESS INSTRUMENTATION OF I²S-LWR

The approach to instrumenting the I²S-LWR has three steps. The first task is to identify all the measurements that need to be made. The second task is to determine which of those measurements can be accomplished with existing technology and applications. The third task is to identify technology gaps and, where possible, propose solutions to fill the gaps. The first two steps occur concurrently, and are broken down by the different systems being instrumented. This begins with reviewing the safety related systems of PWRs and whether or not those systems are present in one form or another in the I²S-LWR. Next, safety related nuclear instrumentation, which measures neutron population, is considered. This is followed by instrumentation of systems inside the vessel, instrumentation of systems outside the vessel, and accident monitoring considerations. The analysis is terminated when secondary steam leaves the flashing drum to carry energy to the turbine. The balance of plant systems are not considered because there is not any reason these systems should be substantially different from a typical large PWR. Analysis of the co-generation application possibilities of the I²S-LWR are a subject for further study. Performance requirements of process instrumentation systems, such as response time and sensitivity are not considered, due to the analysis required to make these conclusions being beyond the scope and resources of the project. At this stage of reactor development, the research is limited to the feasibility of obtaining necessary information for the safety and control of the proposed reactor systems.

2.1 Safety Systems

As a result of reviewing the instrumentation needs of the I²S-LWR a review of reactor safety systems that corresponded to NUREG-800 Chapter 7.2 [U.S. NRC, 2010] has been carried out. The Design Control Document (DCD) for the Westinghouse AP1000 was also consulted along with NRC Regulatory Guide 1.97, Revision Three [U.S. NRC, 1983]. The results of this review include identification of reactor safety systems for I²S-LWR along with proposed methodology for the monitoring of safety system parameters. The analysis focuses on safety systems that are used in traditional nuclear power plants and those that may be unique to the I²S-LWR. The bulk of these unique systems are associated with either the primary side or operating conditions of the flashing drum.

The reactor safety systems will be labeled as all sensors, controls, and all other equipment/instrumentation necessary to monitor the following systems or conditions [U.S. NRC, 2010]:

- Nuclear Steam Supply System (NSSS).
- Parameters responsible for executing reactor trip signals.
- Systems that allow for reliable and rapid reactor shutdown.

The purpose of these systems is to protect the fuel in the core by maintaining acceptable fuel design conditions as well as maintaining the reactor coolant pressure boundary during design basis events of both high and low frequency, and during transient events.

In typical nuclear power plants, reactor trip signals are monitored using four redundant sensors for each trip-related parameter. Of the four sensors, three are used for regular monitoring, and the fourth is maintained as a backup in the event that one of the three in use is malfunctioning. The three sensors used for regular monitoring are interpreted using a “two-out-of-three” logic for trip decisions. This logic structure means that trip decisions are based on two of three sensors indicating a trip condition. If one of the three primary sensors malfunctions, that sensor is excluded from the logic and the fourth sensor is included in its place. The purpose of monitoring with redundant sensors is to minimize false and missed reactor trips (type I and type II errors, respectively). In addition to generating trips, the safety systems have pre-trip alarms that function to alert operators of impending trip conditions so that mitigating actions may be taken, when applicable. Functionally, a reactor trip acts to de-energize the control drive mechanisms (CRDM), causing the control rods to be fully inserted into the core under the force of gravity.

The functions of these systems include [International Atomic Energy Agency, 2002]:

- Provide normal reactivity control within safety limits
- Prevent unacceptable reactivity transients
- Shutdown the reactor as necessary to prevent design limits from being exceeded
- Maintain safe reactor shutdown conditions
- Maintain the ability to safely remove heat from the core

Typical reactor trip signals that may apply or be analogous to some other system of I²S-LWR are as follows [Arizona Public Service Company, 2007]:

- Reactor Variable Overpower

- High Logarithmic Power Level
- High Local Power Density
- Low Departure from Nucleate Boiling Ratio (DNBR)
- High/Low Pressurizer Pressure
- High/Low Steam Generator Water Level
- High/Low Steam Generator Pressure
- High Containment Pressure
- Low Reactor Coolant Flow

2.1.1 Reactor Variable Overpower

This trip signal is determined by monitoring the neutron flux at various positions throughout the core. The flux signal used is the average of three linear sub channel flux signals that originate at different instrumentation lines. Trips are executed based on either the rate of which the flux is increasing or if the neutron flux reaches a preset value. This signal is monitored with ex-vessel power range neutron detectors.

2.1.2 High Logarithmic Power Level

The focus of this trip signal is to monitor the indicated neutron flux. The monitored parameter for this trip is the logarithm of the indicated neutron flux. During startup and shutdown, the flux may increase by several orders of magnitude, which is impractical to monitor on a linear scale, so the logarithmic scale flux is monitored to ensure safe operation. The trip is generated once the measured signal reaches a preset value. Additionally, this system typically has two set points, one that can be bypassed manually, and one that cannot be bypassed.

2.1.3 High Local Power Density

The high local power density trip is provided to trip the reactor when any peak local power density reaches a preset value. The set point of this value is selected as some value lower than that which would cause the fuel centerline to melt. This parameter is usually calculated by the core protection calculator, which is a safety related algorithm that takes into account various reactor conditions such as coolant pressure, neutron flux, and core exit temperature, to determine the local power density of each monitored fuel assembly. The algorithm is designed such that the centerline temperature of the reactor fuel does not approach melting temperatures.

2.1.4 Low Departure from Nucleate Boiling Ratio (DNBR)

If the DNBR reaches a set point value, the reactor will trip. This parameter is typically calculated based on average core power, reactor coolant pressure, and core power distribution. The calculation accounts for the sensor and processing delays and inaccuracies to ensure that a trip is generated before the DNBR value exceeds safety limits. In some cases, this system is tied to several other trips such as a low pressurizer pressure trip. In the event of a trip by a linked system, the DNBR trip will also be reported. Parameters such as primary coolant flow rate and primary coolant pump speed are included in the DNBR calculation. Consequently, a low DNBR trip may be generated due to low core coolant flow rate.

2.1.5 High/Low Pressurizer Pressure

In the event that the system pressure is too high or low, the reactor should trip. For high pressure the trip is based on only the pressurizer pressure; for low pressurizer trips the set point value is based on standard operating power range. In typical systems, this set point can be reduced to a certain minimum value manually when the reactor power is below operating range. Incremental minimum set point values are usually determined for each power level such that an appropriate minimum pressurizer pressure set point can be maintained during plant cool downs. Each power level generally has two low pressure set points, the more conservative of which may be bypassed by the operator.

2.1.6 High/Low Steam Generator Water Level

While the I²S-LWR does not have traditional steam generators, the water level in the flashing drum is controlled to optimize the thermodynamics of the isenthalpic expansion. In an accident scenario, the water in the drum is used to continue to remove heat via the primary heat exchangers in the event of a loss of feedwater flow. If the level cannot be controlled, then there is a serious malfunction of the system, forcing reactor shutdown and investigation.

2.1.7 High/Low Steam Generator Pressure

Similar to the pressurizer pressure systems, the set points for the high pressure is static and the low pressure set point can be adjusted and by-passed based on reactor power level. The adjusted low pressure set point is also used to allow for a minimum set point to be maintained during plant cool down. These systems are another set of analogous systems that can be applied to the flashing drum. The I²S-LWR flashing drums will have high and low set points and the low set point may

also be a function of reactor power level. However, the flashing drum of the I²S-LWR is intended to operate at the same pressure regardless of power level.

2.1.8 High Containment Pressure

The goal of this set point is to monitor the overall containment pressure and trip the reactor if the measured containment pressure exceeds a certain set point value. The set point of this system is selected to prevent pressures exceeding the design containment pressure in the event of a design basis LOCA or main steam line break. Given the integral design of the I²S-LWR this set point may be based on secondary LOCA rather than primary LOCA.

2.1.9 Low Reactor Coolant Flow

In a typical PWR, the low reactor coolant flow trip is provided to trip the reactor when the differential pressure of primary coolant across the steam generator falls below a preset value. It is important to note that this trip is not based on primary flow rate measurement but rather primary pressure drop. This system is not directly applicable to I²S-LWR due to the lack of primary coolant flow outside of the RPV. It may be possible to measure differential pressure across the inlet and outlet plena of each of the eight microchannel heat exchangers, though rigorous analysis of this idea is a subject for further study. Additionally, this trip could be redefined to be based upon flow rate as measured by ultrasonic flow meters mounted on the external surface of the RPV.

To provide a collective result of the safety systems review, Table 2-1 of reactor safety system sensors has been prepared to demonstrate the type, number, and measurement for each reactor trip signal.

2.2 Ex-core Nuclear Instrumentation

The utilization of fixed in-core nuclear instrumentation is not unique to the I²S-LWR concept. Both Combustion Engineering (CE) and Westinghouse Electric Company (WEC) have designed reactor systems utilizing fixed, in-core, self-powered nuclear instrumentation systems. The in-core instruments in CE designs and in the WEC AP1000 reactor are not considered safety related equipment. This is largely due to the high probability of loss of functionality of these devices under severe accident scenarios, when safety related instrumentation is most important. In both the AP1000 and the CE PWRs, safety related nuclear instrumentation is located outside the RPV, in the concrete containment well in which the reactor vessel is installed. Limited information is publically available on the specific placement and allocation of ex-vessel nuclear instrumentation

Table 2-1. Sensor selection for Reactor Safety Systems [US NRC, 1983; US NRC, 2010; Arizona Public Service Company, 2007].

Monitored Variable	Sensor Type	Number of Sensors	Associated Trips	Equipment Range
Neutron Flux Power	Neutron Detector	12	Reactor Overpower High Log Power Level High Local Power Density	10 ⁻⁶ % to 200% power
Average Core Temperature	Thermocouple (Detector strings)	N/A	Low DNBR High Local Power Density	Expected: 315.4°C Vessel Design Temp: 343.3°C
Primary Temperatures (Hot and Cold Leg)	Precision RTD	16	Low DNBR Various Core Protection Calculators	10°C to 398.9°C
Pressurizer Pressure	Pressure Transmitter	4	High/Low Pressurizer Pressure	Design: 15.51 MPa
Primary Heat exchanger Pressure Drop	Differential Pressure Transducer	4/Heat Exchanger	Low Reactor Coolant Flow	Design: 0.456 MPa
Reactor Coolant Pump Speed	Pump Motor Signals	N/A	Low Reactor Coolant Flow	0 to 15498 kg/s
Flash Drum Pressure	Pressure Transmitter	4 per Drum	High/Low Drum Pressure	Inlet: 12.06 MPa Outlet: 7.0800 MPa
Flash Drum Level	Differential Pressure Transducer	4 per Drum	High/Low Drum Water Level	Bottom of drum to steam dryers
Control Rod Position	CRDM reading	4 per Control Rod	Control Position Monitoring	Full in or not full in
Containment Pressure	Pressure Transmitter	4	High Containment Pressure	-0.0345 MPa to 3 times design pressure or 46.53 MPa

for the AP1000, however, the Final Safety Evaluation Report (FSER) indicates that the AP1000 does use data obtained from its in-core instrumentation to calibrate its ex-core detectors [Westinghouse Electric Co., 2004]. More information is available for the CE designs from the Final Safety Analysis Report (FSAR) for Arkansas Nuclear One, unit 2, a CE PWR [Arkansas Power & Light Co., 1978]. To assess the applicability of typical nuclear instrumentation systems to the P-S-LWR, the system employed at ANO is discussed here.

2.2.1 Typical PWR Nuclear Instrumentation

The CE PWR uses four safety channels located in the reactor cavity close to the biological barrier. The channels are placed 90 degrees apart to provide optimal neutron flux information. Each safety channel detector assembly contains three identical fission chambers which are stacked vertically in the reactor cavity. The fission chambers provide neutron flux information within a range of startup flux levels up to 200% of the reactor's operating power. The safety channels send information to the reactor protection system (RPS) and provide information on the rate of change of reactor power, local power density, DNBR, and reactor overpower protection.

Figure 2-1 shows the radial position of the instrumentation channels in a CE PWR with respect to the center of the RPV. Figure 2-2, Figure 2-3, and Figure 2-4 show vertical cross-sections, taken at the center of the RPV, for each pair of instrumentation channels' respective radial position within the reactor cavity.

The CE PWR also contains two startup channels located within the reactor cavity close to the RPV. The detector assembly contains two uranium lined fission chambers that provide 10^{-8} % to 100% power level neutron flux information (corresponding to 0.1 to 10^6 CPS readout from the detector) and boron dilution event monitoring.

Startup channel instrumentation is primarily used during shutdown periods, reactor startup and startup after extended shutdown periods such as after maintenance or refueling. The boron dilution event monitor reads the source range count rate obtained from the startup channel fission chambers and activates an alarm if the count rate has increased by an amount equal to a predetermined value. The startup channels are not connected to the RPS and only provide information and alarms for use by reactor operators.

There are two uncompensated ion chambers located within the reactor cavity. These ion chambers are used as gamma sensitive radiation monitors that are used in accident conditions and have a range of 1 R/hr to 10^8 R/hr.

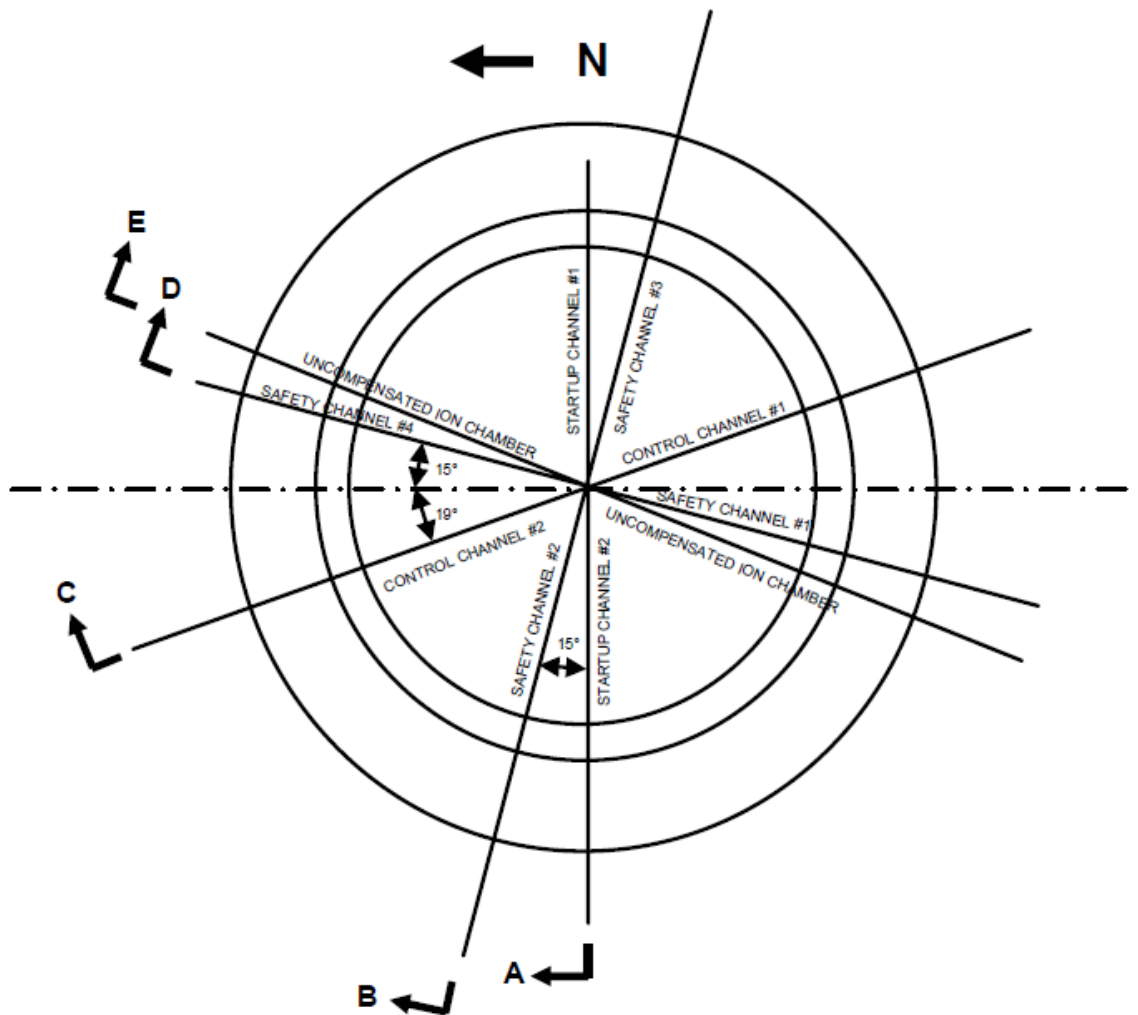


Figure 2-1: Radial locations of instrumentation channels in the Arkansas Nuclear One – Unit 2, a CE design. Upper case letters refer to Figure 2-2 and Figure 2-3 [Arkansas Power & Light Co., 1978].

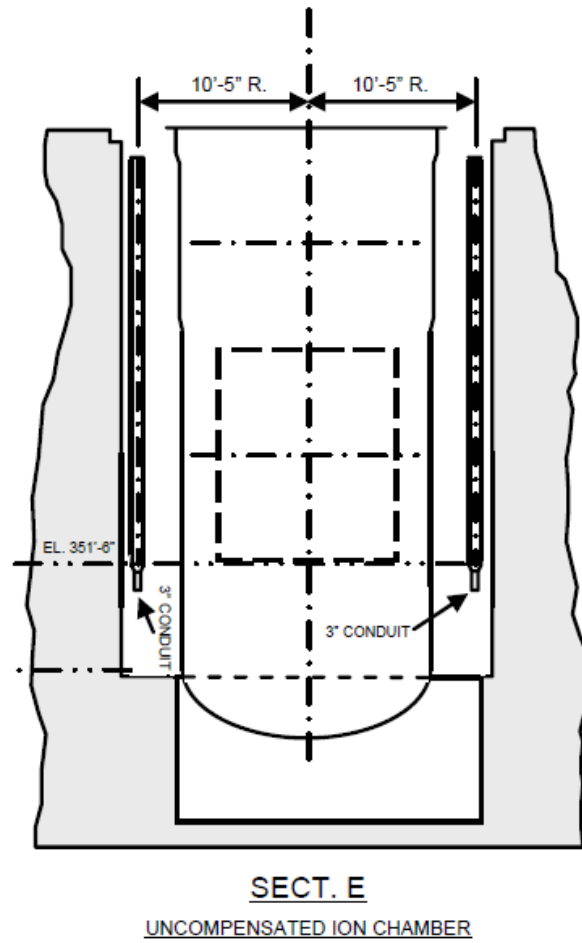


Figure 2-2: Location of the uncompensated ion chambers within the reactor cavity of the Arkansas Nuclear One – Unit 2 CE plant [Arkansas Power & Light Co., 1978].

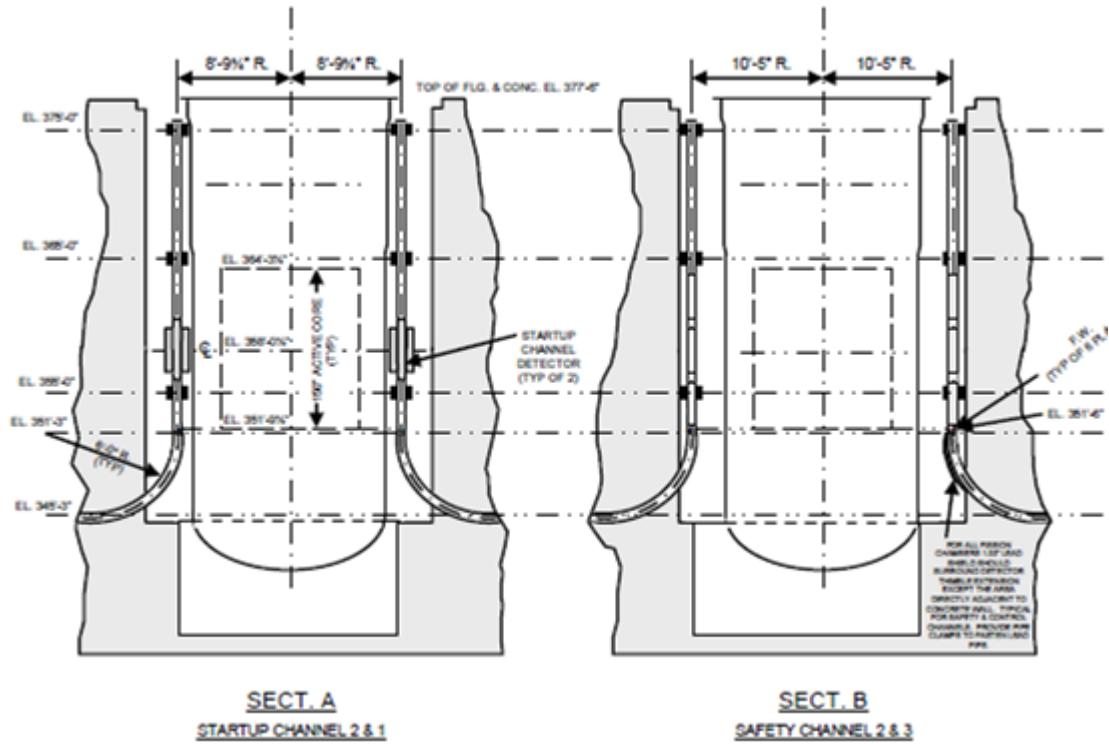


Figure 2-3. Instrumentation channel locations for cross-sections A and B [Arkansas Power & Light Co., 1978].

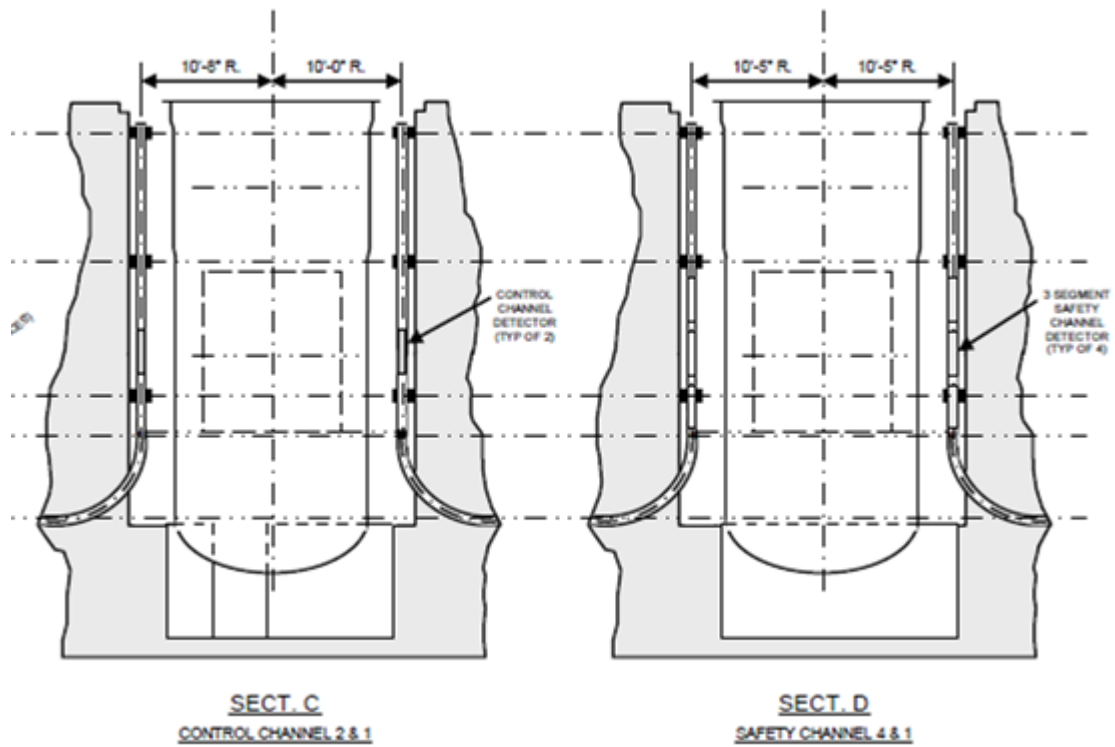


Figure 2-4. Instrumentation channel locations for cross-sections C and D [Arkansas Power & Light Co., 1978].

The chambers contain a U-235 source that provides a baseline reading of 1 R/hr during normal operating conditions. To protect the chambers in accident conditions, both chambers have a stainless steel casing that can protect the detectors at temperatures up to 350 °F.

The I²S-LWR design concept will have a larger downcomer region than that of CE plants and other conventional PWRs, which will reduce the thermal neutron flux in this region. A typical PWR has a downcomer thickness of approximately half a meter, whereas the I²S-LWR downcomer is nearly a full meter from the outside of the core barrel to the inside of the RPV. An analysis of neutron flux through the vessel and outside of the vessel, at full power operation, was performed by researchers at the Georgia Institute of Technology and is shown in Figure 2-5 [Petrovic and Flaspoebler, 2015]. The flux ranges of the detectors used in a standard WEC PWR are shown in Figure 2-6 [Westinghouse Electric Co, 1984].

Figure 2-5 shows that the thermal neutron flux in the reactor cavity of the I²S-LWR design is 1×10^6 n/cm²-s at full power. This is less than half of the zero-power flux seen by the power range detectors in a WEC PWR, which is shown in Figure 2-6 as 2.5×10^6 n/cm²-s. The full power flux at power range detector locations is roughly 5×10^8 , two orders of magnitude greater than that seen in the ex-vessel region around the I²S-LWR. The IRIS design faced a similar challenge. With a downcomer of approximately 1.68 m, the neutron flux outside the vessel was shown to be 5-6 orders of magnitude below the levels of typical PWRs [Lombardi, et al, 2002]. While the issue is not as severe with the I²S-LWR design concept, it remains that direct application of typical PWR nuclear instrumentation to the containment cavity outside the I²S-LWR RPV will likely be insufficient to meet the safety and control needs of the plant.

As in all the areas of instrumentation development for this reactor, it is desirable to use existing technology and solutions postulated for other systems whenever possible. During the development of the IRIS design, advanced flux monitors were proposed, such as silicon carbide (SiC) semiconductor based neutron detectors in lieu of traditional fission chambers and ionization chambers. The SiC matrix interacts with fast neutrons, but not thermal neutrons. Since the population of thermal neutrons in the downcomer is much greater than the population of fast neutrons and also of more direct interest to the monitoring of the core power during startup, it is beneficial to measure the thermal neutron population by means of a ⁶Li converting layer surrounding the SiC matrix of the detector.

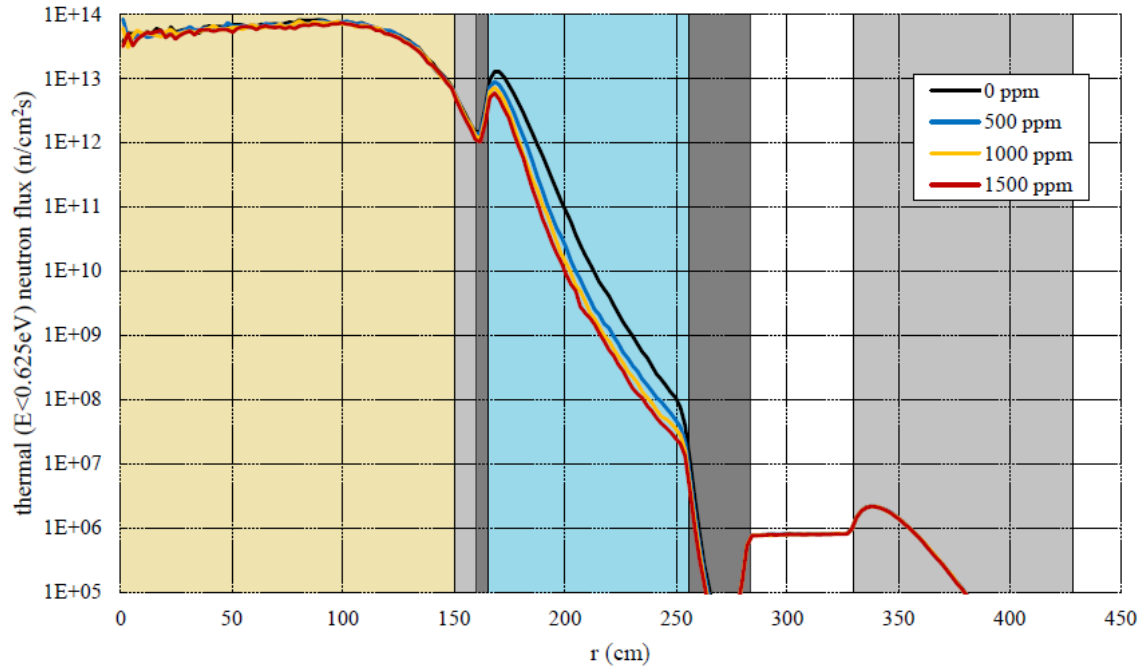


Figure 2-5: Thermal neutron flux profile of the I²S-LWR reactor design concept at full power and with various concentrations of dissolved boron [Petrovic and Flashpoehler, 2015]. The innermost shaded region is the reactor core from centerline to outer radius (tan). Outside of that region is the neutron reflector and core barrel (light and dark grey), followed by the downcomer (blue), RPV (dark grey), reactor cavity (white), and biological containment (light grey, outermost).

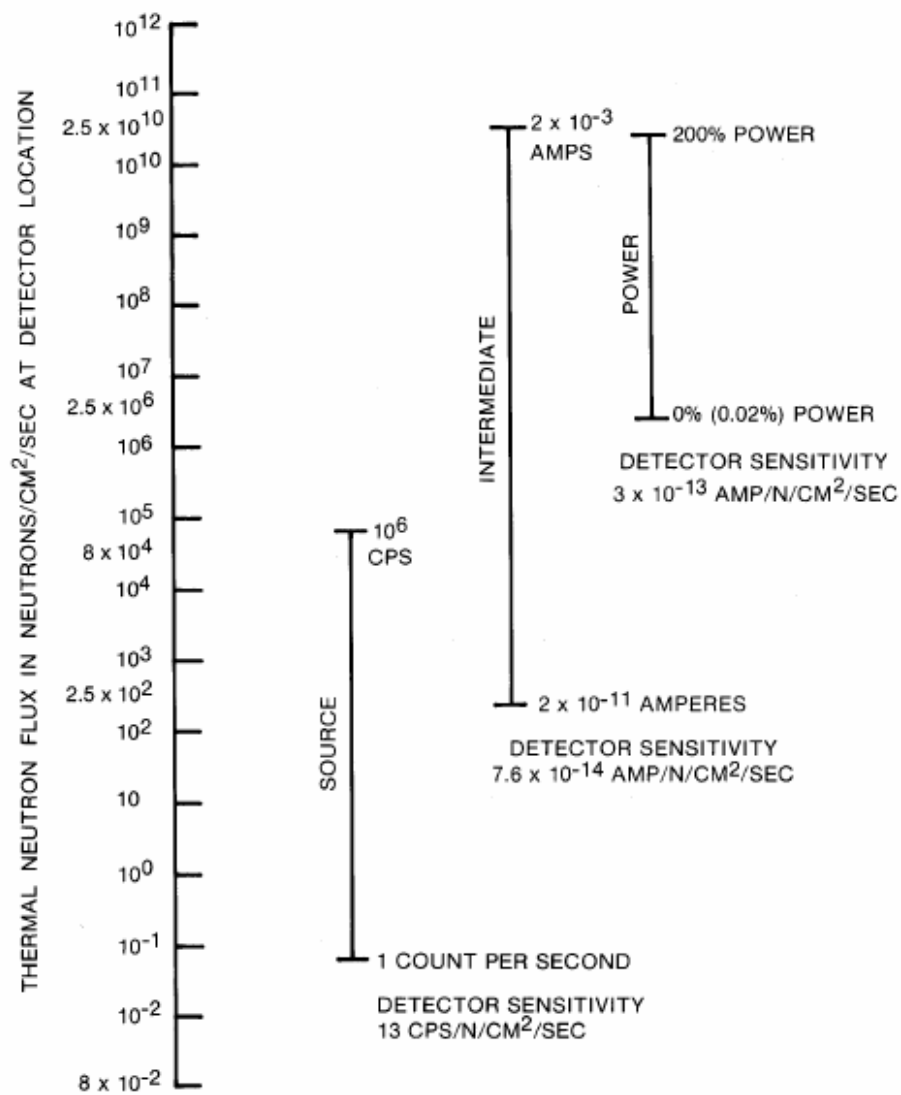
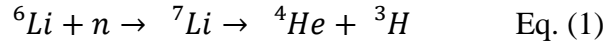


Figure 2-6. Flux ranges of detectors in a standard Westinghouse PWR [WEC, 1984].

The converting layer undergoes the following reaction:



The energized alpha and tritium products enter the SiC matrix, depositing energy and promoting electrons to the conducting band, which produces a proportional current when a reverse bias voltage is applied to the detector. Fast neutrons interact directly with the nuclei of carbon and silicon in scattering interactions, but with smaller cross sections than the thermal neutron absorption cross section of ${}^6\text{Li}$.

The downside to using a ${}^6\text{Li}$ conversion mechanism is that the lithium converting layer is consumed in the process. Once this layer is gone, the detector must be replaced. Such a detector suitable for detecting source range levels of neutrons in the downcomer is rapidly consumed under the fluence levels of the reactor at full power. The radial position of the detector in the downcomer can be varied to increase the lifetime, but this adversely affects detector sensitivity at low power. Another possible solution to the lifetime versus sensitivity problem is to locate the detector for optimum sensitivity during startup, but include a moveable shield in the detector assembly that would partially or completely cover the detector once the reactor power level increased above the range monitored by the in-vessel SiC detectors, when ex-vessel detectors could take over monitoring duties.

In the IRIS design, it was proposed to place these detectors, with a converting layer, inside the RPV, but outside the core, in the downcomer region. Analysis showed a balance of detector lifetime versus detector sensitivity could be achieved in this region without additional shielding [Petrovic, et al, 2002]. This approach was recently evaluated for the I²S-LWR design, using SCALE modeling of the radiation environment throughout the RPV and into the ex-vessel cavity and concrete containment well. It was determined that there was a similar balance between detector lifetime and sensitivity which could be struck by strategically placing SiC detectors in the downcomer region of the I²S-LWR [Petrovic and Flaspoepler, 2015].

These detectors have the additional benefits of being resistant to radiation as well as appropriate for high temperature applications such as the conditions found in the downcomer region of an integral reactor. It is also suggested that SiC detectors also be used as redundant and

diverse detectors for intermediate and power range nuclear instrumentation outside the pressure vessel, with or without thermal neutron detecting conversion layers as appropriate.

2.3 Instrumentation of In-Vessel Systems

2.3.1 In-core Instrumentation

For calibration of ex-vessel nuclear instrumentation and to monitor reactor performance, it is valuable to measure neutron flux throughout the core, and coolant temperature at the core exit. In current generation PWRs designed by WEC, periodic measurement is accomplished with moveable detector assemblies that are driven into position within the core through guide tubes that penetrate the bottom of the RPV. The I²S-LWR will not have any penetrations in that region to help prevent the possibility of core uncover, so that approach is not viable. Self-powered neutron detectors (SPND) in fixed in-core detector (FID) strings are used in CE designed PWRs and will be part of the in-core instrumentation in the new WEC AP1000 PWRs under construction at the Vogtle and V.C. Summer sites in Georgia and South Carolina, respectively.

FID assemblies typically consist of multiple SPNDs and a core-exit thermocouple. SPNDs operate based upon the interactions of neutrons and/or gamma rays with the emitter element of the detector to produce a current proportional to the local flux. Typical emitter elements are rhodium, platinum, and vanadium. Various properties of emitter elements are compared in Table 2-2. FIDs have the added benefit of providing continuous monitoring as opposed to the periodic monitoring capability of movable in-core detectors.

The standard CE design uses rhodium self-powered detectors. AP1000 reactors employ vanadium based detector elements in a design called OPARSSEL, an acronym for “optimized proportional axial region signal separation, extended life.” The number of neutron detectors in each string depends mostly upon the height of the core. Sensors that are too close together generate indistinguishable signals. WEC AP1000 has a 14-foot active core and uses seven SPNDs. The I²S-LWR has a 12 foot core and will use six SPNDs per instrument tube. WEC reports that the OPARSSEL instrument assemblies provide reduced uncertainty and exhibit better fault tolerance than the standard CE style rhodium based design [Heibel and Kistler, 2009]. A sketch of the AP1000 in-core instrument thimble assembly (IITA) is shown in Figure 2-7. The orientation of the detectors within the thimble assembly is shown along with the dimensions of the thimble.

Table 2-2. Comparison of SPND emitter elements for use in FID assemblies [Heibel and Kistler, 2009].

Emitter	Rhodium	Vanadium	Platinum
Source	Neutron	Neutron	Gamma
Response delay	Small	Medium	Prompt
Physics model	Medium	Simple	Complex
Signal level response	Large	Small	Small
Response proportional to	Surface	Volume	Volume
Sensor depletion	Large	V. Small	V. Small
Sensitivity change	Large	V. Small	FP Buildup
Sensitivity variation among detectors	Medium	V. Small	Small
Lead-wire compensation	Easy	Critical	Critical

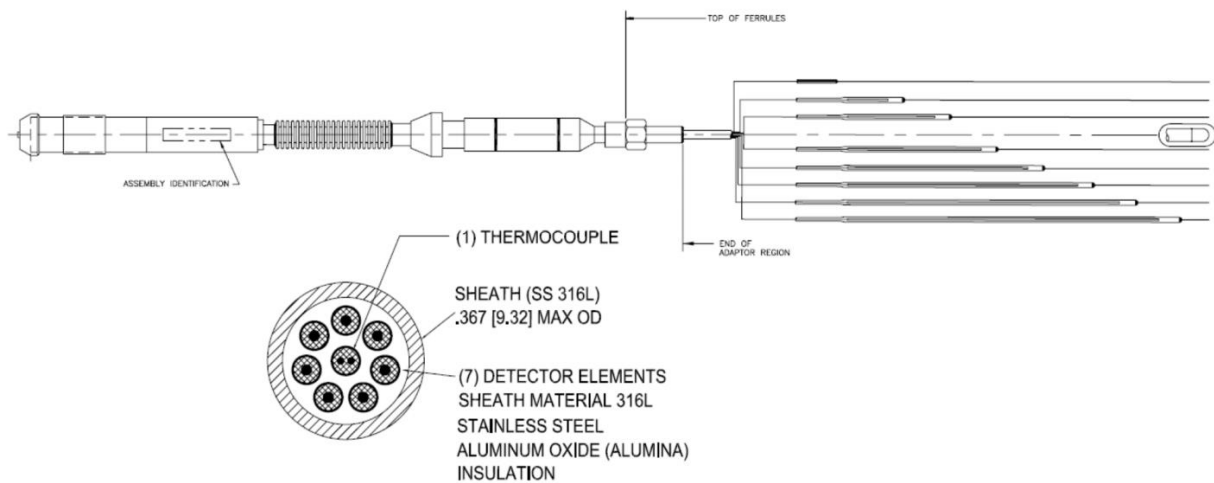


Figure 2-7. Westinghouse ITTA In-core detector assembly [Heibel and Kistler, 2009].

The downside to vanadium only based detectors is that they do not exhibit fast enough response to changes in neutron population for core protection applications. The next generation design of WEC in-core detectors may incorporate both vanadium and platinum detectors to improve response time for direct use in the reactor protection system. The I²S-LWR will take advantage of the latest licensable technology at the time of deployment.

The proposed distribution of the in-core instrumentation assemblies throughout the core of the I²S-LWR is based upon the core fuel assembly map and the distribution patterns found in CE designs [Upadhyaya, 1984]. Figure 2-8 shows the distribution of 34 IITAs within the 121 fuel assemblies of the core. Each thimble assembly goes inside an instrumentation tube at the center of the indicated fuel assembly, providing 34 core-exit temperature measurements and 170 neutron flux measurements.

2.3.2 Pressurizer Instrumentation

The I²S-LWR pressurizer is located in the top of the pressure vessel and requires pressure transmitters and differential pressure level sensors to monitor and control the pressurizer. Four level sensors and four pressure transmitters are sufficient for two-out-of-three reactor trip logic, with one sensor in reserve service. Typical pressurizer pressure monitoring instruments have a range of zero to 3000 PSI (~20.68 MPa) and a calibration span of 1700 to 2500 PSI (~11.72-17.24 MPa). Qualified lifetime of these pressure transmitters depends strongly on ambient temperature of the instrument, and ranges from less than three years to upwards of 30 years. The electronics generally have a shorter lifetime than the pressure transmitting module itself. Response times are on the order of tenths or even hundredths of a second with accuracies around 0.25%, though ambient temperature and pressure can create an additional 0.50% uncertainty [Rosemount, 2008]. There is no particular reason to suspect that the I²S-LWR would require better performance than currently operating PWRs enjoy from currently licensed nuclear grade pressure transmitters. However, the speed of transient events must be analyzed in conjunction with the response time of instrumentation, decision making, and actuation equipment in order to specifically characterize the performance requirements of any of the process instrumentation. Such an analysis is a subject for future study.

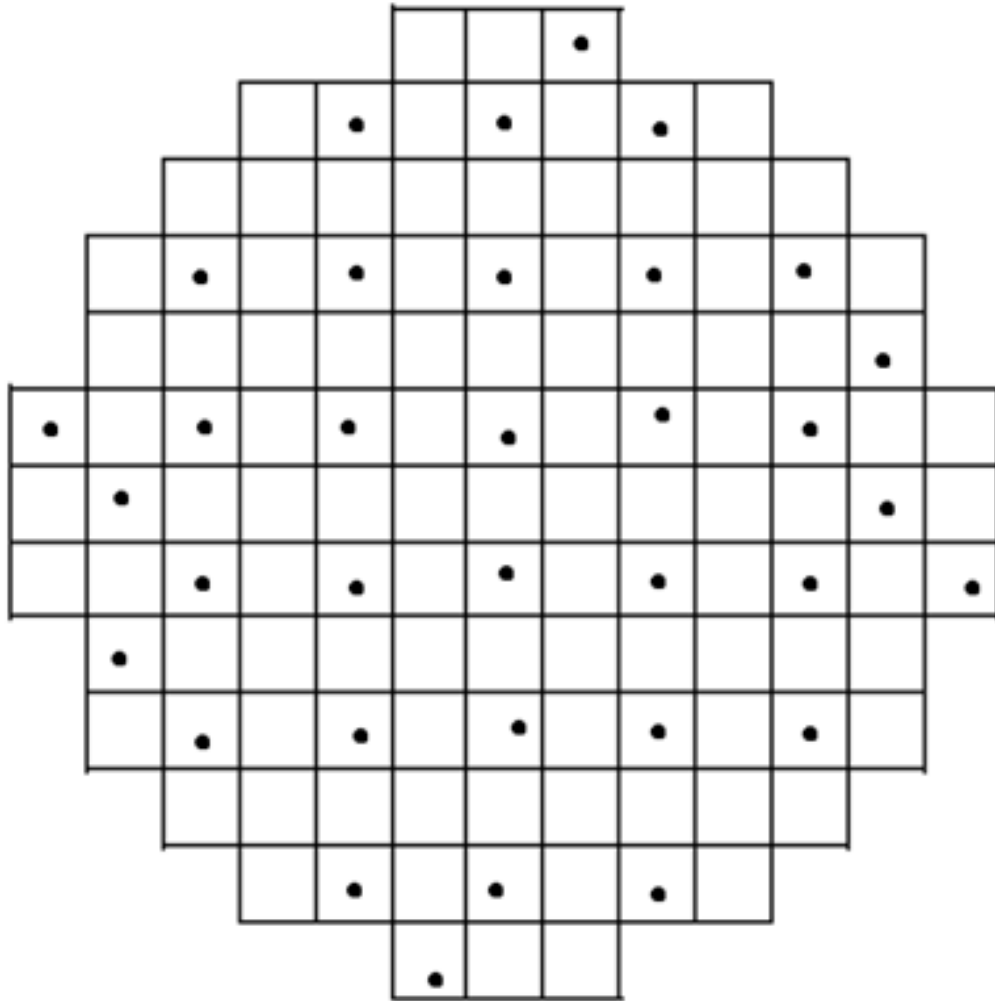


Figure 2-8: Proposed detector configuration for P^2S -LWR.

2.3.3 DHRS Instrumentation

The instrumentation needed for the decay heat removal system must be able to verify proper operation of the system by determining the energy extracted from the primary coolant by each DHRS for post-accident monitoring. The DHRS operates completely by natural circulation, and is designed to maintain the core at safe temperatures indefinitely in a post-accident cool down scenario, even in the event of loss of off-site power and backup electricity.

The primary DHRS heat exchanger (DHRS-HX) for each of four DHRS loops is inside the RPV. It consists of a helical coil tube for primary coolant within a larger pipe for secondary coolant, which enters and exits the RPV at the same elevation as the penetrations for the primary, power operation heat exchangers. The core barrel features fail-open valves just above the core to allow the DHRS primary intake access to the coolant rising out of the core if the reactor coolant pumps (RCP) are offline. There are four DHRS units in the I²S-LWR system, for a total of eight secondary coolant pipes that conduct coolant to and from the final heat sink, air cooled heat exchangers. Figure 2-9 shows the placement of the DHRS-HX on the outside of the core barrel, in between two primary heat exchanger units. The primary and secondary inlet and outlet locations are shown along with the associated instrumentation.

In order to monitor the overall operation of the DHRS, flow meters suitable for the slower, natural circulation flow in the secondary coolant loops are employed along with RTDs to monitor the temperature and flow rate of the coolant entering and leaving the pressure vessel, from which the power removed may be readily calculated. The terminal heat exchanger, utilizing air as the ultimate heat sink, is monitored similarly.

Verifying the operation of the internal components is not straightforward. Measuring inside the RPV is restricted by space limitations and harsh operating environment. The parameters of importance for the primary coolant are its temperature and flow rate at the intake and outlet of primary loop. The lower plenum contains RTDs for normal operation ‘cold leg’ monitoring that can provide exit temperature. If space permits, RTDs can be placed around the outside of the core barrel, proximal to the ‘hot’ inlet, to monitor inlet temperature. If space does not permit, core exit thermocouples (TC) contained in the in-core instrumentation assemblies may be sufficient for post-accident monitoring.

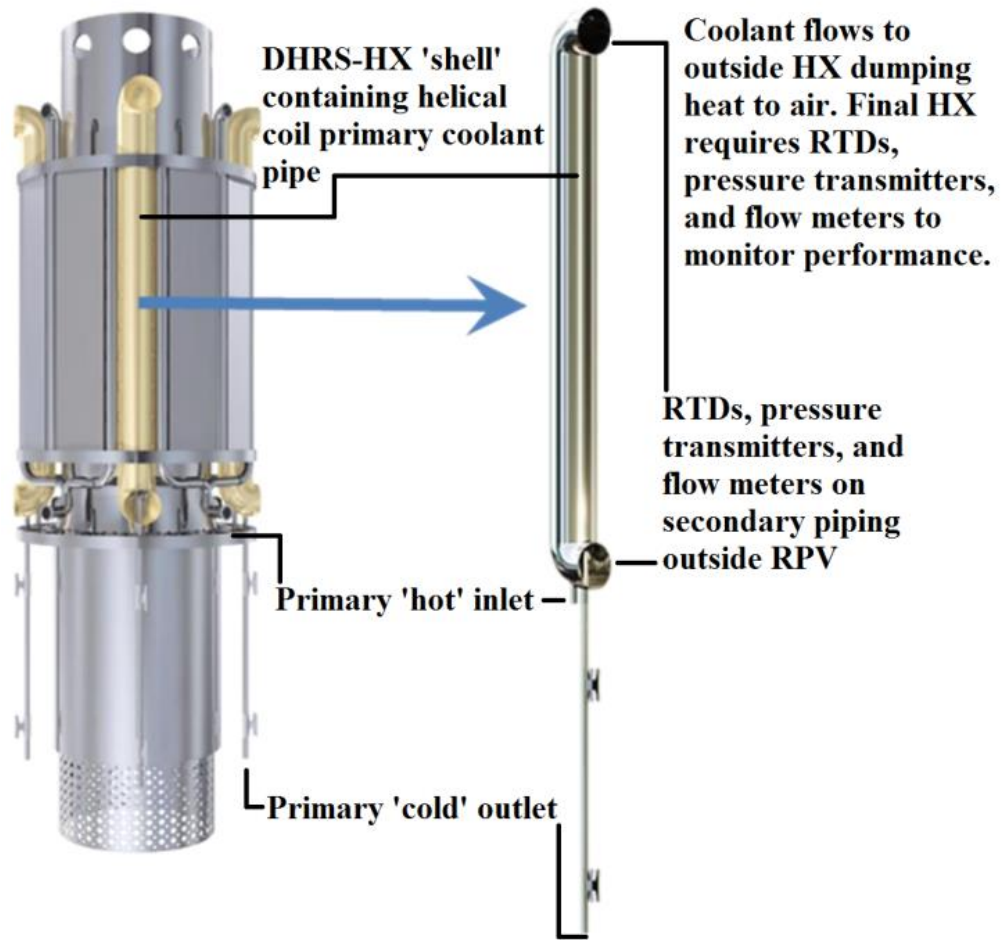


Figure 2-9. DHRS heat exchanger and associated instrumentation (Figure from [Memcott, et al, 2014], annotation by author).

It may be possible to include a flow meter on the primary coolant ‘cold’ pipe of the DHRS-HX if space permits and a suitable instrument is available. If primary flow cannot be measured directly, it has to be inferred from the coolant temperatures and the power removed from the secondary side. However, that approach assumes the system is otherwise the same as at the time of calibration.

The primary coolant could fail to flow through the tube side of the heat exchanger for a number of reasons. The primary coolant level could drop below the hot inlet, near the elevation of the top of the core, though the entire safety system is designed to prevent core uncover. Only a beyond design basis accident could result in such circumstances. It may also be possible for the tube to become sufficiently fouled under some accident condition to resist natural circulation.

If correct power is being extracted by the secondary coolant, then the primary coolant is necessarily flowing, so it is not critical to measure it directly. If correct power is not being extracted from the primary coolant and dumped through the air sink, the information from the instruments may help identify the cause.

If coolant level were to fall and approach the DHRS-HX intake, it would be detected by the primary coolant inventory monitoring system, discussed later. If fouling is the issue then the flow rate through a particular exchanger would be necessarily slowed, reflected in less power extraction measured on the secondary side of that particular unit. If there is some issue with the terminal heat exchanger, which dumps the decay heat to air, the instrumentation which brackets that equipment would show a decrease in power extracted from the secondary coolant by the terminal heat sink.

2.3.4 CRDM/RCCA Instrumentation

The CRDMs in the I²S-LWR are located in the primary coolant riser section. Enclosing the control rods and CRDMs inside the pressure vessel eliminates the possibility of a full rod ejection event. However, the position of every control rod must be monitored. The CRDMs include rod position indicator equipment inside each CRDM, bundling the power, control, and instrument cabling together for each CRDM. The diameter of each cable is approximately 0.8 inch (20.32 mm) [Ferroni, Private Communication 2015].

2.3.5 Primary Coolant Inventory Monitoring

Two techniques are proposed for primary coolant inventory monitoring to ensure core submersion in post-accident scenarios. They are thermal probe level sensors (TPLS) and the torsional ultrasonic wave-based in-vessel level measurement system. Differential pressure

transmitters are not applicable to RPV coolant level monitoring in the I²S-LWR because they would require pressure tap penetrations in the pressure vessel in the lower portion of the pressure vessel, violating a design constraint of the I²S-LWR concept.

TPLS monitor the presence of water or vapor at their location based upon the difference in thermal conductivity of liquid versus gaseous water. The sensitivity of such an implementation depends on how close together the sensors are placed. For example, if they are one foot apart, then the coolant level in the reactor would be known to be at least the level of the highest submerged sensor, but less than one foot above that sensor.

The torsional ultrasonic wave-based in-vessel level measurement system is a system designed at Oak Ridge National Laboratory [ORNL, 2005] specifically for monitoring coolant level in integral LWRs. The system estimates the regional density throughout the RPV to determine the elevation of the surface of the coolant [Wood, et al, 2003]. Either of these is a suitable approach to post-accident primary coolant inventory monitoring in the I²S-LWR.

2.3.6 Primary Coolant Temperature Instrumentation

The primary coolant ‘hot leg’ and ‘cold leg’ temperatures must be measured accurately and with rapid response time. These values are critical for reactor protection and control. RTDs are the instrument of choice, but access and placement are challenges. The ‘hot leg’ measurements may be made with RTDs inserted into thermowells that are supported by vessel internal structure. The lower plenum temperature (‘cold leg’) is measured using submersible RTDs. A suitable submersible RTD assembly is not commercially available, but conceptually, encasing an RTD in its own small ‘pressure vessel’ should be feasible. Placement and number of sensors within the available space should be addressed to ensure an accurate average coolant temperature measurement. Temperature stratification of the coolant in the plenum volumes will have to be investigated to aid in sensor placement. The hot and cold leg RTDs should have a calibration span of 70 °C surrounding the nominal values of the respective coolants at full power. Typical nuclear grade RTD accuracy is around 0.18 °C, with response times less than seven seconds [Ultra Electronics, 2014]. The accuracy and response time of these temperature sensors satisfy the coolant temperature monitoring requirements of the I²S-LWR. RTD response times are very slow in comparison to pressure transmitters, due to the fact that heat must transfer from the process, through the thermowell material, detector sheath, then to the actual transmitter before a change in temperature can be detected. In a pressure sensing line the pressure travels at the speed of sound

in the medium to a diaphragm or cantilever based pressure transmitter which detects the change in pressure very quickly via its mechanics of operation. The rapid response times of pressure transmitters provides rapid detection of a partial or total loss of flow accident (LOFA). This means that any indirect measure of primary coolant flow based upon temperature measurements is too slow to base the reactor safety systems on.

2.3.7 Primary Coolant Flow Measurement

The flow rate of primary coolant in a typical PWR is monitored by the change in pressure of the coolant across the U-tube steam generator. The low flow reactor trip is activated when the magnitude of the pressure drop falls below the set point. However, this is not an extremely accurate method of primary coolant flow measurement. It is extremely fast, which is most important in responding to LOFA. Improved measurement of the primary coolant flow rate lends itself to improved safety and performance. Further, the absence of a typical steam generator makes this traditional approach unavailable to the I²S-LWR system.

Pursuant to this end, several potential techniques for measuring the primary coolant flow rate are presented as candidates for use in the I²S-LWR. This includes the use of existing process instrumentation placed primarily for other purposes for flow rate estimation. First, ultrasonic flow measurement is discussed.

2.3.7.1 Ultrasonic Flow Meters

Ultrasonic flow meters operate by emitting ultrasonic pulses between two sets of transceivers. An ultrasonic transceiver is both a transmitter and a receiver of ultrasonic pulses. One transceiver sends pulses against the flow while the other sends pulses in the direction of the flow. The flow velocity is then determined by measuring the difference between the times of flight of the two pulses. Ultrasonic flow meters provide advantages over other direct measurement techniques. These include:

- No pipe penetrations
- No obstruction in coolant flow
- Multiple sensors can be applied to develop a liquid flow profile in the vessel
- These devices can maintain accuracy despite fouling of coolant conduit
- Capable of measuring flow rate of non-fully developed flows

Applying ultrasonic flow meters to measure primary coolant flow rate can offer many advantages over other measurement techniques. Given that there is a limited distance past the

micro-channel heat exchangers there may not be enough length to create a fully developed flow. Transit time ultrasonic flow meters can be very useful for this application because they do not require a fully developed flow. Another advantage is that the velocity profile of the primary flow channel can be determined by using multiple sets of transceivers around the exterior of the pressure vessel. Additionally, if these are installed in a “clamp-on” fashion, by which the meter is external to the fluid conduit, sending ultrasonic pulses through the conduit and the working fluid, no penetrations to the reactor vessel will be needed to accommodate these meters. They also present no obstructions to the primary coolant flow path within the conduit [Papadakis, 1999].

In the proposed application, the objective is to configure ultrasonic flow meters vertically along the reactor vessel wall, directed toward the central axis of the core. In this arrangement, the transceivers generate pulses that penetrate the vessel wall, cross the flow, reflect off the core barrel, and return to another corresponding transceiver. This is a common configuration for ultrasonic flow meters that is referred to as reflection mode. This allows for the primary flow measurements to be performed in the region below the heat exchangers, in between the lower sections of the passive decay heat removal system. Placing these meters in this location also serves to monitor core coverage by primary coolant in case of a loss of coolant accident.

The transit time of an acoustic wave is dependent upon the density of the medium it travels through. Consequently, if the core coolant level drops below the level of the highest ultrasonic pulse generator, the ultrasonic wave will pass through some region of the lower plenum occupied by lower density gas, thus significantly lengthening the transit time. This would alert personnel, responding to an accident, of the core uncover condition. Furthermore, it should be possible to correlate the ultrasonic instrument response to the height of the liquid level in the region of monitoring, providing accurate liquid primary coolant inventory within that section of the down-comer. Figure 2-10 shows a conceptual design of the placement of ultrasonic instrumentation in the down-comer region of the I²S-LWR. Ultrasonic pulses are directed toward the core barrel both in the direction of the flow, and counter to the flow. Correlation of the received signals allows for calculation of the difference in transit time of the two pulses, which corresponds to the coolant transit time between the two transceivers. The known distance between the transceivers then yields the coolant velocity. Figure 2-10 shows the orientation of the transceivers to the core, as mounted on the outside of the reactor vessel. The figure is not to scale.

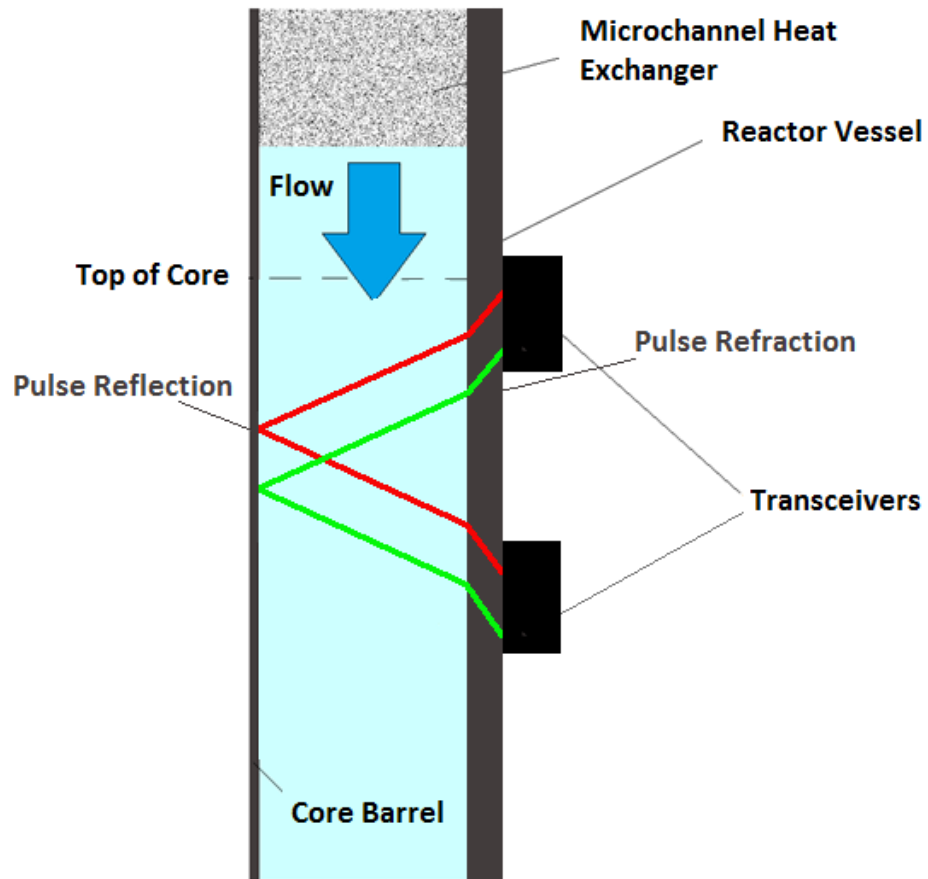


Figure 2-10. Side profile of conceptual application of ultrasonic flow meter in the down-comer of P^2S -LWR for measurement of non-fully developed flow rate of primary coolant. The red and green paths indicate pulses going against and with the flow, respectively [Upadhyaya, et al, NET 2015].

2.3.7.2 Measurement Principle and Pulse Energy Attenuation

As stated previously, ultrasonic flow meters measure flow rate by evaluating the difference in transit times between an upstream and downstream pulse pathway. The total transit time for each pulse can be calculated with the following equations [Papadakis, 1999].

$$t_{down} = \frac{L}{c + V_{flow} \sin(\varphi)} + t_p \quad \text{Eq. (2)}$$

$$t_{up} = \frac{L}{c - V_{flow} \sin(\varphi)} + t_p \quad \text{Eq. (3)}$$

$$\Delta t = t_{up} - t_{down} \quad \text{Eq. (4)}$$

$$V_{flow} = \frac{L \cdot \Delta t}{2 \sin(\varphi) \cdot t_{down} \cdot t_{up}} \quad \text{Eq. (5)}$$

t_{down} = Transit time of downstream pulse (in direction of flow)

t_{up} = Transit time of upstream pulse (opposite direction of flow)

t_p = Transit time of pulse through reactor vessel wall

Δt = Change in transit time between the upstream and downstream pulses

L = Ultrasonic pulse path length in the coolant

V_{flow} = Velocity of coolant flow

φ = Refracted pulse angle (of axis perpendicular to the flow direction)

The estimate of the flow velocity is dependent only on the path length and transit times. The flow velocity measurement is independent of fluid properties such as pressure, temperature, Reynolds number, etc. Due to a small number of parameters affecting flow measurement, these devices require minimum calibration after the initial installation.

One of the important issues in the use of this type of ultrasonic device is the attenuation of pulse strength as it traverses the various media. As the signal changes from one medium to another, part of the pulse is reflected while the remaining part is transmitted forward. This decreases the strength of the signal at each medium of transition. The ultrasonic transmitters can be placed around the RPV, thus allowing the estimation of an average reactor coolant flow rate.

Ultrasonic flow measurement at high temperatures is challenging due to the restricted temperature tolerances of normal acoustic couplants. Acoustic couplant is a material that allows

for an ultrasonic pulse to travel from the transceiver to the conduit wall with little to no losses by matching the impedance of the steel with the impedance of the coupling material. Without the coupling the ultrasonic pulse would be greatly dampened by the impedance mismatch between the steel conduit wall and air. There are now applications of high temperature couplants that have high temperature tolerance, can match the acoustic impedance of steel, and provide thermal shielding between the ultrasonic transducer and high temperature conduits. An example outside the nuclear industry, which is of relevance to the potential application of this technology in the I²S-LWR concept, is the wave injector from FLEXIM [Flexim, 2013]. These ultrasonic meters are augmented with thermal shielding and acoustic coupling between the instrument housing and the surface of the working fluid conduit that allow them to measure very high temperature flows, up to 600 °C, while maintaining normal operating temperatures in the instrument. Proper calibration accommodates for the transit time effect of the thermal insulating material on the ultrasonic wave. This indicates that these devices are able to handle the peak temperatures of the primary coolant, approximately 330 °C.

Over the past few years, several nuclear utilities have begun using ultrasonic flow meters to measure feed water flow rates. In some cases, Venturi meters have been replaced by ultrasonic flow meters in order to help recover lost megawatts caused by errors in venturi flow measurements. A report by Caldon, a trademark of Cameron International, details the history of their ultrasonic flow measurement technology, called LEFM, from its development by Westinghouse in the 1960s, through widespread application in the commercial nuclear power industry, beginning with the use for measuring reactor coolant system flow in Prairie Island Unit 2 in 1974 [Caldon, 2006]. Ultrasonic measurement techniques were also applied for RCS temperature and flow measurements at Ginna and Watts Bar nuclear plants, as well as achieving a 1% power uprate at Comanche Peak nuclear plant [Shankar, 2001].

2.3.7.3 Alternative Approaches to Primary Flow Monitoring

A few alternate methods of evaluating coolant velocity are possible with fast sampling rates of instrumentation that is already in the reactor system. Coolant passing through the core flows sequentially past neutron flux monitors and core exit thermocouples.

Cross-correlation algorithms can be employed to detect the same pattern in the signals of different detectors. The time delay between the signals of sequential detectors relates to the velocity of the coolant by the distance between the detectors [Upadhyaya, et al, 1980]. Another

method of inferring the primary flow rate is to balance the energy extracted by each heat exchanger with the change in temperature across the primary side of the same heat exchanger. These are related to the primary flow rate through the heat exchanger according to the following equation:

$$\eta(\dot{m}_P c_{pP} \Delta T_P) = \dot{m}_S c_{pS} \Delta T_S \quad \text{Eq. (6)}$$

In the equation, " \dot{m} " is coolant mass flow rate, c_p is the heat capacity (at constant pressure) of the working fluid, and ΔT is the change in temperature of the working fluid due to heat transfer in the heat exchanger. The overall efficiency of the heat exchanger is specified by η . The upper-case subscripts S and P denote secondary and primary working fluids. Since the working fluid experiences a pressure drop across the exchanger, this simplified relationship is not exact. However, this discrepancy can be accounted for with experimentation and data based model generation, treating η as a correction factor rather than a strict efficiency of heat transfer.

Reactor coolant pumps are typically powered by three-phase induction motors. Motor power exhibits a direct relationship to pump flow rate, though not necessarily a linear relationship [Upadhyaya, et al., 2014]. Motor power can be measured continuously based upon the current and voltage drawn by the motor. The same data is also used for monitoring the operational integrity of the reactor coolant pumps for signs of wear or malfunction. Early detection of RCP degradation allows for maintenance or replacement during scheduled outage time as opposed to a sudden pump failure requiring an unscheduled outage.

It may be possible to measure pressure of the primary coolant before and after it passes through the primary heat exchangers. If this proves feasible, the pressure drop across the heat exchangers can be correlated to flow rate. This is the same measurement used for primary coolant flow rate based trips in operating PWRs. Improvements over this technique benefit the system performance and safety by providing more precise evaluation of the flow rate, which improves the capability of monitoring and diagnostic algorithms to detect and isolate anomalous conditions more rapidly.

Ultimately, the uncertainty of each of these methods must be characterized so that a combined uncertainty of the aggregate of all of these methods may be established. The response time of the methods is difficult to characterize. Calorimetric methods are inherently too slow because they rely on temperature sensors with multi-second response times. Pump motor power monitoring

should, in theory, have a very fast response time to measure the actual change in power, but the sensitivity of this technique, along with how quickly a change in flow is reflected in the power level, have not been characterized. The response time of cross-correlation methods has also not been well characterized for non-bubbly flows. The determination of the response time actually required of primary coolant flow instrumentation to maintain the plant within safety margins is a subject for future research.

2.3.8 Cable Routing

When determining how to get instrumentation signals out of the reactor, several factors come into consideration. The first considerations are those to design constraints and operational realities. The I²S-LWR cannot have penetrations in the RPV at any elevation lower than four feet (1.22m) above the top of the reactor core. The instrumentation placement and cable routing must be compatible with removing the vessel head, containing the pressurizer, as well as all internals above the core. This is due to the riser tapering inward above the core to provide additional space in the downcomer for the primary heat exchangers and DHRS. Refueling requires the removal of all systems above the core in order to reach fuel assemblies at the outside diameter of the core. Additional considerations include reducing the number and size of instrumentation cabling penetrations, consistent with ensuring no large LOCA possibility and minimizing the total number of LOCA initiating event locations associated with instrumentation cabling. Also of significance is the length of the cable runs. The longer the run, the more noise that is introduced into the signal, making the measurements obtained less useful.

Taking all of this into consideration, the initial strategy was to rout all in-vessel instrumentation cables out through the top of the RPV, passing through the pressurizer. This approach was determined to not be viable by collaborators, as the volume required would compromise the performance of the pressurizer, located in the upper hemisphere of the RPV. The revised approach to cable routing is presented in Figure 2-11.

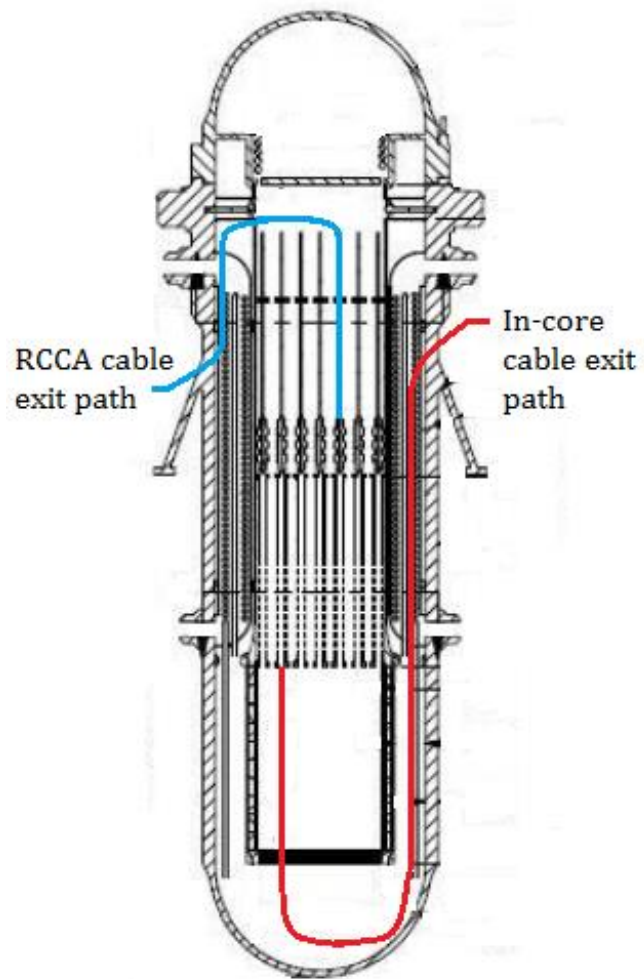


Figure 2-11: Proposed cable routing for in-core detectors and rod control cluster assemblies.

The power, control, and rod position indicator (RPI) cables for each RCCA are contained within a single cable with a diameter of 0.8 in (20.32 mm). The in-core detector cables have a diameter of 0.367 in (9.32 mm). The minimum radius of curvature for these cables is approximately 5 in (127 mm) [Ferroni, private communication, 2015].

RCCA cables will be routed vertically from each RCCA, parallel to the control rods, to the top of the riser, where they will bend outward into the downcomer, meeting with the interior wall of the RPV. Then they will travel down to exit at either the flange connecting the upper and lower halves of the RPV, or a more suitable elevation if the flange region is overly crowded. There are 45 such cables. These cables will have to be disconnected from the RCCAs during refueling outages to allow for the removal of the control rods, support structure, and RCCAs. They can either be withdrawn from the vessel or set into racks attached to or hung from the upper flange until it is time to reattach them to their respective RCCAs. This will have to be done systematically to avoid connection errors.

It is proposed that the in-core detector cables will be routed out the bottom of each assembly in which they are placed, through guide tubes which arc through the lower plenum toward the wall of the RPV, then track up the vessel until they exit at the same flange or alternative location as the RCCA cables. During refueling, the cables can be withdrawn out the guide tubes until the detector arrays are fully removed from the fuel assemblies, but only just so. Once refueling or other service is complete, the in-core detectors will be inserted back into the core in the same locations. This approach necessitates long cable runs for the in-core detector assemblies, raising concerns of cable aging, radiation damage, and unacceptable signal to noise ratios. These concerns need to be addressed in the next phase of research and development.

2.4 Secondary Side Instrumentation

The secondary coolant loop includes eight microchannel heat exchangers (MCHX) inside the RPV, with the following components outside the RPV: four steam flashing drums, four secondary coolant pumps, and the piping between components as well as that for feedwater delivery and steam removal. The balance of plant (BOP) portion of the secondary coolant loop should not be significantly different from a typical PWR, so it is not addressed. The secondary side instrumentation is shown in Figure 2-12. The secondary loop piping has instrumentation similar to the primary loop of a typical PWR.

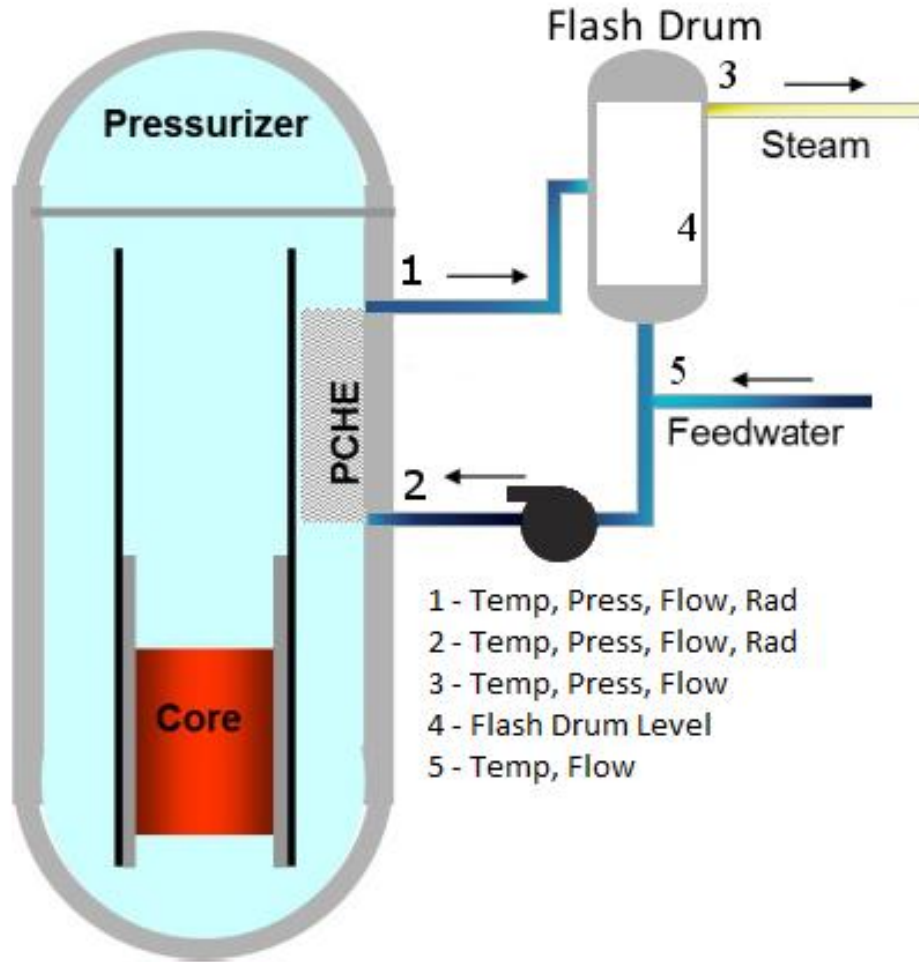


Figure 2-12. Instrumentation for the secondary coolant loop and steam flashing drum of I²S-LWR [Upadhyaya, et al, 2015].

For measuring secondary coolant temperature, each loop consists of four resistance temperature detectors (RTD) on both the hot and cold legs of the secondary circuit.

Three RTDs on each leg will be distributed evenly about the circumference of the pipe, in thermowells at 120 degrees apart.

Distribution of the RTDs in this fashion provides an accurate temperature measurement from the average of the signals, despite stratification of the different layers of the pipe flow due to temperature differences. These sensors are narrow range RTDs. The fourth RTD on each leg is a wide range RTD suitable for coolant temperature monitoring during startup and shutdown. The accuracy and sensitivity of the averaged narrow range RTDs are only necessary when the system is at power. Normal power operation is when small changes in the temperature are important for detecting changes in reactor power as measured by the power removed by the secondary coolant.

Differential pressure transmitters and orifice/venturi meters are used for measuring pressure and flow rate of the secondary coolant before and after it passes through the heat exchangers. If more precise measurement of flow rate is necessary, ultrasonic flow meters would be used. These are discussed more in Section 2.3.7.1. Radiation detectors will also be on the secondary coolant piping to monitor the integrity of the isolation of the primary coolant.

Steam pressure measurement uses pressure transmitters. Steam temperature is measured with three or four RTDs. Steam flow rate is measured using an orifice plate or a vortex meter. Multivariable vortex flow meters are capable of measuring pressure, volumetric flow rate, and temperature. They then calculate the mass flow rate. It is advantageous to use such an instrument because it reduces the number of cables which must be routed out of the containment to the instrumentation cabinets in the control building. If the flow, temperature, and pressure measurements are taken separately and the mass flow rate calculated by the plant computer, then each instrument requires its own signal lines. If a single instrument is used that measures multiple parameters of the process, performs a calculation, then sends this data to the plant computer, cabling capital and maintenance costs can be reduced.

The flashing drum coolant level would also be monitored by differential pressure measurement. This is important because drum coolant level is a controlled parameter. Much the way the level of a U-tube steam generator is maintained to a set point, so is the water level in the flashing drum. This is done with four differential pressure transmitters located in the lower region

of the drum. The drum level is controlled by adjusting the feedwater flow rate using a throttling valve.

Feedwater temperature is maintained at a set point by the feedwater heaters, so it too must be measured. The measurement does not require four RTDs because the accuracy is not as important as in the power related temperature measurements. Three RTDs, two narrow range and one wide range, are adequate for each feedwater line. If the calibration or functionality of one of the narrow range RTDs is compromised, the other may be used exclusively until the next scheduled outage, or replaced in service. RTDs have very good records of maintaining calibration as long as they are not adversely affected by maintenance operations (such as being jostled by a worker, moving the assembly slightly out of position within its thermowell, increasing response time significantly and altering calibration). The flow rate of the feedwater must be measured as well. This is necessary for drum level control as well as for reactor operation. Traditionally, venturi tubes have been used for this application, though they are known to become fouled over time, causing reductions in power. Ultrasonic flow meters have been used to replace venture meters, garnering power uprates. For an advanced plant such as the I²S-LWR, it is proposed to use ultrasonic technology from the outset.

2.5 Accident Monitoring

Instrumentation becomes even more important in a nuclear power plant if abnormal conditions arise. The instrumentation provides all the information that is available to operators and emergency response personnel in dealing with an accident scenario. Consequently, it is important to consider the information that is critical to have when responding to an accident when designing an instrumentation system and to optimize this design with accident mitigation in mind.

The International Atomic Energy Agency (IAEA) considers the terms accident monitoring, and post-accident monitoring to be equivalent. In this paper, the term accident conditions refers to conditions or states that are less frequent and more severe than normal operational occurrences. Normal operational occurrences are events which the plant is intended to experience at least once during the lifetime of the plant. Accident conditions include two classes of unexpected conditions, design basis accidents (DBA) and design extension conditions (DEC). DBAs are postulated events the plant is designed to recover from, to a safe condition, according to conservative methodologies. DECs are considered in the design of the plant according to best estimate methodology. They are

not extensions of the DBA scenarios but general extensions of states the plant may enter resulting in accident conditions. In some cases, the effects of DEC are limited by the described scenarios of one or more DBAs. In other cases, DEC results in significant fuel damage. This subset of DEC is referred to as severe accidents [IAEA, 2015].

The monitoring of an accident is performed with both installed, permanent instruments used for normal operation, installed, permanent instruments not normally in service, and portable instruments and equipment that are incorporated into an accident response plan. This section discusses the instrumentation used for normal operation and how it is applicable to accident monitoring.

There are several ways in which the proposed instrumentation systems support accident monitoring. The primary system instrumentation is designed to provide the necessary information to operators to respond quickly and appropriately to any accident which leaves the instrumentation systems operational. The primary coolant inventory monitoring approach provides continuous monitoring of the inventory of primary coolant in the event of a LOCA. This information, coupled with core power monitoring by core-exit TCs and the DHRS instrumentation, which verifies the energy extracted from the primary coolant during DHRS operation, yields a complete picture of decay heat removal process. These instruments also aid in isolating any malfunctions which may occur in the DHRS systems.

Appropriate response to an accident scenario is predicated largely on knowledge of the malfunction or failure which leads to the accident condition. If a reactor is losing primary coolant and no one knows why, the response is limited to indefinite replacement of the coolant. When prepared, ultra-pure makeup water runs out and must be replaced with water from a general purpose supply, such as the nearest potable water supply, the rates of reaction for corrosion processes will increase as the water chemistry of the reactor is unbalanced by the uncontrolled ion content of the replacement coolant. This increases the probability of fuel failure, as well as providing the potential to exacerbate the original leak or cause new leaks to initiate. Consequently, it is desirable to be able to isolate the source of equipment failure resulting in the accident such that the failure may be mitigated to bring the reactor system to a stabilized, safe condition. One of the principal benefits of the ultrasonic level monitoring system developed at ORNL is that if a penetration in the RPV is spraying primary coolant out of it, it should be spatially isolatable from the instrumentation as a difference in density as compared to both the pressure vessel wall and the

air and insulation surrounding the pressure vessel. If a leak can be found, it can potentially be stopped.

The integrity of the fuel is another important factor for accident monitoring [IAEA, 2015]. If the integrity of the fuel can be maintained, large release of radionuclides can be prevented. Hydrogen monitors in the pressurizer can provide indication of fuel integrity based upon the presence of hydrogen gas, a corrosion product. If nucleate boiling or significant hydrogen gas bubble production is occurring in the core, it may be detected by cross-correlation of the signals from in-core flux monitors and core-exit TCs. This cross correlation algorithm will already be running on the appropriate signals for core flow mapping, so gas detection becomes a matter of implementing an appropriate monitoring algorithm to look at the cross-correlation data for patterns indicative of gas bubble formation.

3 DYNAMIC MODELING OF THE I²S-LWR PRIMARY AND SECONDARY SYSTEMS

When determining how to approach a dynamic modeling problem, it is useful to consider the objectives of the modeling effort and the resources available to complete the modeling effort. Resources include both human effort and computational effort. A more detailed model can generally provide more insight into the system which is modeled, but also requires more human resources to realize and more computational resources to evaluate. With a given amount of human and computational resources, a compromise must be established between the scope of the modeling and the detail of the modeling. For this project, the minimum scope of the modeling work is established by the objectives: to evaluate strategies for monitoring and controlling the I²S-LWR. This means that all the systems of the plant, for which existing monitoring and control approaches are not demonstrated, must be included in the modeling work. For the I²S-LWR, these systems are the primary coolant loop components and the secondary coolant loop components, excluding the balance-of-plant systems. The BOP systems are all systems in the secondary coolant flow path from where the steam exits the flashing drum until the reheated feedwater joins the drum recirculating coolant to enter the primary heat exchangers. The BOP systems are excluded from the modeling scope because there are no significant differences in the BOP systems for the I²S-LWR compared to other LWRs. Therefore there are no monitoring or control considerations to be evaluated for those systems at this stage of research and development. If deployed for co-generation applications, the additional systems associated with that functionality will need to be evaluated, and any feedback from those systems incorporated into the analysis for this system.

The level of detail required is also informed by the objectives. If the objectives include a detailed design of a control system, then the model must have sufficient detail to simulate with high fidelity the spatial and temporal evolution of matter and energy for every postulated physical scenario in the design basis of the system, as well as the instrumentation which monitors the processes in the system, the controllers which interpret data from the instruments to determine the control action to be taken, and the actuators which execute the control action. At this stage of the development process, the control objective is limited to evaluating the approaches to controlling the systems mentioned above. In practice, what this requires is a model with sufficient detail to demonstrate the feedback mechanisms present in the systems, as well as evaluate the ranges of

operational states of the systems, so that these bounding conditions can inform upon the best approaches to controlling the plant. The monitoring and diagnostic objectives require the model to simulate slow changes in the operating conditions of selected process equipment and instrumentation.

These objectives can be accomplished with low fidelity models. While high fidelity models are more useful, as they can be applied to the objectives of this research as well as objectives of future research on the same systems, efficiency is more important to this work than utility due to the wide scope and limited resources. The limitations and impacts of using low fidelity models in this research are discussed for each system in the section discussing the modeling of that system.

The assumptions used in each system model are discussed with that system, but it is useful to keep in mind some deviations from reality that are consistently assumed in all of the models. The first is the reduction of the modeling space to a single dimension. All movement of mass and energy is modeled in the single dominant dimension of transport, within each system model. All material within a given discretely modeled block of that material is assumed to be well mixed at all times, and uniform in intrinsic properties of pressure, temperature, density, and heat capacity. The I²S-LWR is not designed to boil primary or secondary coolant, and so it is assumed that boiling does not occur anywhere in the system. Losses in coolant pressure and energy due to friction between fluid and conduit, as well as increases in pressure and energy due to pumping power, are neglected. Each system is assumed to be well sealed and insulated, exchanging no material or energy with the external environments. No instrument hardware, controller hardware, actuator hardware, safety equipment, or anything other components not explicitly described are modeled.

These assumptions affect the outcomes of the modeling in several ways. The lack of modeled I&C hardware causes controller feedback to begin nearly instantaneously after a deviation in a controlled parameter is simulated. This is obviously unrealistic, and a principal reason why the model can only address plausibility of control strategies, rather than inform the design of real controllers, in terms of the design parameters of those controllers. Another consequence is the artificial widening of the temporal evolution of information from one point to another. This is true of all lumped parameter nodal models to some degree or another. The greater the number of nodes used to represent a particular space, the more accurately the time evolution of a change in an intrinsic property can be simulated. The amount of deviation from reality when simulating the time it takes for a transient to propagate through a system depends upon the rate at which the change

occurs in the node in which the change is introduced to the system, the rate at which the change propagates in the real system, and the simulation time step.

Consider a step increase in the temperature of the water entering a pipe of a given length, flowing at a constant velocity. This change enters the pipe as a narrow delineation between hotter water and colder water. That is what defines a step change. As it travels down the pipe, the dividing line broadens due to random, Brownian motion of molecules, or groups of molecules, of water. If the resident time of the water is fast compared to the rate of broadening, the line between hotter and colder water will maintain its shape when it reaches the end of the pipe, resembling a step change. The time it takes for the information that a step increase in temperature has entered the pipe is the same as the time that it takes for the water to flow from one end of the pipe to the other. In a nodal model of the pipe, the step change is reflected as an increase in the temperature of all of the water in the first node. In the first time step after the step change occurs, a certain amount of water from the first node is moved into the second node, according to the flow rate of the water. Because the nodes are well mixed, the temperature of the water in the second node is calculated by distributing the energy added to the second node by the hotter water from the first node throughout the entire mass of the second node. Depending on the length of the time step, the actual front of the hotter water may still be in the first node. So in the real system, after one time step, the line between the hot and cold water is in the region represented by the first node, and the water in the region represented by the second node is still at the original temperature before the introduction of the step increase. However, in the modeled system, the second node has already increased in temperature. After as many time steps as there are nodes in the pipe model, the downstream end node in the pipe model shows an increase in temperature, while the real front of hotter water lags behind. Further, this forward diluting of the energy of the hot water front into the nodes causes the time it takes for the modeled temperature in each node to reach the final temperature of the step increase to lag behind the real front of hot water. So the information front is broadened in the modeled pipe as compared to the real pipe. This causes the simulated movement of information about changing conditions to move artificially quickly from one system of the plant model to another.

This reduces the effective magnitude of transients as well as artificially speeding up feedback processes between systems. It also contributes to artificially speeding up controller responses. It may seem that a simple solution is to set the time step such that it matches the resident time of a

given node. In such a scenario, in the first time step after the step change, all of the coolant in the second node would be replaced with coolant from the first node, while the temperature front would have advanced to the dividing line between the first and second node. In this fashion, the simulation front would arrive one time step ahead of the real front, and arrive all at the same time, just like a step increase. For a simple system with one process happening, this approach works. When modeling a nuclear power plant, there are many processes occurring simultaneously and at different rates, and with different energetic and material resident times. Further, for computational efficiency when working with a large model, variable time step solvers are used to allow the computational software the ability to shorten the time step when rapid changes are occurring, so that it can more accurately simulate them, and lengthen the time step when the system is at steady state, saving data storage space and computation time. In order to accurately model a rapid change, a model needs both a short time step and many nodes, so that the resident time of the fast process in the node is close to the time step. Since it is not important to achieve high fidelity in the modeling work presented here, few nodes are used. However, similarly designed models have been used before for the same types of applications to which these models are utilized [Upadhyaya, 2011a; Upadhyaya, 2011b].

3.1 Reactor Core Model

3.1.1 Modeling Approach

The standard approach to dynamic modeling employed in this work is to separate the material in the process being modeled into spatial nodes. Ordinary differential equations (ODEs) are used to describe the changes in mass and energy, over time, in each spatial node of the process being modeled. They are solved for the change in temperature of the material: fuel, tubing, coolant, etc. This is illustrated in Figure 3-1 for the nodal modeling of heat transfer from the nuclear fuel to primary coolant. This shows one fuel node representing all of the fuel in the core, and two coolant nodes representing all of the coolant in the core. It is necessary for this approach to use two coolant nodes for every fuel node. The ODEs representing the time rate of change of the fractional reactor core power, delayed neutron precursor concentration, fuel temperature, and coolant temperatures, are given after Figure 3-1. The output of the core model is the primary coolant hot leg temperature, which is passed into the heat exchanger model.

Nuclear fission is modeled by point reactor kinetics, where the change in reactor power is determined by the change in neutron population, as reflected in prompt neutron generation and delayed neutron precursor concentrations. It also incorporates feedback effects from changes to the fuel and coolant temperature. Most of the energy from nuclear fission is deposited in the fuel. A small fraction, generally around three percent, is deposited directly into the coolant via gamma radiation. The energy deposited in the fuel is distributed evenly throughout the mass of fuel, just as energy drawn by conduction from the fuel to the coolant is withdrawn evenly from the fuel. The driving force for heat transfer from fuel to coolant is the same for each coolant node. It is the difference between the fuel temperature and the temperature in the first coolant node. Energy transfer between coolant nodes and out of the reactor core into the hot leg is modeled by convection. The hot leg is considered to be all of the coolant from the top of the core, through the riser, in the upper plenum and up to the entrance to the primary heat exchangers.

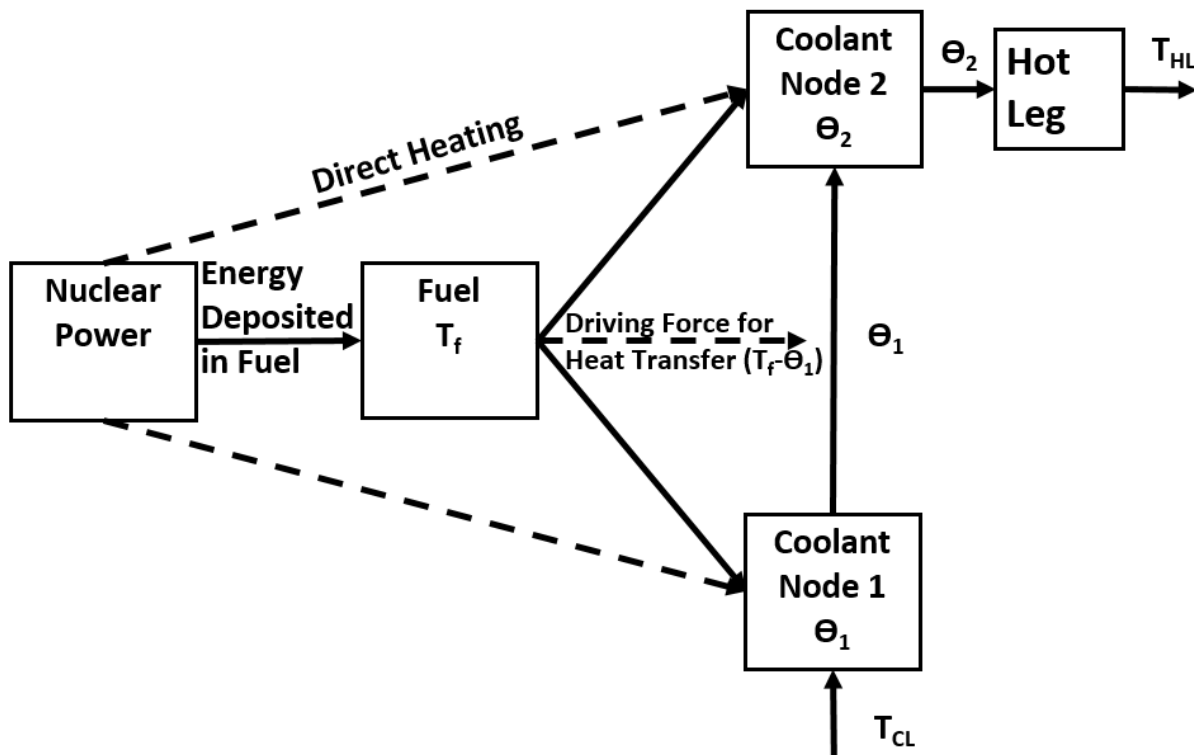


Figure 3-1. Nodalization of point kinetics and heat transfer from nuclear fuel to primary coolant in the core.

$$\frac{d}{dt} \left(\frac{P}{P_0} \right) = \frac{\rho_{tot} - \beta}{\Lambda} \left(\frac{P}{P_0} \right) + \sum_{i=1}^6 \lambda_i C_i \quad \text{Eq. (7)}$$

$$\frac{d}{dt} C_i = \frac{\beta_i}{\Lambda} \left(\frac{P}{P_0} \right) - \lambda_i C_i \quad \text{Eq. (8)}$$

$$\frac{d}{dt} (T_f) = \frac{f P_0}{m_f C_{pf}} \frac{P}{P_0} - \frac{U_{fc} A_{fc}}{m_f C_{pf}} (T_f - \theta_1) \quad \text{Eq. (9)}$$

$$\frac{d}{dt} (\theta_1) = \frac{(1-f)P_0}{2m_{c1} C_{pc}} \left(\frac{P}{P_0} \right) + \frac{U_{fc} A_{fc1}}{m_{c1} C_{pc}} (T_f - \theta_1) + \frac{\dot{m}_c}{m_{c1}} (T_{CL} - \theta_1) \quad \text{Eq. (10)}$$

$$\frac{d}{dt} (\theta_2) = \frac{(1-f)P_0}{2m_{c2} C_{pc}} \left(\frac{P}{P_0} \right) + \frac{U_{fc} A_{fc2}}{m_{c2} C_{pc}} (T_f - \theta_1) + \frac{\dot{m}_c}{m_{c2}} (\theta_1 - \theta_2) \quad \text{Eq. (11)}$$

$$\frac{d}{dt} (T_{HL}) = \frac{\dot{m}}{m} (\theta_2 - T_{HL}) \quad \text{Eq. (12)}$$

P_0 = Nominal reactor thermal power

C_i = Concentration of i^{th} group delayed neutron precursor

θ_1 = Coolant node-1 temperature

θ_2 = Coolant node-2 temperature

T_f = Fuel node temperature

T_{HL} = Hot leg coolant temperature

T_{CL} = Cold leg coolant temperature

β = Total delayed neutron fraction

λ_i = Decay constant of i^{th} group delayed neutron precursor

Λ = Mean generation time of prompt neutrons.

ρ_{tot} = Total reactivity (\$) = External reactivity + Fuel and Coolant temperature feedback

m_f = Mass of fuel

m_{c1} = Mass of coolant in node-1

m_{c2} = Mass of coolant in node-2

\dot{m}_c = Total core coolant mass flow rate

A_{fc} = Total fuel-to-coolant heat transfer area

U_{fc} = Overall fuel-to-coolant heat transfer coefficient

C_{pf} = Specific heat capacity of fuel

C_{pc} = Specific heat capacity of coolant

f = Fraction of nuclear power deposited in the fuel

3.1.2 Parameters for Reactor Core Model

The majority of the parameters to operate the model come from other design teams on the I²S-LWR project, or are design basis parameters. This is facilitated by a Plant Parameter List (PPL), which is periodically updated with the latest values that the individual research groups are working with, and a material property database compiled a collaborator from WEC. Some parameters necessary for modeling were not provided and had to be estimated based upon available data. For the core model, these parameters are:

- Upper and lower plenum volumes, or the volumes between core exit and MCHX inlet, and between MCHX exit and core inlet
- Overall fuel to coolant heat transfer coefficient.

Upper plenum volume is approximated as the volume of the riser. No volume is added for the area between the top of the riser and the heat exchanger inlet, because there are no dimensions provided to calculate volume from for this regions. However, volume is not removed for the space excluded by the RCCAs and control rods. There is no way to know which of these is larger, but together they reduce the error in the approximation. Lower plenum volume is approximated more accurately as a hemisphere plus a hollow cylinder with the dimensions of the downcomer below the heat exchanger outlet. No volume is subtracted for instrument guide tubes, flow directing vanes, core support structure, etc. It is important to note that the only way the volume affects the modeling is via the mass of coolant in the hot and cold leg nodes. This mass affects transient behavior of the model, but not steady state behavior, where the hot leg temperature matches the core exit temperature, and the cold leg temperature matches the heat exchanger outlet temperature. It is useful to recall that that this approach to modeling inaccurately treats transients regardless of the nodal masses used in the modeling. Parameters for the reactor core and primary coolant loop are given in Table 3-1.

Table 3-1. Reactor core and primary coolant loop parameters.

Parameter (units)	Value
Core thermal power (MWth)	2850
Overall Plant efficiency (%)	34
Plant electrical output (MWe)	969
Overall fuel-to-coolant heat transfer coefficient ($\text{W}\cdot\text{m}^{-2}\cdot\text{K}^{-1}$)	1,492.5
Total effective fuel-to-coolant heat transfer area (m^2)	4272
Core diameter (m)	3.08
Core (or fuel rod) active length (m)	3.658
Cladding material	Kanthal APMT
Cladding outer diameter (cm)	0.914
Cladding thickness (cm)	0.041
Pellet diameter (cm)	0.810
Coolant Volume in Upper Plenum (m^3)	71.587
Coolant Volume in Lower Plenum (m^3)	57.17
Fuel assembly lattice array	19 x 19
Number of assemblies	121
Number of fuel rods per assembly	336
Total number of fuel rods	40,656
Fuel material	U_3Si_2
Fuel Loading (kg U)	83,027
Total mass of fuel (kg U_3Si_2)	89,559
Average fuel temperature ($^{\circ}\text{C}$)	761
Average fuel specific heat capacity ($\text{J}\cdot\text{kg}^{-1}\cdot\text{K}^{-1}$)	236.345
Control rod type (material)	Ag-In-Cd
Number of control rod assemblies	121
Number of control rods per assembly	24

Table 3-1 continued.

Parameter (units) (nominal at full power)	Value
Total coolant flow rate (kg/sec)	14,723 kg/sec
Core coolant velocity (m/sec)	4.233 m/sec
Coolant pressure (MPa)	15.51
Core coolant inlet temperature (°C)	298
Core coolant outlet temperature (°C)	330.5
Average coolant specific heat capacity (kJ·kg ⁻¹ ·K ⁻¹)	5.9410
Average coolant density (kg·m ⁻³)	691.88
Total coolant volume in core (m ³)	19.6
Total mass of coolant in core (kg)	13,561
Delayed neutron importance factor	0.97
First Delayed Neutron Group Fraction	0.000200
Second Delayed Neutron Group Fraction	0.001265
Third Delayed Neutron Group Fraction	0.001152
Fourth Delayed Neutron Group Fraction	0.00248
Fifth Delayed Neutron Group Fraction	0.000927
Sixth Delayed Neutron Group Fraction	0.00023
First Group Decay Constant (1/sec)	0.0128
Second Group Decay Constant (1/sec)	0.0316
Third Group Decay Constant (1/sec)	0.1214
Fourth Group Decay Constant (1/sec)	0.3231
Fifth Group Decay Constant (1/sec)	1.4027
Sixth Group Decay Constant (1/sec)	3.8835
Moderator Temperature Coefficient of Reactivity (K ⁻¹)	-3.6e-4
Fuel Temperature Coefficient of Reactivity (K ⁻¹)	-2.97e-5
Mean Prompt Neutron Generation Time (sec)	1.0632e-5
Fraction of Total Power Deposited in Fuel	0.974

Overall fuel to coolant heat transfer coefficient is calculated as that required to transfer nominal power over the effective fuel to coolant heat transfer area, subject to a driving force of the average coolant temperature subtracted from the average fuel temperature. The mass of fuel in the core is not explicitly provided, but the mass of uranium loaded into the core is provided. The total fuel mass, into which most of the energy of fission is deposited, is calculated by determining the mass of silicon from the molecular masses of uranium and silicon, and the ratio of silicon to uranium in the fuel form. The mass of silicon added to the provided mass of uranium is the total fuel mass.

3.2 Micro-channel Heat Exchanger (MCHX) Model

3.2.1 Modeling Approach

The micro-channel heat exchanger (MCHX) model differs from other heat exchanger models in one key feature. Typically, and as seen in the core heat transfer equations, the driving force for heat transfer is the difference in temperature between two materials, such as primary coolant and tube material in a shell and tube heat exchanger model. The counter-flow and micro-channel characteristics of the heat exchanger used in this reactor concept require a different mathematical treatment of the driving force for heat transfer. This is called the log-mean temperature difference (LMTD) [Garimella, et al, 2005]. In the case of counter-flow heat exchangers, the rate of heat transfer across any given spatial node is best modeled by the differences in temperature between the hotter and colder fluids at each end of the spatial node. The difference between the coolant temperatures at one end is subtracted from the difference at the other end. This value is divided by the natural logarithm of the ratio of the two differences. This relationship is shown in the following equation for arbitrary ends A and B of a counter-flow heat exchanger, or a spatial node within.

$$LMTD = \frac{\Delta T_A - \Delta T_B}{\ln\left(\frac{\Delta T_A}{\Delta T_B}\right)} \quad \text{Eq. (13)}$$

The nodal model of the MCHX in the I²S-LWR is shown in Figure 3-2. The equations are given following the figure. The inputs to the MCHX model are the primary hot leg temperature and secondary cold leg temperature. The outputs of the model are the primary cold leg temperature and the secondary hot leg temperature. The primary cold leg returns to the core model while the secondary hot leg is passed to the steam flashing drum model, discussed in Section 3.3.

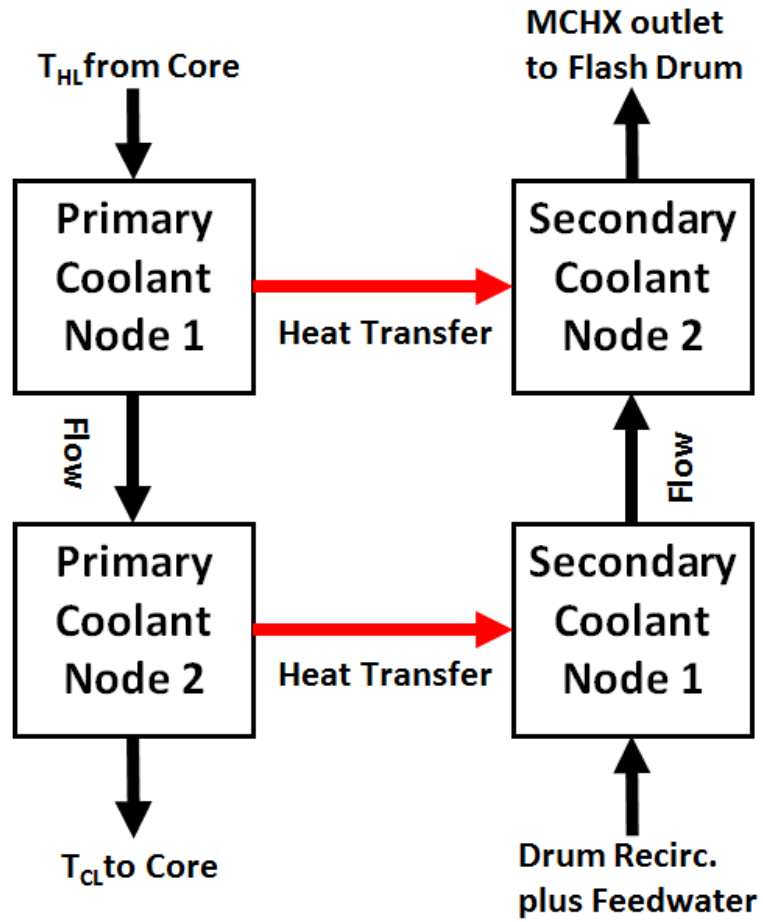


Figure 3-2. Nodal model of counter-flow micro-channel heat exchanger in I²S-LWR. Each node models half the length of the micro-channels for each coolant.

$$\frac{dT_{p1}}{dt} = -\frac{U_{ps} * A_{ps}}{M_{cp1} * C_{pcp}} * \frac{(T_{p1} - T_{s1}) - (T_{HL} - T_{s2})}{\ln\left(\frac{(T_{p1} - T_{s1})}{(T_{HL} - T_{s2})}\right)} + \frac{W_{cp}}{M_{cp1}} * (T_{HL} - T_{p1}) \quad \text{Eq. (14)}$$

$$\frac{dT_{p2}}{dt} = -\frac{U_{ps} * A_{ps}}{M_{cp2} * C_{pcp}} * \frac{(T_{p2} - T_{FW}) - (T_{p1} - T_{s1})}{\ln\left(\frac{(T_{p2} - T_{FW})}{(T_{p1} - T_{s1})}\right)} + \frac{W_{cp}}{M_{cp2}} * (T_{p1} - T_{p2}) \quad \text{Eq. (15)}$$

$$\frac{dT_{s1}}{dt} = \frac{U_{ps} * A_{ps}}{M_{cs1} * C_{pcs}} * \frac{(T_{p2} - T_{FW}) - (T_{p1} - T_{s1})}{\ln\left(\frac{(T_{p2} - T_{FW})}{(T_{p1} - T_{s1})}\right)} + \frac{W_{cs}}{M_{cs1}} * (T_{FW} - T_{s1}) \quad \text{Eq. (16)}$$

$$\frac{dT_{s2}}{dt} = \frac{U_{ps} * A_{ps}}{M_{cs2} * C_{pcs}} * \frac{(T_{p1} - T_{s1}) - (T_{HL} - T_{s2})}{\ln\left(\frac{(T_{p1} - T_{s1})}{(T_{HL} - T_{s2})}\right)} + \frac{W_{cs}}{M_{cs2}} * (T_{s1} - T_{s2}) \quad \text{Eq. (17)}$$

$T_{p1,p2,s1,s2}$ = temperature of primary and secondary nodes 1 and 2, respectively.

$T_{HL,FW}$ = temperature of primary hot leg and secondary feedwater respectively.

U_{ps} = overall heat transfer coefficient from primary to secondary coolant.

A_{ps} = area for heat transfer in each node.

$M_{cp1,p2,s1,s2}$ = mass coolant in primary and secondary nodes 1 and 2, respectively.

$C_{pcp,s}$ = isobaric heat capacity of primary and secondary coolant, respectively.

$W_{cp,cs}$ = flow rate of primary and secondary coolant, respectively.

The operational parameters of the heat exchanger model come from the research group designing the heat exchangers and performing experiments on laboratory scale versions, led by Garimella at the Georgia Institute of Technology [Kromer, et al, 2016, submitted]. A limitation of this model is that at low power conditions, the temperature of coolants in the nodes may cause ΔT_A or ΔT_B to become negative, at which point the simulation terminates because the computer cannot evaluate the logarithm of a negative number.

3.2.2 Parameters for MCHX Model

The parameters for the primary heat exchanger modeling are given in Table 3-2. Masses of coolant are determined from the appropriate volume and average density. Heat capacities and densities for primary coolant are the same as those used in the reactor core model. Heat capacity and density for secondary coolant comes from steam tables for the average pressure and temperature of secondary coolant in the heat exchanger at full power. Total primary coolant flow rate is higher in the heat exchanger than in the reactor core, due to the absence of core bypass flow contribution. Core bypass flow is used to cool the neutron reflector shield surrounding the core, a process that is not modeled in this work.

Table 3-2. Micro-channel primary heat exchanger modeling parameters.

Parameter (units)	Value
Overall primary-to-secondary heat transfer coefficient ($\text{W}\cdot\text{m}^{-2}\cdot\text{K}^{-1}$)	9,259.4
Total effective primary-to-secondary heat transfer area (m^2)	20,082
Volume coolant in primary channels (m^3)	4.8162
Volume coolant in secondary channels (m^3)	4.8162
Secondary coolant flow rate (kg/s)	13,016
Primary coolant flow rate (kg/s)	15,498
Secondary coolant inlet temperature (oC) (full power)	279.3
Secondary coolant outlet temperature (oC) (full power)	318.2
Outlet pressure of secondary coolant in MCHX (Mpa)	12.066
Average isobaric heat capacity of secondary coolant ($\text{J}\cdot\text{kg}^{-1}\cdot\text{K}^{-1}$)	5,553.4
Average density of secondary coolant ($\text{kg}\cdot\text{m}^{-3}$)	722.42

3.3 Steam Flashing Drum Model

3.3.1 Modeling Approach

In order to achieve the best possible model, a literature review of dynamic modeling of steam flashing drums was conducted to ascertain appropriate approaches to the modeling project in the Mathworks MATLAB and Simulink computation and simulation platform. Two papers [Goncalves, et al, 2007; Lima, et al, 2008] presented very similar approaches to modeling flashing drums for chemical plant applications in separating organic compounds, a common industrial application of flash vaporization. Their approach involves treating the entire drum as a single control volume for mass and energy balance, calculating thermodynamic properties rigorously via empirical equations of state, and iteratively calculating the solution to the flashing process, at each time step, using nested loops. The flashing outcome is the equilibrium between the liquid and vapor phases, and is therefore calculated as the minimization of a thermodynamic state function. The thermodynamic state function to minimize depends upon the specified conditions of the flashing process. For an isenthalpic process at specified downstream pressure and enthalpy (PH-flash), such as the I²S-LWR flashing drum, the state function to be minimized is the negative of

the system entropy [Michelsen, 1999]. For an isothermal flash problem at specified pressure and temperature (PT-flash), the minimization problem is unconstrained and can be readily solved. However, for the other specifications, including isenthalpic, the state function minimization is subject to nonlinear constraints, which removes the guarantee of convergence present in the unconstrained minimization of the PT-flash. To work around this, Michelson suggests further generalizing the problem using an objective function Q , which allows the optimization to be solved in two steps using nested loops. Instead of trying to solve the PH-flash by minimizing $-S(T, P^{spec}, v, l)$, subject to $H(T, P^{spec}, v, l) - H^{spec} = 0$, where ‘spec’ refers to specified conditions, S, H, T , and P refer to entropy, enthalpy, temperature and pressure respectively, and v and l are downstream vapor and liquid molar outputs, we define Q for the PH-flash as $Q = (G - H^{spec})/T$, where G is the Gibbs energy. Then the maximum of Q with respect to T is solved by finding the minimum of $G(P^{spec}, T, v, l)$ for each T , such that a saddle point in Q exists where Q is minimized in composition (v and l) while maximized in T . This allows the system to work in the familiar variables of temperature, pressure, and composition, while preserving the unconstrained minimization of G , as in the PT-flash. This requires that the minimization of G be performed for each temperature, in a nested loop.

Another approach for modeling the thermodynamic state properties of a dynamic system relies upon partial derivatives of the Helmholtz energy with respect to density and temperature [20]. In this representation, the reduced Helmholtz energy is represented by an ideal gas component equation and a deviation from ideality residual equation. Both are empirical models derived from fitting a function to data. The ideal portion is composed of nine terms while the residual portion is composed of 56 separate terms. The terms include polynomials, exponentials, logarithms, and constants. The independent variables in the empirical Helmholtz equations are the dimensionless, reduced density and inverse reduced temperature. Reduced values are obtained by dividing the actual value of the parameter by the critical point value of that parameter for the given substance. This formulation of the Helmholtz energy, along with all of the empirical model parameters, is given in [Thorade and Saadat, 2013]. From the combined ideal and residual empirical equations, the partial derivatives with respect to inverse reduced temperature and reduced density can be calculated. The partial derivatives are then used to calculate state variables in a thermodynamic system. While this approach does not require nested loops, it also does not specifically address the

flashing calculation. The flashing calculation would still need to be performed in a separate manner.

While these rigorous approaches to modeling the flashing process produce highly accurate results, they are ultimately unnecessary for modeling the flashing of a single component liquid as part of the NSSS of the I²S-LWR. The purpose of such detailed and complicated techniques is to accurately realize the simulation of flash vaporization of multi-component liquids. Single component liquids are quite straightforward. A simple energy balance across the throttling device of a flash vaporization system accurately predicts the mass fraction that will become vapor in the isenthalpic expansion. The difference in upstream and downstream liquid enthalpy is the amount of energy available, per unit mass, to vaporize part of the stream, and the difference in downstream liquid and vapor enthalpy, or the heat of vaporization of the substance, is the energy required, per unit mass, to vaporize a portion of the substance. Consequently, the ratio of these two values is the mass fraction vaporized [Marshall and Ruhemann, 2001]. This relationship is shown in the equation below, where X_v is the mass fraction of the inlet flow that ends up as high quality (99.9%) steam, H_i , H_l and H_v are the enthalpies of the inlet flow, drum liquid, and drum vapor respectively.

$$X_v = \frac{H_i - H_l}{H_v - H_l} \quad \text{Eq. (18)}$$

Certain assumptions are made in the modeling of the flashing drum, which are also implicit to this treatment of the flashing dynamics. The first assumption is that the rates of mass and energy exchange between the vapor and liquid volumes (during a transient, for at steady state these rates are equal and opposite, otherwise the system would not be at equilibrium) is so small compared to the rates of mass and energy transfer due to coolant entering and exiting the drum, that they can be neglected. Closely tied to this is the assumption that the drum is a well-insulated container, which exchanges no energy with the outside environment. Together, these assumptions serve a dual purpose. The first benefit is that the vapor and liquid phases can be subsequently considered as separate control volumes with independent mass and energy balance equations. However, the volumes are linked in that they are constrained to the same total volume, thus the mass balance of the liquid control volume dictates the volume available in the vapor control volume. The second advantage of these assumptions is that the flashing process can be modeled simplistically as a purely isenthalpic expansion, where all of the enthalpy of the flow entering the drum ends up in the vapor and liquid components of the drum. The energy lost by the liquid component as it decreases from inlet temperature and pressure to saturation temperature at the drum operating

pressure is conserved in overcoming the heat of vaporization of the fraction that becomes vapor, leading to the equation previously discussed. The third assumption is that isobaric heat capacities do not change over the range of operation of the drum or the secondary coolant loop, excluding the balance of plant (which is not yet modeled for this reactor). Heat capacities for various nodes are calculated for the steady state conditions of the plant at full power, and fixed thereafter. This assumption is made because the heat capacities do not change very much over the operating range of the plant and simulation. Further, the actual values of computed model outputs are not critical at this stage of research and development, for the reasons described at the beginning of this chapter.

From this we arrive at the nodal model of the flashing drum shown in Figure 3-3. Unlike the spatial models of the core and MCHX, this nodalization is based upon how the controlled variables are arrived at by the model. Differential equations are used for the inventory of liquid and vapor in the drum. Enthalpies used to calculate the flash vaporization fraction are derived from functional fits of steam table data. Steam table data comes from the International Association for the Properties of Water and Steam [IAPWS, 2009].

Functional fits of the enthalpy data for the MCHX outlet, drum liquid, and drum vapor are shown in Figure 3-4, Figure 3-5, and Figure 3-6. Equation 19 through Equation 26 describe the dynamics of the two control volumes in the flashing drum. The R^2 values of the first and second order functional fits show that there is little difference between first and second order approximations of the data within the ranges shown. All the models have R^2 values of at least 0.99, though the second order models outperform the first order models in each case. It is not erroneous that as pressure increases, drum vapor saturated enthalpy decreases. This is accurate behavior for steam at high pressure.

$$\frac{d(\text{drum level})}{dt} = \frac{d(M_l)}{dt} / (A_d * \rho_l) \quad \text{Eq. (19)}$$

M_l is liquid mass; A_d is cross-section area of drum; ρ_l is liquid density.

$$\frac{d(M_v)}{dt} = W_{hx} * X_v - W_s \quad \text{Eq. (20)}$$

W_{hx} and W_s are flow rates for the heat exchanger and steam; X_v is vaporization fraction.

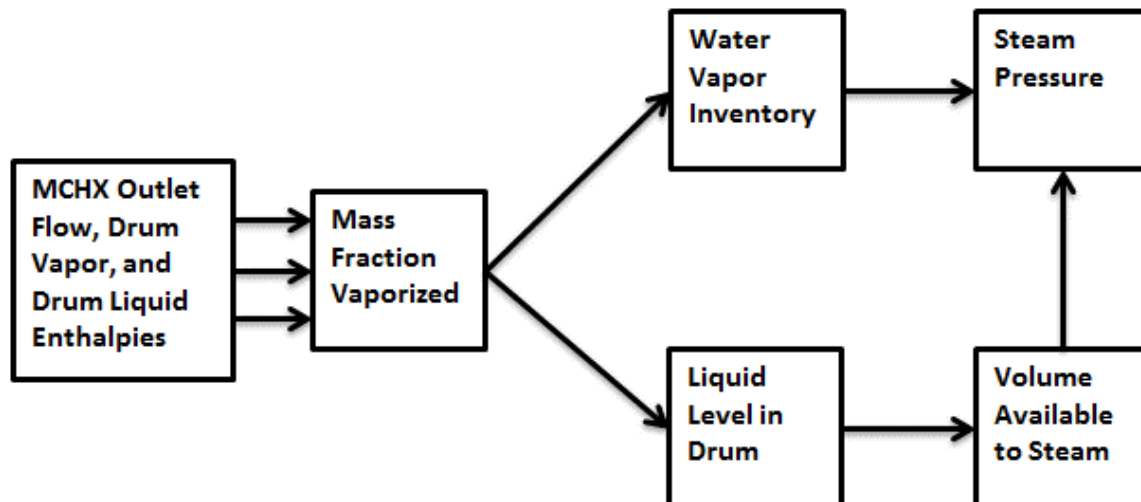


Figure 3-3. Nodal representation of steam flashing drum model.

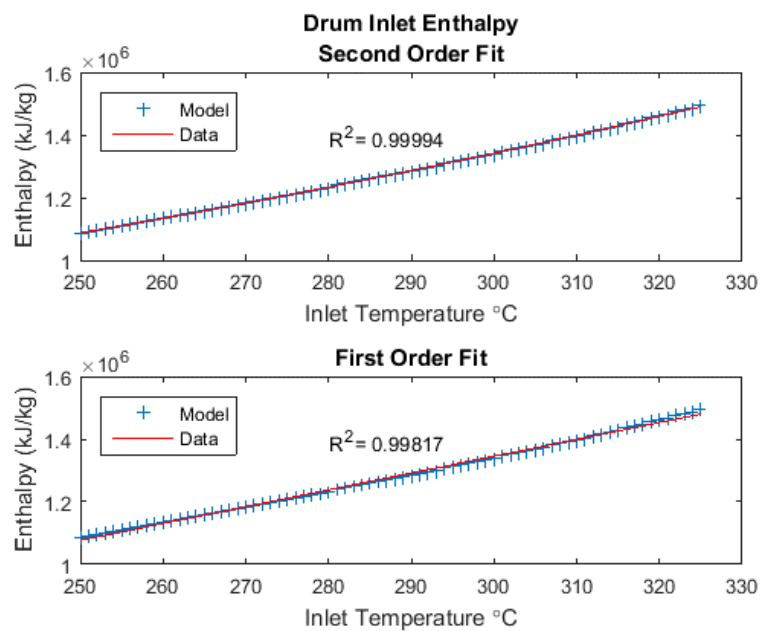


Figure 3-4. Drum inlet enthalpy functional fit comparison. The parabolic fit shows an improvement in the R^2 value.

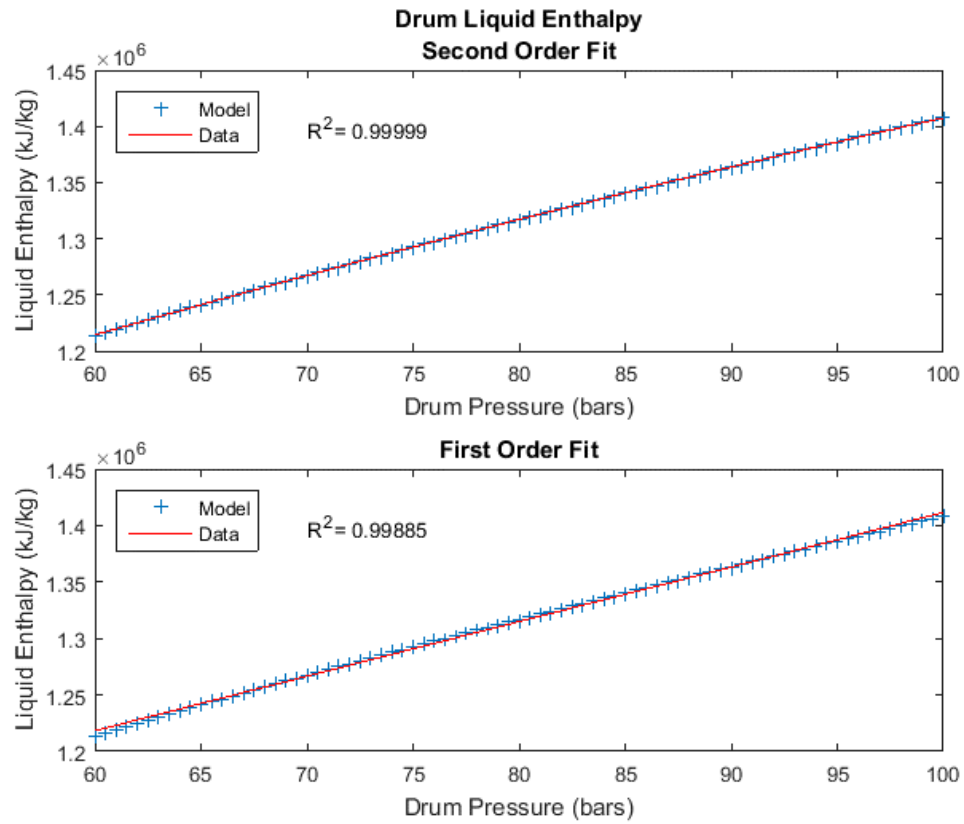


Figure 3-5. Drum saturated liquid enthalpy as a function of pressure. Deviations are apparent in the linear fit at the ends and in the middle. The parabolic fit shows an improvement in the R^2 value.

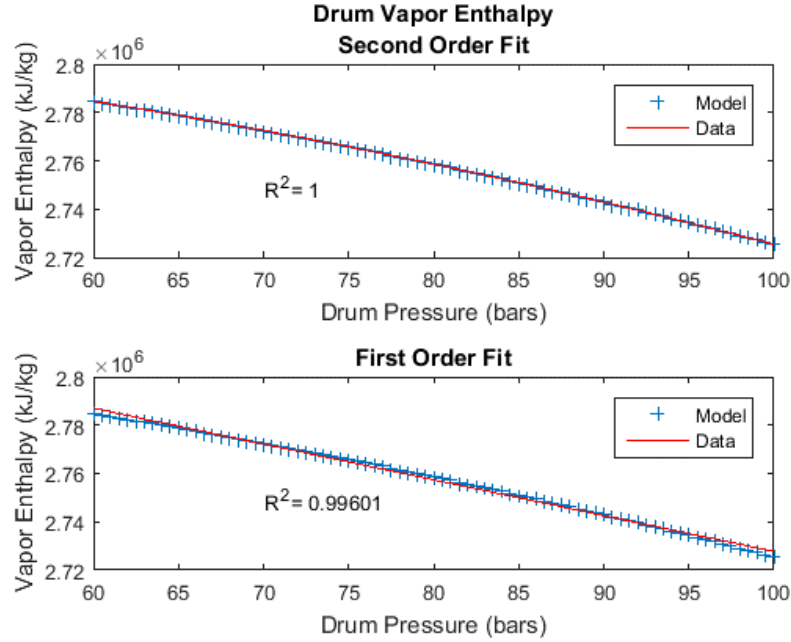


Figure 3-6. Drum saturated vapor enthalpy as a function of pressure. The most significant difference between the linear and parabolic functional fits is in the vapor data. The parabolic fit is rounded to one from the sixth decimal place.

$$\frac{d(V_v)}{dt} = -A_d * \frac{d(\text{drum level})}{dt} \quad \text{Eq. (21)}$$

$$P = \frac{\left(\frac{M_v}{mm_v}\right)R}{V_v} (T_{v,o_c} + 273.15) \quad \text{Eq. (22)}$$

P is pressure (MPa); mm_v is molar mass of water; R: gas constant ($\text{MPa} \cdot \text{m}^3 \cdot \text{K}^{-1} \cdot \text{mol}^{-1}$); T_{v,o_c} is vapor temperature ($^{\circ}\text{C}$).

$$\frac{d(T_v)}{dt} = \frac{\frac{d(M_v)}{dt} H_v}{M_v C_{p_v}} \quad \text{Eq. (23)}$$

T_v is vapor temperature in $^{\circ}\text{C}$; C_{p_v} is isobaric heat capacity of vapor at nominal pressure of drum.

$$\frac{d(M_l)}{dt} = W_{l,i} - W_{l,o} \quad \text{Eq. (24)}$$

$W_{l,i}$ and $W_{l,o}$ are inlet and outlet liquid flow rates,

$$\frac{d(T_l)}{dt} = \frac{d(M_l)}{dt} * H_l / (M_l * C_{p_l}) \quad \text{Eq. (25)}$$

T_l is liquid temperature; C_{p_l} is liquid isobaric heat capacity.

$$\frac{d(T_{si})}{dt} = \frac{(W_{hx} - W_{fw}) * C_{p_l} * (T_l - T_{si}) + W_{fw} * C_{p_l} * (T_{fw} - T_{si})}{C_{p_{si}} * M_{si}} \quad \text{Eq. (26)}$$

T_{si} is temperature of secondary coolant entering heat exchanger; $C_{p_{si}}$ and M_{si} are heat capacity and mass of coolant in node.

3.3.2 Parameters for Flashing Drum Model

Flashing drum sizing parameters and operating conditions were determined by the research group responsible for this system, currently at Brigham Young University. These values are taken from the PPL and reproduced in Table 3-3.

3.4 Testing Models for Stability

To evaluate the stability of the models, open-loop, or uncontrolled simulations are performed in which transients are introduced to examine model behavior. The complete model is operated without any external reactivity control, drum level control, or steam pressure control. Feedwater and steam flow rates are constant. This assumes a steam throttling valve controlled to deliver constant steam flow rate to a turbine under constant load. In actuality, since the steam condition may change during a transient, constant flow rate is not an accurate representation of steam flow controlled to maintain turbine speed, but a better approximation is not readily available. The first transient tested is a positive reactivity insertion and the second is a feedwater flow rate reduction.

3.4.1 Reactivity Insertion

The 10-cent positive step insertion reactivity perturbation is initiated at 500 seconds of simulation, and the simulation is continued for a total of 1000 seconds. Plots are focused to the time window surrounding the transient so that the modeling behavior can be readily observed. Figure 3-7 shows the response of the reactor power (fraction with respect to the nominal thermal power) for a step insertion of reactivity of +10 cents, without any reactivity controller. The reactor power dynamics are consistent with the first order response typical of a point reactor kinetics model. Fuel temperature response, shown in Figure 3-8, reflects the feedback of temperature and coolant coefficients of reactivity on energy deposition in the fuel during the transient.

Table 3-3. Flashing drum simulation parameters.

Parameter (units)	Value
Nominal steam and feedwater flow rate (kg/s)	398.1
Nominal mass fraction vaporized	0.1082
Inlet water temperature (°C)	320.1
Inlet water pressure (MPa)	12.066
Inlet water flow rate (per drum) (kg/s)	3149.25
Drum operating pressure (MPa)	7.08
Drum operating temperature (°C)	286.6
Steam outlet quality	0.999
Drum vapor volume (m ³)	451.18
Drum liquid volume (m ³)	223.66
Drum inner diameter (m)	6.626
Drum height (m)	22.068
Drum liquid height (level set point) (m)	7.263

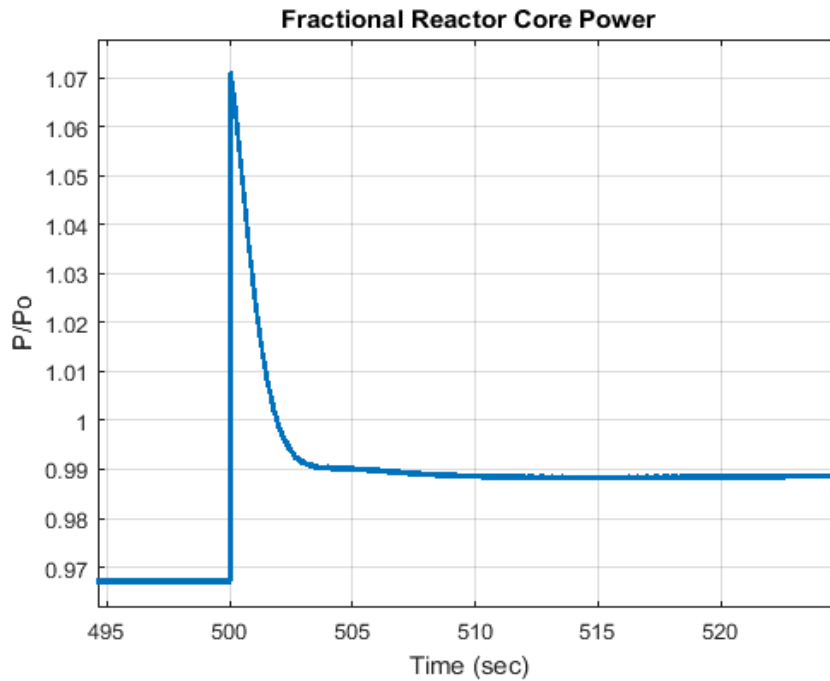


Figure 3-7. Fractional power response to +10 cent reactivity insertion.

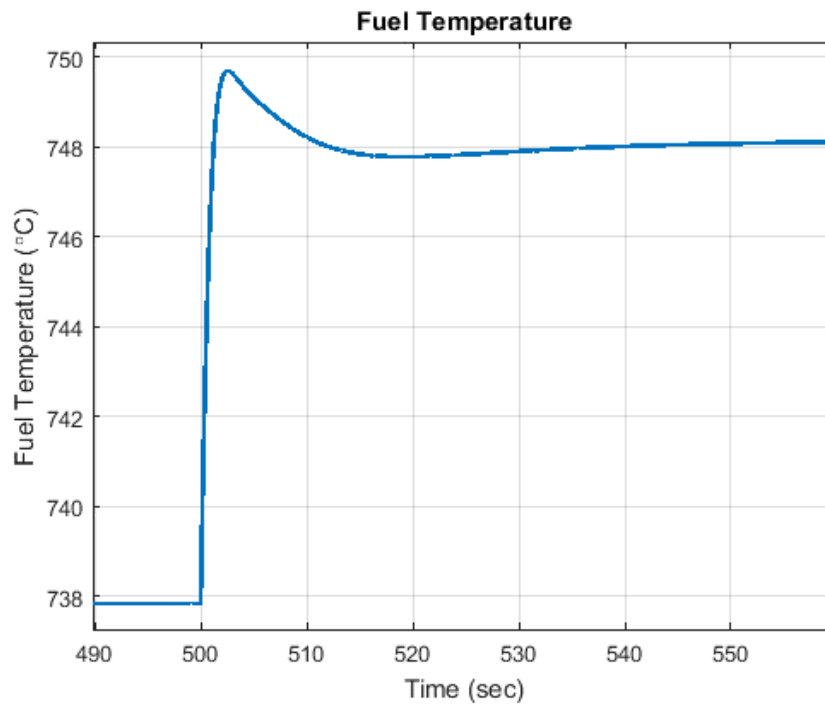


Figure 3-8. Fuel temperature response to a +10-cent reactivity insertion.

Figure 3-9 shows the core exit and hot leg temperature responses to the same perturbation. This should look like a pure transport delay, if the modeling of the fluid dynamics was high fidelity. However, it can be seen in the figure that the hot leg response looks more like the temperature response of a tank being filled with hotter liquid than a transport delay system. The temporal separation of the two signals in the early versus later part of the transient illustrates the spreading of information discussed as a limitation of the modeling approach at the beginning of the chapter. Based upon the amount of coolant in the hot leg node and the flow rate of that coolant, the resident time of coolant in the hot leg is estimated to be 3.36 seconds. At the beginning of the transient, the hot leg has increased by two tenths of a degree Celsius only 1.5 seconds behind the core exit temperature, less than half the resident time. At the end of the transient, the hot leg is lagging six seconds behind the core exit temperature, nearly twice the resident time. This confirms the limitation of simulating transient behavior for control purposes with this model, because the model does not accurately simulate the time it takes for a transient event initiating in one part of the plant to be measureable in another part of the plant. This is critical for the next phase of control system development, when performance requirements such as sensor and actuator response time must be determined.

The secondary coolant responds to the reactivity predictably. The coolant leaving the primary heat exchanger increases in energy (Figure 3-10), and therefore enthalpy, causing more of the stream to vaporize upon entering the flashing drum (Figure 3-11). This raises drum pressure (Figure 3-12), and decreases drum level (Figure 3-13). The rise in pressure brings the vaporization fraction back to the pre-transient level and the system achieves a new steady state. Steam and feedwater flow rates remained constant throughout the simulation.

3.4.2 Feedwater and Steam Flow Reductions

Reducing feedwater flow rate while maintaining steam flow rate does not allow the uncontrolled system to return to steady state. Simulating a feedwater reduction of 5% as a step decrease at 500 seconds causes, after an initial spike in the opposite direction, the reactor power and fuel temperature to increase linearly while all coolant temperatures decrease linearly, along with the flashing drum water level and steam pressure. They do not self-stabilize.

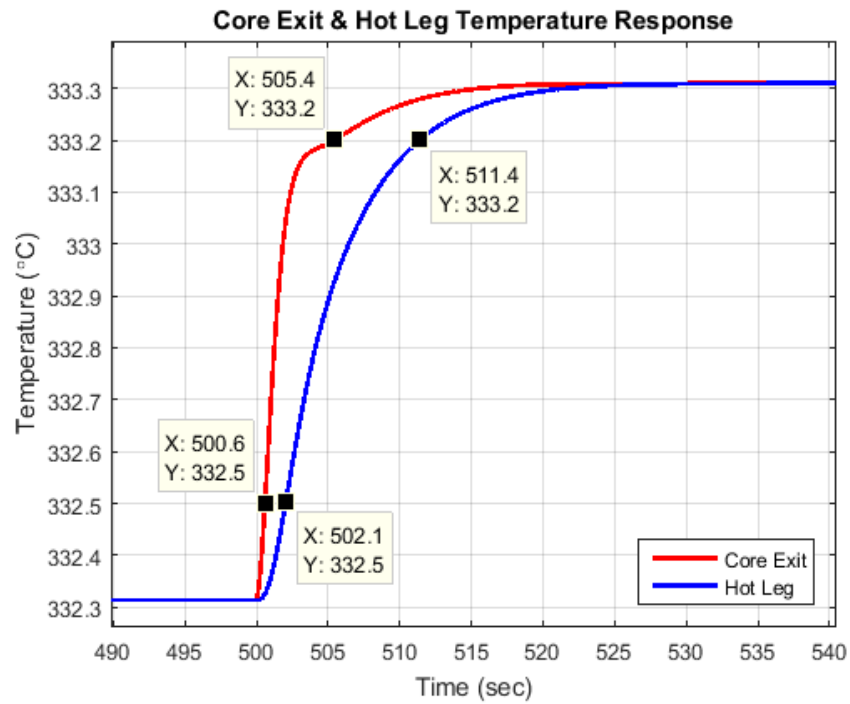


Figure 3-9. Core exit and hot leg temperature responses to a +10-cent reactivity insertion.

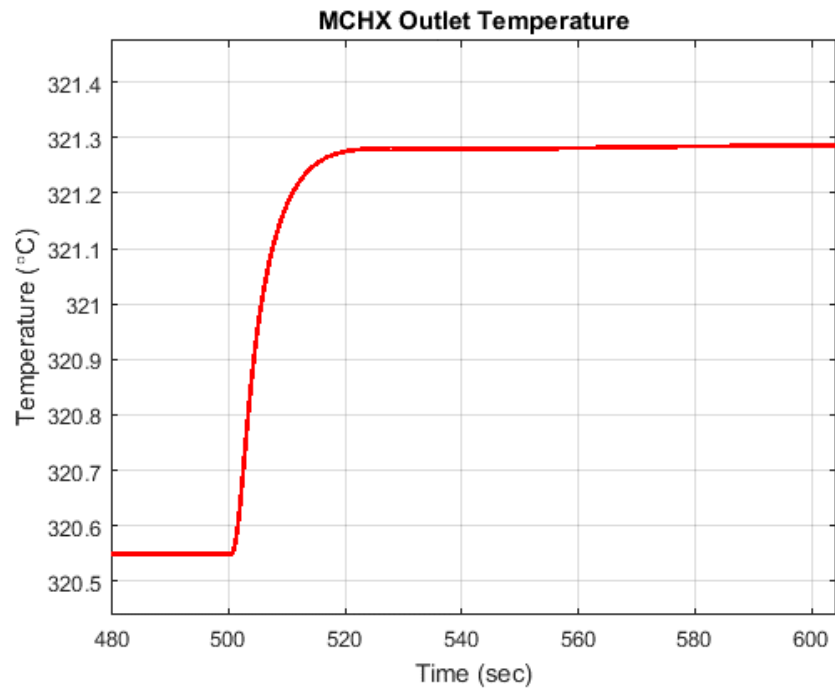


Figure 3-10. Heat exchanger secondary outlet response to +10cent reactivity insertion.

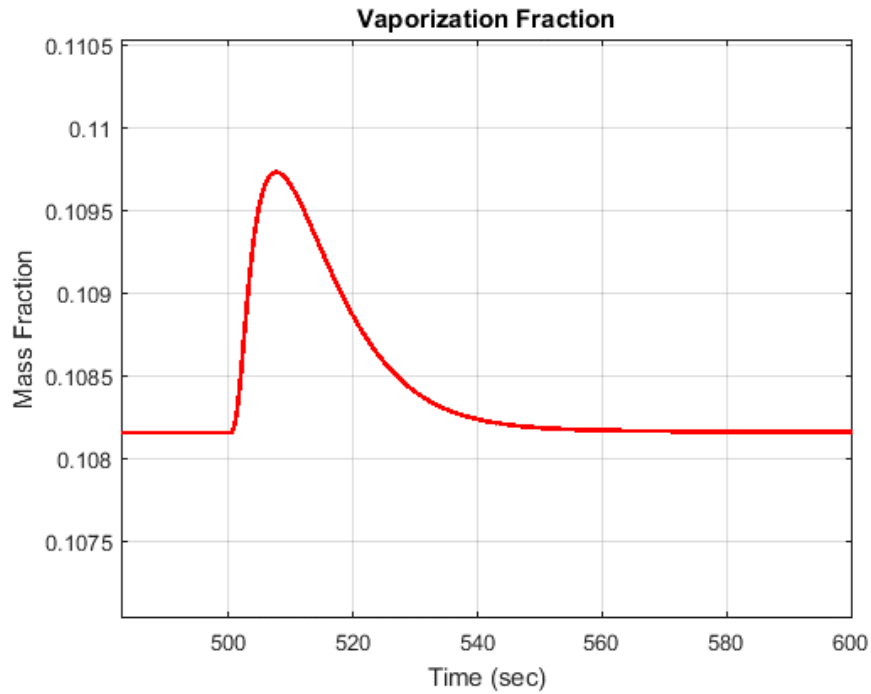


Figure 3-11. Fraction of inlet flow vaporized in flashing drum response to +10 cent reactivity insertion. Vaporization fraction achieves similar value at increased operating pressure and inlet temperature as prior to perturbation.

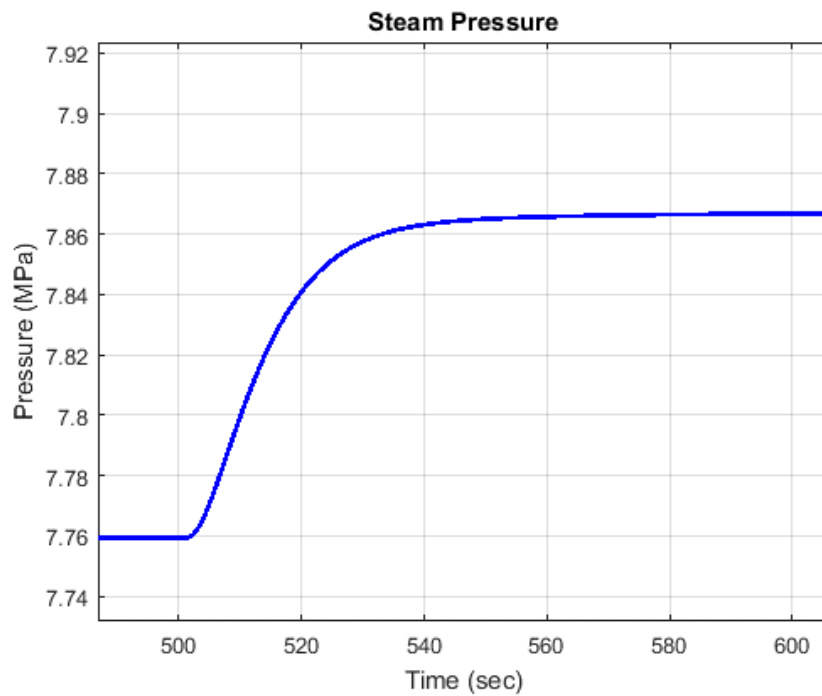


Figure 3-12. Flashing drum uncontrolled pressure response to +10 cent reactivity insertion.

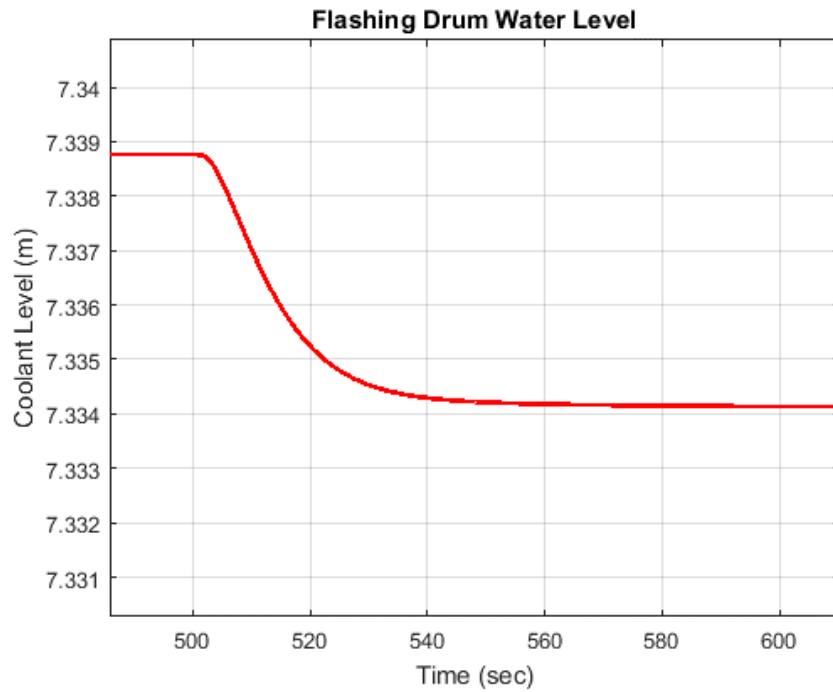


Figure 3-13. Flashing drum uncontrolled level response to +10 cent reactivity insertion.

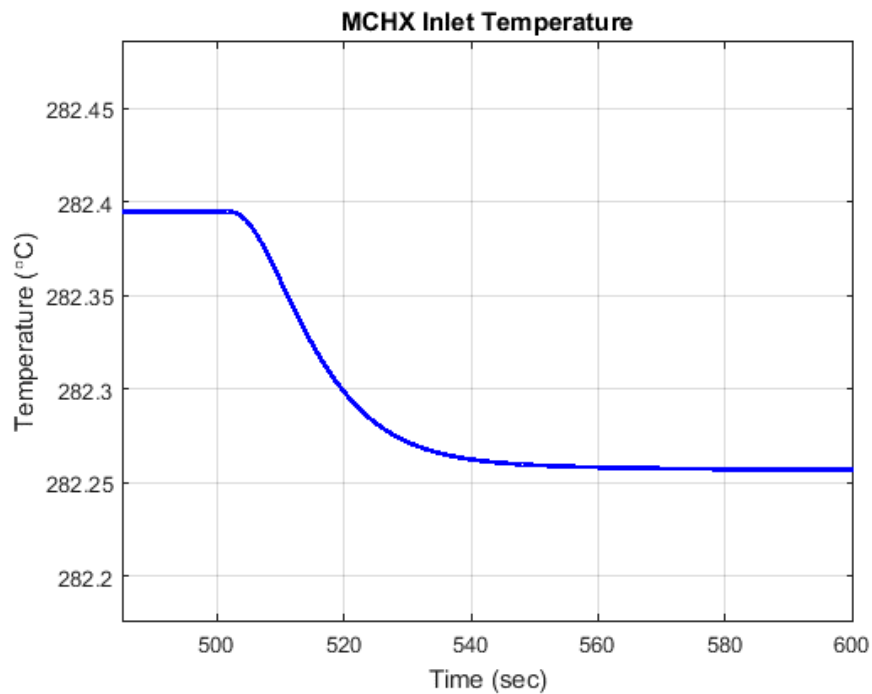


Figure 3-14. Heat exchanger secondary inlet response to +10 cent reactivity insertion.

If, at 600 seconds, the steam flow rate is reduced by the same amount as the feedwater flow rate, the system stabilizes. Maintaining steam flow rate after a decrease in feedwater flow rate is not a very realistic simulation, as it would require decreasing pressure on the turbine side of the steam throttling valve in order to keep a sufficient pressure drop to draw the same flow rate of steam while the steam flow rate falls. The decreasing pressure increases the steam enthalpy, causing an increase in the steam enthalpy rate that matches the increase in power during the linear transition portion of the simulation.

The progression of these flow changes through the reactor system begins with the increase in MCHX inlet temperature (Figure 3-15), due to the decrease in colder feedwater mixing with the flashing drum recirculation flow. This spikes the primary coolant cold leg (Figure 3-16), which in turn enters the reactor core, negatively affecting reactivity (Figure 3-23) and core power (Figure 3-17). Fuel temperature (Figure 3-18) falls while core exit coolant temperature (Figure 3-19) increases, in turn increasing the MCHX secondary coolant outlet temperature (Figure 3-20). This increases the enthalpy of the flashing drum inlet flow, increasing the vaporization fraction (Figure 3-24), which causes less liquid to be added to the recirculation flow, decreasing drum level (Figure 3-21). Drum level falls continuously, further decreasing drum pressure (Figure 3-22). Vaporization fraction only stabilizes because the drum liquid volume decreases in temperature as the pressure falls, due to saturation condition. This decreases the MCHX secondary inlet temperature, primary coolant temperatures, and MCHX secondary outlet temperature, lowering the enthalpy of the drum inlet flow, such that the ratio which determines vaporization fraction stabilizes slightly lower than before the flow transient begins. In order to bring the plant back to a steady state, the steam flow rate must be adjusted to reflect the difference in feedwater flow rate. After all, a coolant loop cannot have a steady state with more coolant leaving the process than is replaced. Once the steam flow rate is adjusted, the plant achieves a new steady state at lower coolant temperatures, higher fuel temperature, and higher power level.

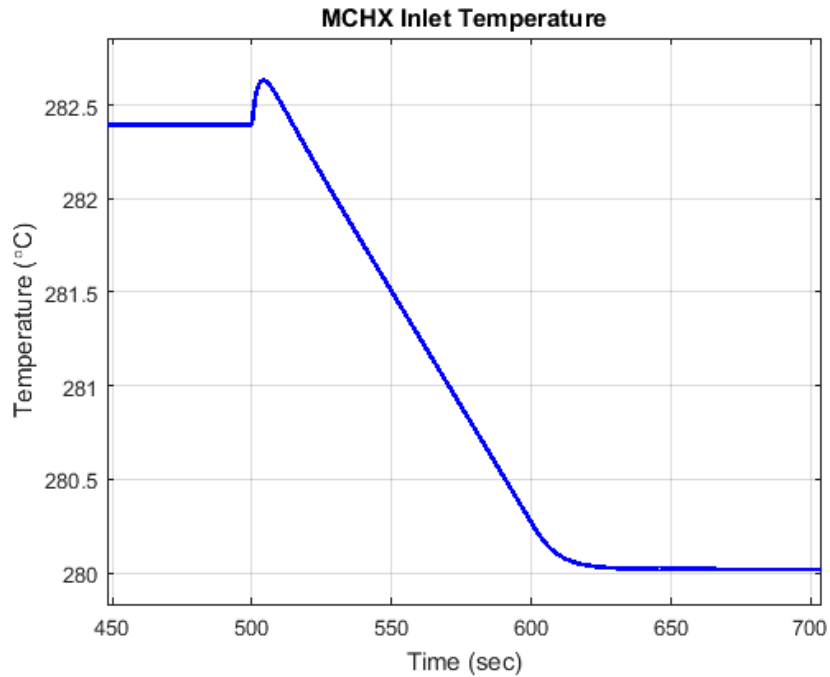


Figure 3-15. Response of the secondary coolant MCHX inlet temperature for a 5% decrease in the feed flow rate at 500 seconds followed by a 5% reduction in steam flow rate at 600 seconds.

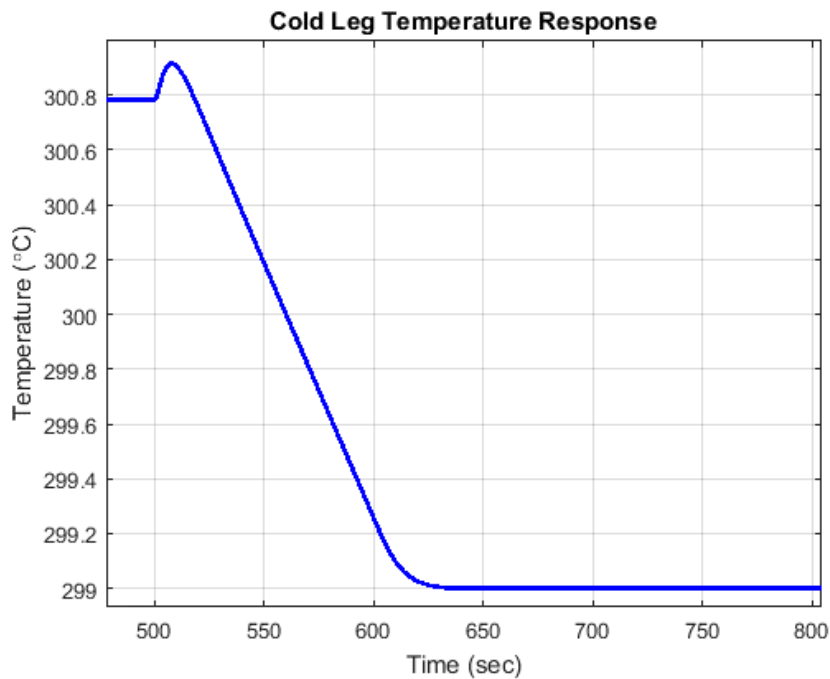


Figure 3-16. Primary coolant cold leg temperature response for a 5% decrease in the feed flow rate at 500 seconds followed by a 5% reduction in steam flow rate at 600 seconds.

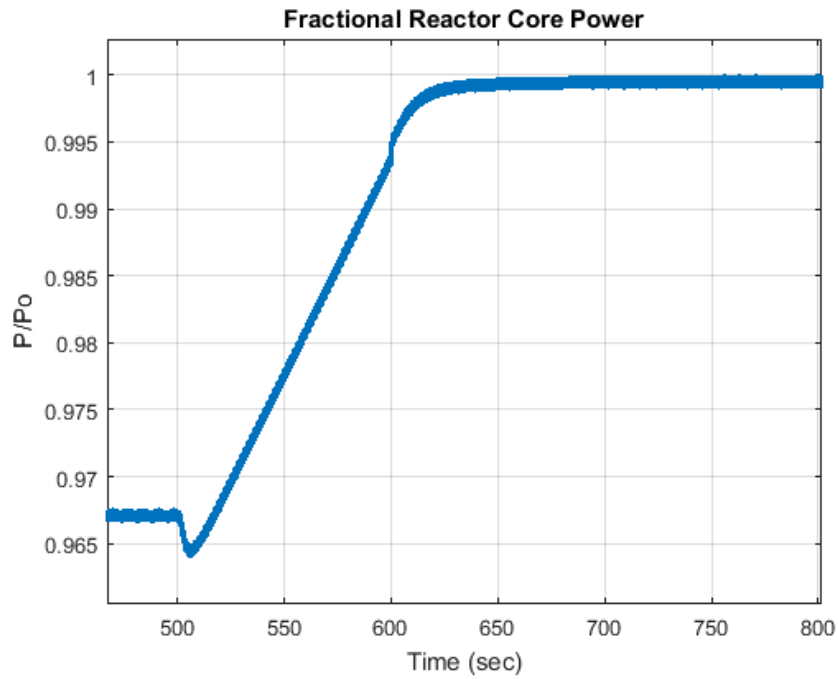


Figure 3-17. Response of the fractional reactor power for a 5% decrease in the feed flow rate at 500 seconds followed by a 5% reduction in steam flow rate at 600 seconds.

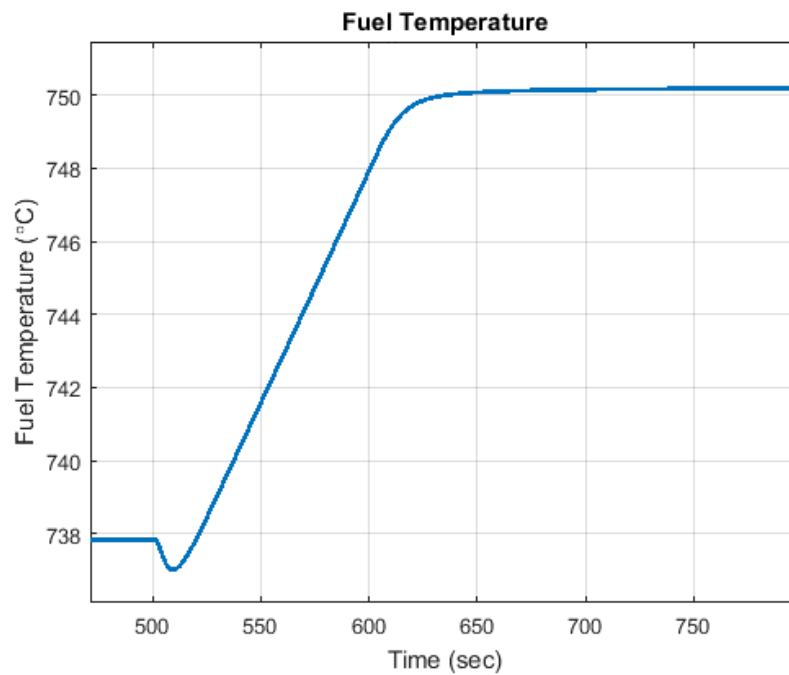


Figure 3-18. Response of the fuel temperature for a 5% decrease in the feed flow rate at 500 seconds followed by a 5% reduction in steam flow rate at 600 seconds.

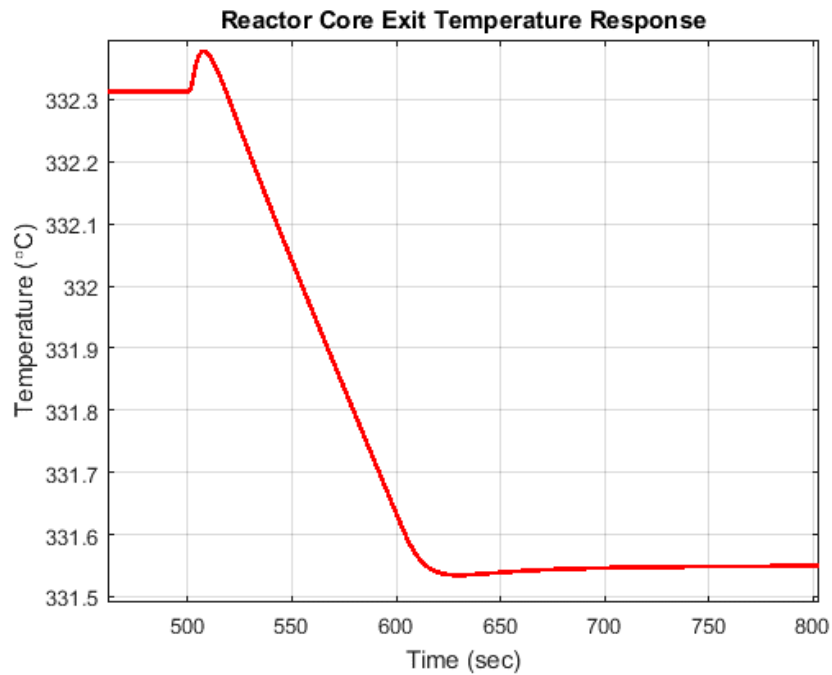


Figure 3-19. Response of the primary coolant core exit temperature for a 5% decrease in the feed flow rate at 500 seconds followed by a 5% reduction in steam flow rate at 600 seconds.

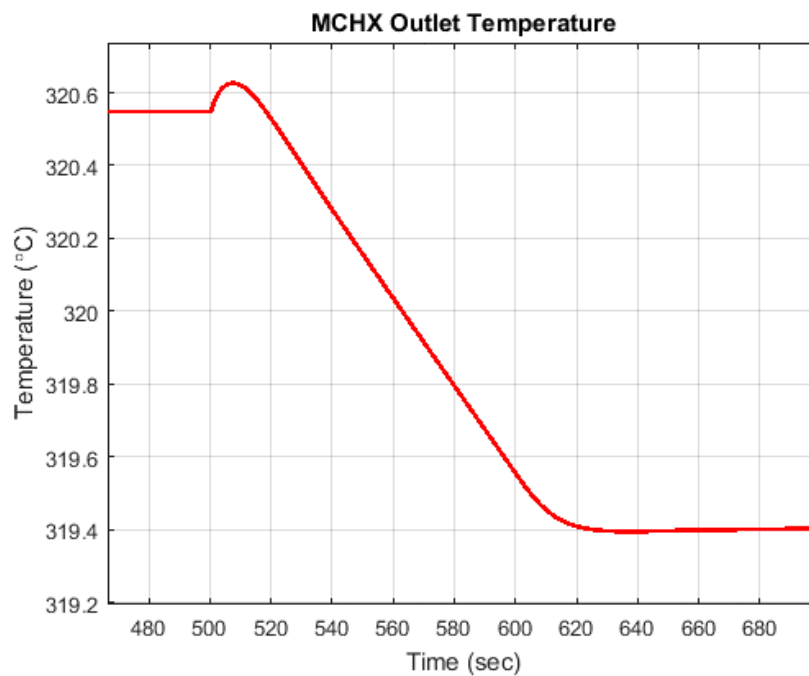


Figure 3-20. Response of the MCHX water exit temperature for a 5% decrease in the feed flow rate at 500 seconds followed by a 5% reduction in steam flow rate at 600 seconds.

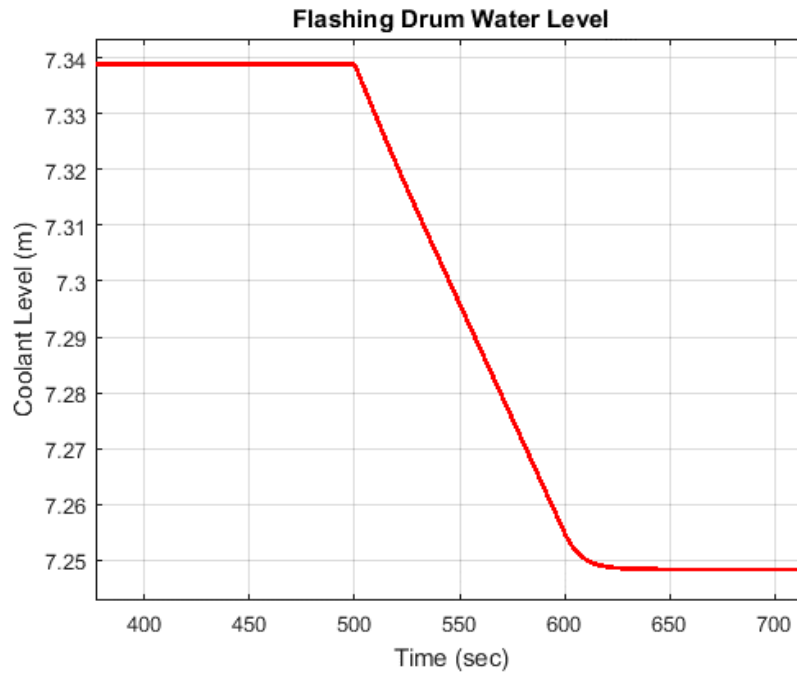


Figure 3-21. Response of the flashing drum water level for a 5% decrease in the feed flow rate at 500 seconds followed by a 5% reduction in steam flow rate at 600 seconds.

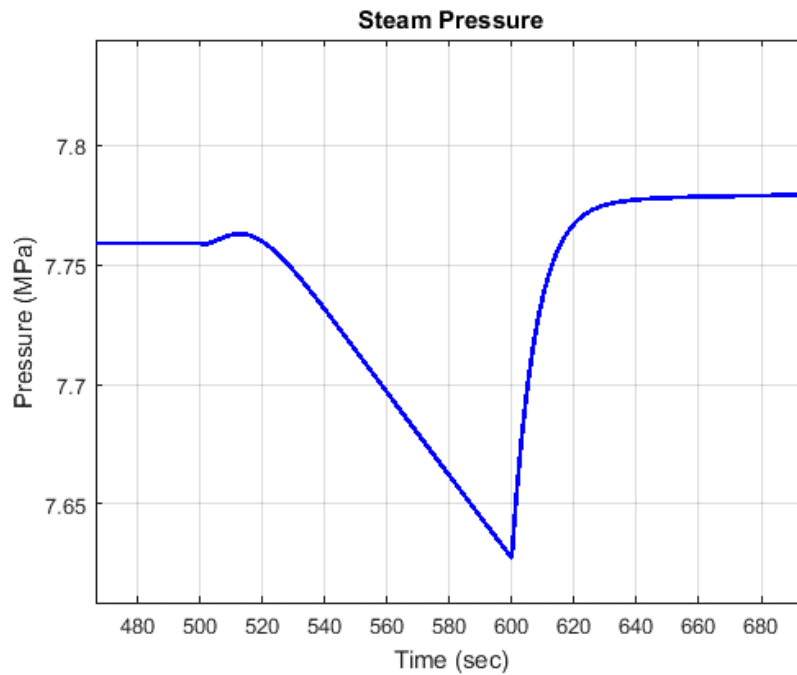


Figure 3-22. Response of the flashing drum steam pressure for a 5% decrease in the feed flow rate at 500 seconds followed by a 5% reduction in steam flow rate at 600 seconds.

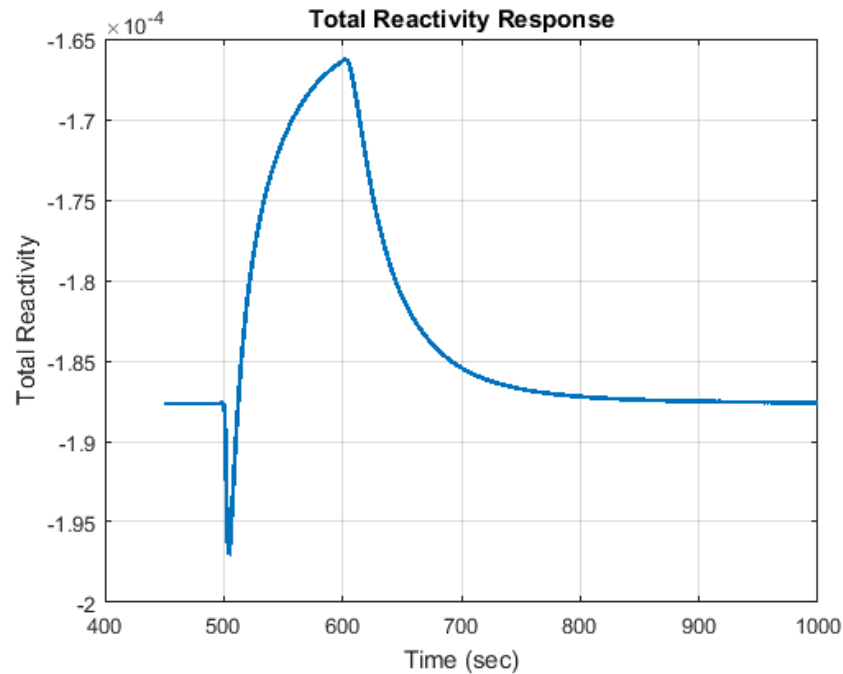


Figure 3-23. Response of the nuclear core total reactivity (sum of feedback effects) level for a 5% decrease in the feed flow rate at 500 seconds followed by a 5% reduction in steam flow rate at 600 seconds.

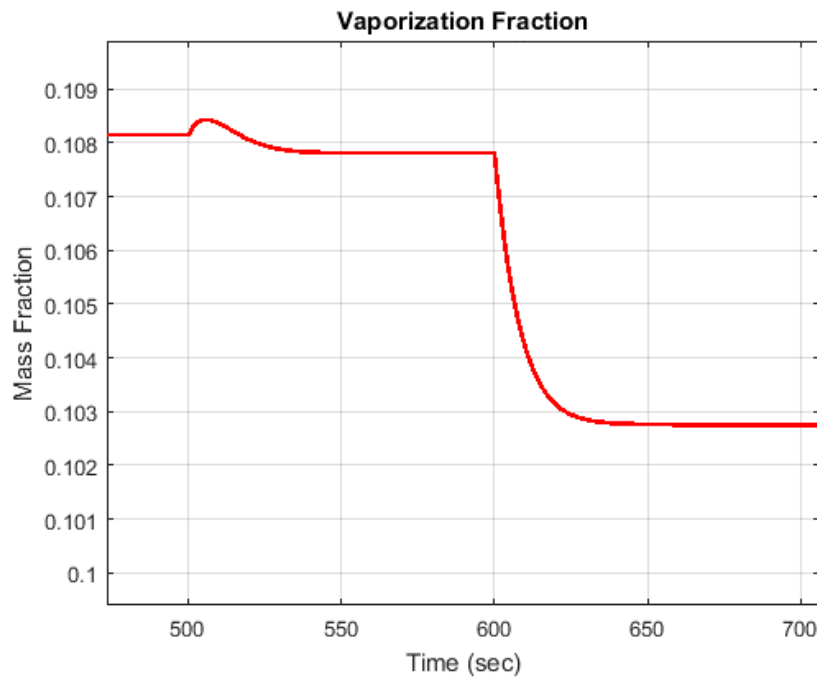


Figure 3-24. Response of the flashing drum vaporization fraction for a 5% decrease in the feed flow rate at 500 seconds followed by a 5% reduction in steam flow rate at 600 seconds.

4 DEVELOPMENT OF CONTROL SYSTEMS

The approach to controlling the I²S-LWR is similar to that for any process system. First the steady state control is established, then the control approach to move the plant from one state to another state is analyzed. To define the steady state control problem, it is necessary to establish which variables of the system will be used to maintain the system at steady state. These are the controlled variables. Often they are selected for their operational or surveillance significance. Temperature can be measured with a high degree of accuracy and sensitivity, so it is used to control reactor power in PWRs by means of primary coolant temperature based control. The I²S-LWR is no different from other PWRs in this regard. This desire to use primary coolant temperatures for control purposes further highlights the need to solve the measurement challenges posed by the primary coolant cold leg volume. Also of operational importance to the I²S-LWR is the flashing drum coolant level and operating pressure. Level and pressure must be maintained at particular values to maximize the thermodynamic efficiency of the power conversion system, which is of critical importance for the economic competitiveness of the design concept.

4.1 Control Measurements and Control Actions

4.1.1 Reactor Power Control

Reactor power control is accomplished with control rods, the movement of which is based upon primary coolant temperature measurement, performed with highly accurate RTDs. The controlled parameter is the primary coolant temperature in a particular region, or the average primary coolant temperature. Typically the average primary coolant temperature is controlled to a set point. This set point may be fixed or move with power level. This is discussed with load following control. In the model, the average primary coolant is controlled to a set point by introducing external reactivity into the core model. The average temperature is the mathematical mean of the simulated hot-leg and cold-leg temperatures. A Simulink block representing a proportional integral differential (PID) controller is used to determine the sign and magnitude of external reactivity to send to the core model, based upon the difference between calculated average primary coolant temperature and the set point. This difference is called the error. In the absence of modeling the sensors, signal processing equipment, control hardware, and control rod drive mechanisms (actuator for external reactivity insertion), the operational parameters of this

controller have no physical interpretation with regards to the control of a real plant. A PID controller works by summing three functions of the deviation from controller set point: the linear, or proportional function of the error, the integral of the error over time, and the derivative of the error at a particular time. Each of these functions is weighted by a constant. These constants are used to tune the controller performance to achieve the desired control dynamics. Since the output of the control block in the Simulink model is the actual reactivity adjustment, in Dollars, as opposed to a certain number of control rod steps into or out of the core, the PID constants used in this controller do not have any real meaning in the design of the control system. The use of these control blocks serves only to demonstrate that the PID control approach can reasonably be expected to bring the controlled system from one operational state to another, but cannot be used to evaluate controller performance because the controller input (measurements) and output (actuators) are not modeled.

4.1.2 Flashing Drum Steam Flow Control

The steam flashing drum must operate at a design value for pressure inside the drum in order to maximize the thermodynamic efficiency of the power conversion system. The drum operating design pressure is 7.08 MPa. However, if the actuator of this pressure control is to be the throttling valve between the NSSS and the high pressure turbine of the PCS, it presents a conflict of control. This valve is typically used to adjust the energy applied to the turbine according to the turbine demand, such that the torque applied by the steam matches the torque applied by the induced current, so that the turbine speed, and electrical frequency remain constant. If electrical demand decreases, and steam flow rate does not, the turbine speed will increase as the steam applies more torque than the current flowing out of the generator is applying in the opposite direction. In practice, this steam flow control uses the mismatch between reactor power and steam power delivered to the turbine as the error signal. For steady state modeling, the drum pressure is controlled by adjusting steam flow rate, using a PID controller simulation block implemented similarly to core reactivity control. In the steam flow controller, the input is the error between drum pressure and drum pressure set point, and the output is the change to the steam mass flow rate.

4.1.3 Flashing Drum Feedwater Flow Control

Just as the coolant liquid level of a U-tube steam generator is controlled to a set point, so too must the liquid level of the I²S-LWR steam flashing drum be controlled. The flashing drum level set point is 7.263 m. Maintaining a constant volume for the expansion of the flash vaporized inlet

coolant flow maximizes the efficiency of the isenthalpic expansion in the drum. There is an important distinction between U-tube steam generator operation and flashing drum operation that simplifies the level control for the flashing drum. U-tube steam generators boil secondary coolant. Doing so means that as power level changes, the boiling rate also changes. This changes the fraction of coolant below the surface of the liquid in the steam generator which is in the liquid phase versus the vapor phase. At higher power, more of the volume below the surface of the liquid coolant is in the vapor phase, as compared to lower power level. This results in a phenomenon known as shrink and swell, referring to the expansion and contraction of the liquid volume of the steam generator during power changes. This can cause the level sensor to detect a higher-than-set-point coolant level during a power increase, resulting in a reduction in feedwater flow rate, when in actuality an increase in feedwater flow rate is needed to accommodate the increased steam production rate. Consequently, an approach called three element control is used to control steam generator level. In this approach, the feedwater flow controller considers both the drum level error as well as the mismatch between feedwater flow rate and steam flow rate when determining control actions on the feedwater regulating valve. By using both error signals, the controller does a better job of controlling level during power changes.

In I²S-LWR control development, it was initially presumed this same approach would be used for flashing drum level based control of the feedwater flow rate. However, implementation of this approach in the dynamic model proved unstable when the drum model was interfaced with the reactor core and heat exchanger models. Upon reflection on the process, it was noted that since there is no boiling process in the I²S-LWR flashing drum, there is no shrink and swell effect, and therefore no need for the three element control approach. Drum level is most efficiently controlled by adjusting feedwater flow rate based upon the level signal alone.

4.2 Steady State Control

4.2.1 Controller Stability

For steady state control testing, PID controllers are implemented to control primary coolant average temperature, flashing drum vapor pressure, and flashing drum liquid level by modulating external reactivity, steam flow rate, and feedwater flow rate respectively. Each parameter is controlled separately by a single PID controller. System stability is evaluated for a variety of controller implementations. The model is first tested with all three controllers implemented. Then,

each controller is implemented individually, while the other two actuator variables remain constant. Finally, each combination of two out of three controllers are implemented while the third actuator variable remains constant. For stability testing combinations of controlled and uncontrolled parameters, no transients are introduced. The results of these tests are conveniently presented by separately plotting twelve parameters in a single figure to show how and whether the system achieved stability under the described controller implementation.

The top row of each figure shows the fractional reactor core power, along with the controller adjusted parameters external reactivity, feedwater flowrate, and steam flowrate. The second row shows the primary and secondary coolant temperatures. The third row shows the steam enthalpy rate, mass fraction vaporized in the flashing drum, drum coolant level and drum steam pressure. Figure 4-1 through Figure 4-3 show the plant with only one active controller operating on external reactivity, feedwater flowrate, and steam flowrate respectively. In these cases the other controlled parameters remain constant. Figure 4-4 through Figure 4-6 show pairs of implemented controllers with a single controlled variable held constant. These figures correspond to external reactivity plus feedwater flowrate, external reactivity plus steam flowrate, and feedwater flowrate plus steam flowrate respectively. Figure 4-7 presents the case of all three controllers implemented together.

The only one of these implementation scenarios which does not lead to a steady state condition is the use of external reactivity and steam flowrate controllers, while holding feedwater flowrate constant. This is shown in Figure 4-5. It appears that the steam pressure controller demands a higher flow than the fixed feedwater flow rate, so the system slowly runs the flashing drum out of coolant, while increasing power to maintain the constant primary coolant average temperature. This is largely due to the fact that the mass flow rate into the liquid volume of the drum is less than the mass flow rate out of it. The cooling of the drum liquid, despite the maintenance of the pressure, and therefore the maintenance of the temperature of the liquid component of the inlet flow, may be an erroneous artifact of the way the temperature change in a node is modeled. For a node in which energy transport is based solely upon convection, the energy entering the node is the mass of coolant entering the node multiplied by the temperature and heat capacity. The energy leaving the node is the same. If the flow rate out of the node is greater than the flow rate into the node, this model, along with the well mixed node assumption, will cause the calculated temperature of the node to decrease. However, conceptually, a well-insulated water tank at a particular temperature with water entering the tank at the same temperature and draining at a

slightly faster rate, should not change temperature. It is the cooling of the tank that drives the cooling of the primary cold leg, and the associated increase in reactor power by the reactivity controller. A higher fidelity modeling approach could address this.

4.2.2 Transient Control

The controllers are further evaluated by applying the same transients used to test the open-loop model to the model with the three PID controllers implemented on their respective variables. These perturbations are a 10-cent positive reactivity insertion and a 5% reduction in feedwater flow rate. Given the implementation of the controllers, the steam flow rate reduction will not have to be implemented manually as it was in the open-loop simulation in order to achieve steady state.

With the controllers driving the system to particular points, the system takes longer to achieve initial steady state after simulation startup than the open loop system. For this reason, the runtime of the reactivity transient simulation is 5,000 seconds, and the perturbation is introduced at 2,500 seconds. This suggests that the initial conditions of the model could be adjusted to match steady state conditions of the open loop model, rather than the design set points of the plant. As these are not high fidelity models, it is expected for the simulation response to differ somewhat from the design values for the plant.

Figure 4-8 and Figure 4-9 show the system responses to the two transients in the same style of figure used to evaluate stability of different controller implementations. The plots show that in response to both transients the controllers bring the plant back to the set operating point. This is in contrast to the open-loop plant response, in which the plant comes to a new steady state reflecting the natural feedback of the system. Controller feedback forces the plant to correct back to the original state, rather than settling at a new equilibrium condition. These simulations suggest that established PID controller approaches should be successful at controlling the I²S-LWR during steady state operation. In the next section, load following needs and control strategies are discussed.

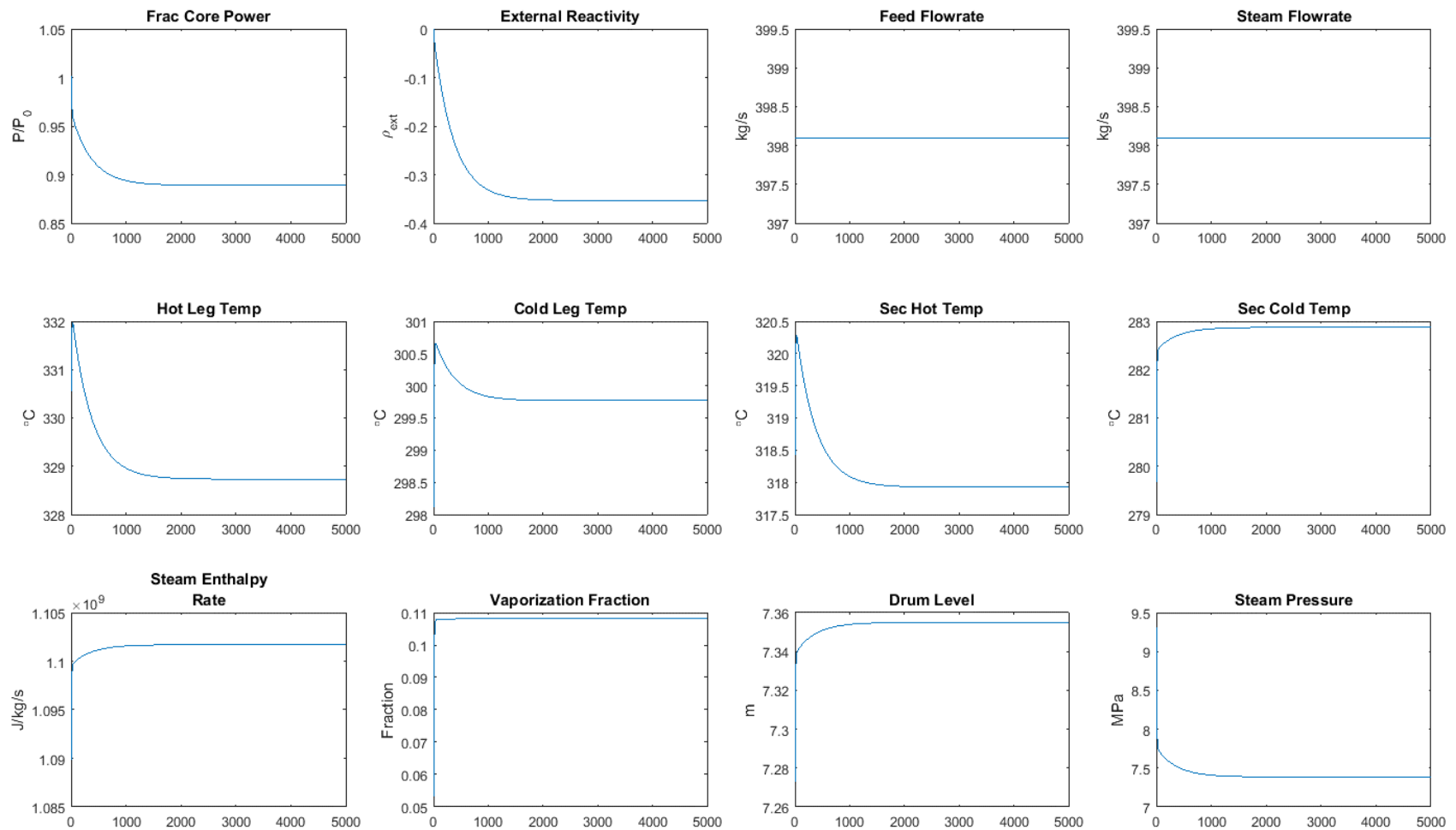


Figure 4-1. Average primary coolant temperature controlled by external reactivity insertion for P^2S -LWR with constant feedwater and steam flow rates.

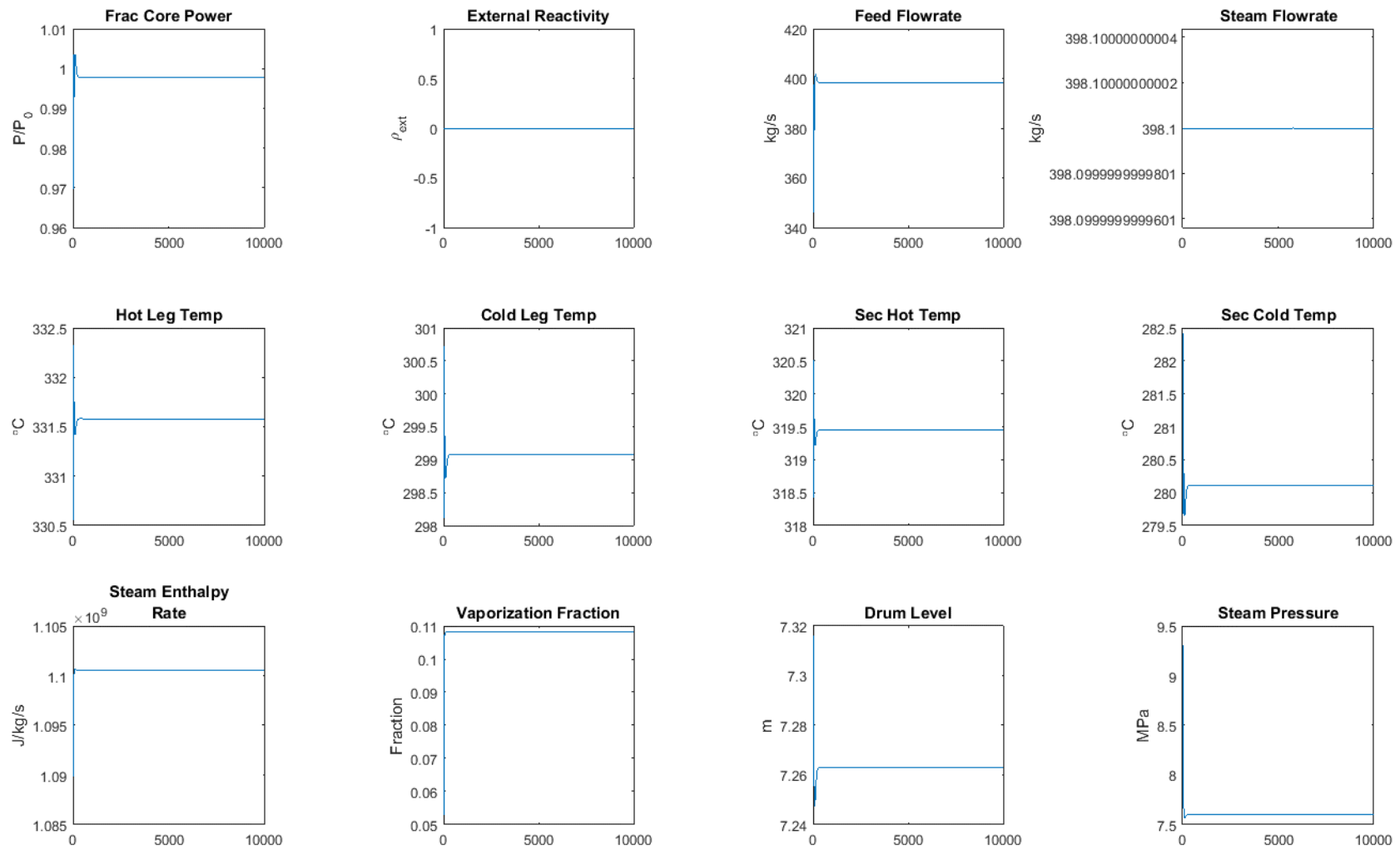


Figure 4-2. Drum level controlled by feedwater flow rate for P^2S -LWR with constant external reactivity and steam flowrate.

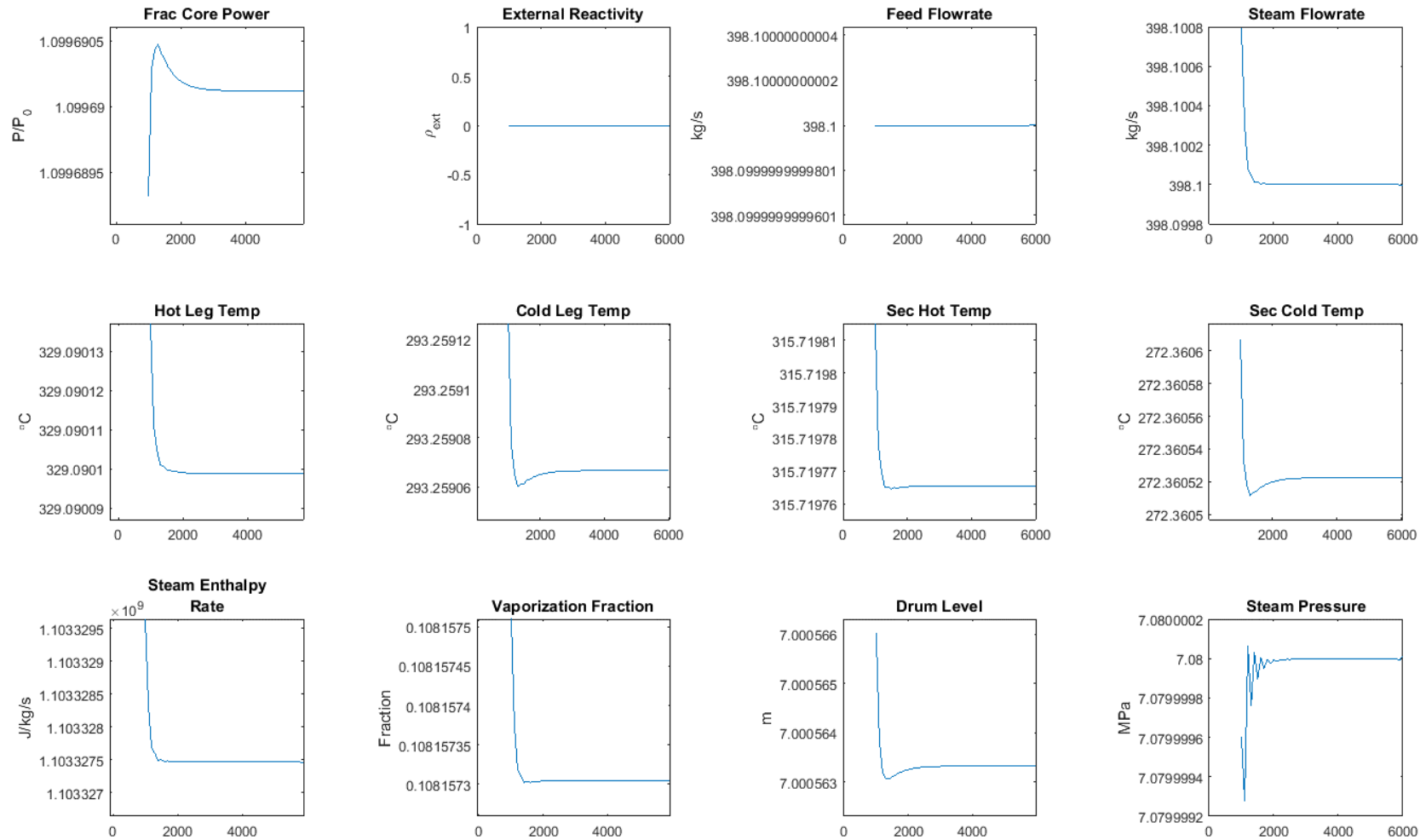


Figure 4-3. Steam pressure controlled by steam flowrate for P^2S -LWR with constant external reactivity and feedwater flowrate.

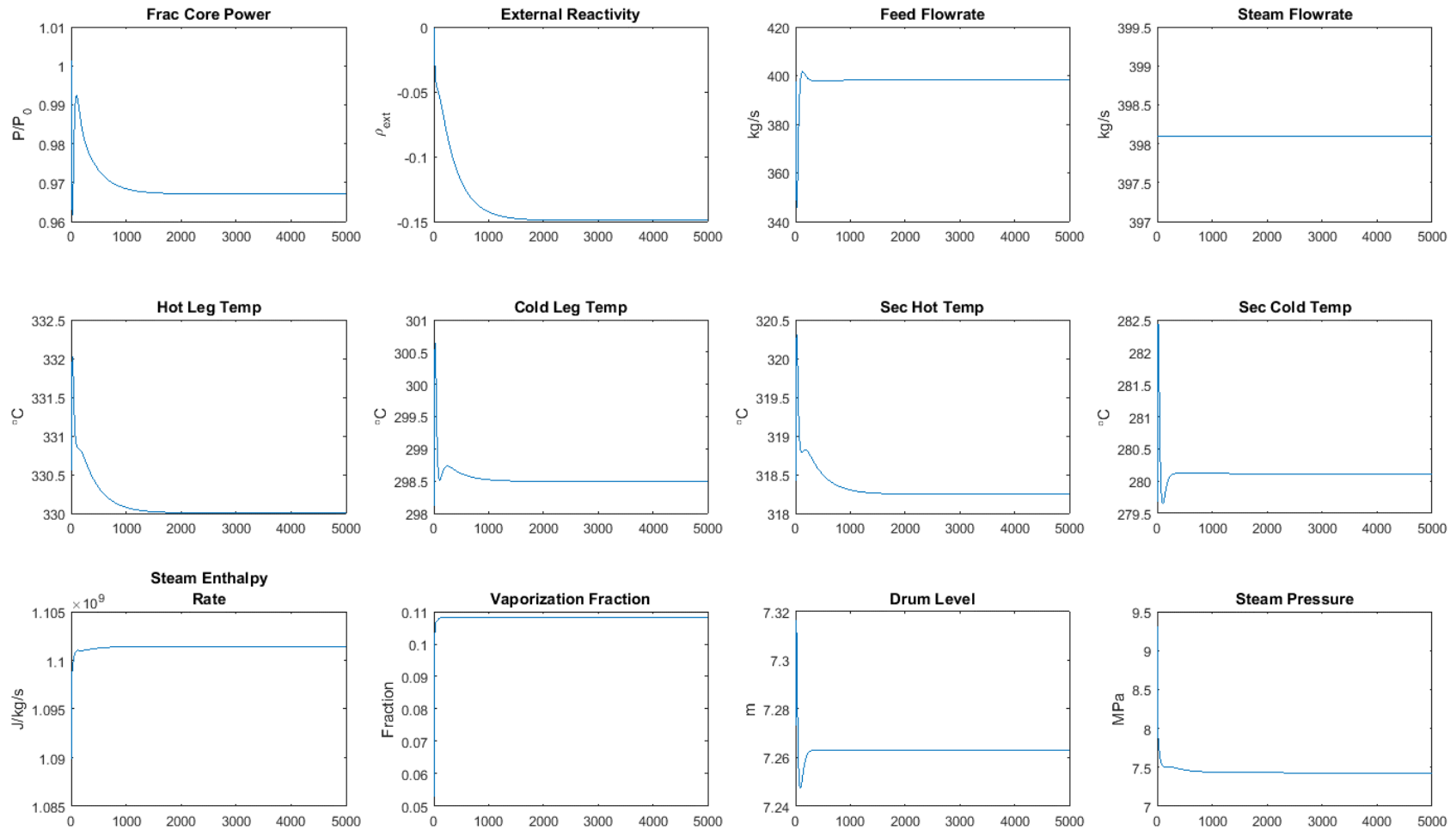


Figure 4-4. Average primary coolant temperature based reactivity control plus drum level based feedwater flowrate control for P²S-LWR with constant steam flowrate.

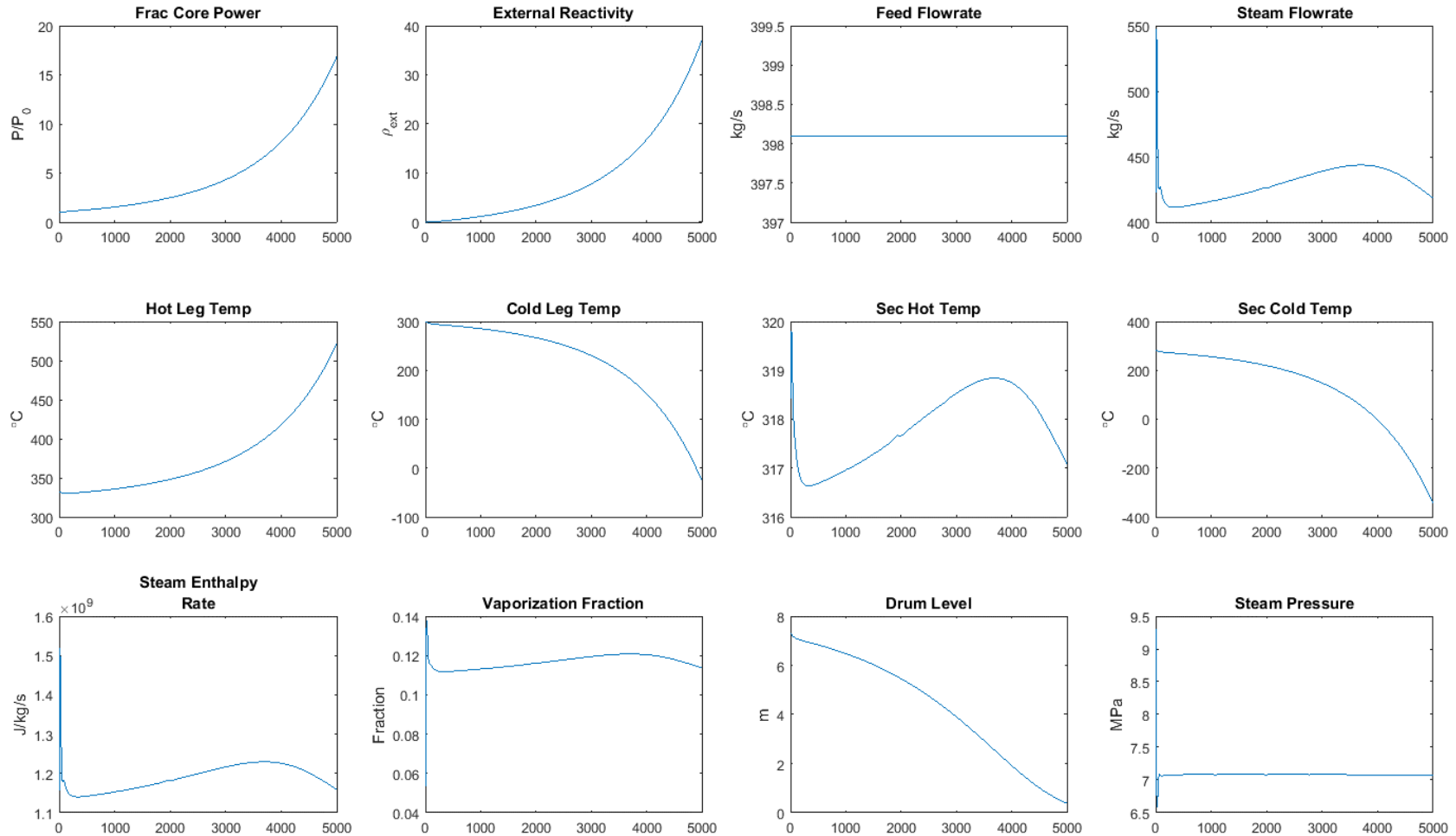


Figure 4-5. Average primary coolant temperature based reactivity control plus steam pressure based steam flowrate control for P²S-LWR with constant feedwater flowrate. This approach is clearly unstable.

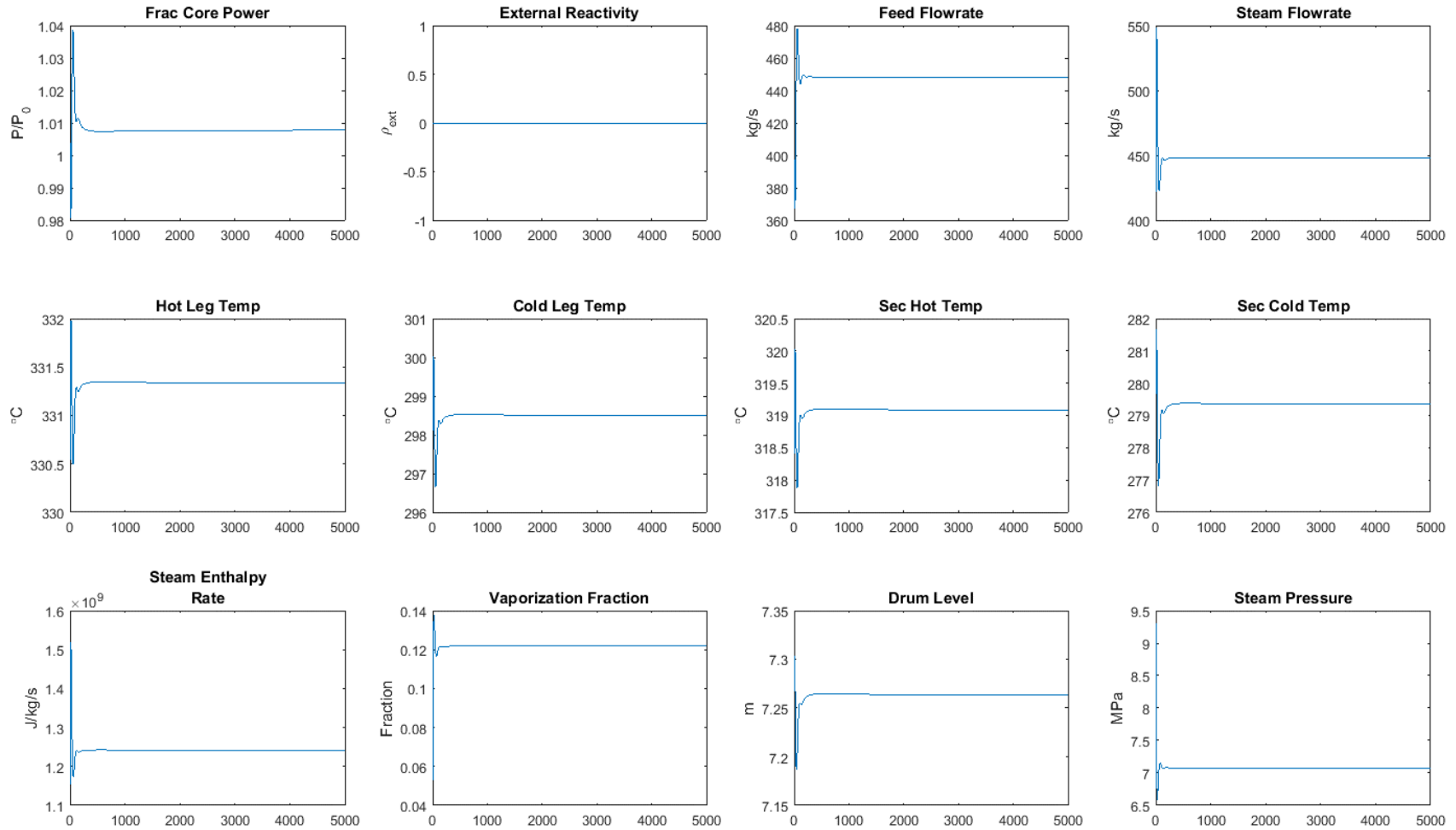


Figure 4-6. Steam pressure based steam flowrate control plus drum level based feedwater flowrate control for P^2S -LWR with constant external reactivity.

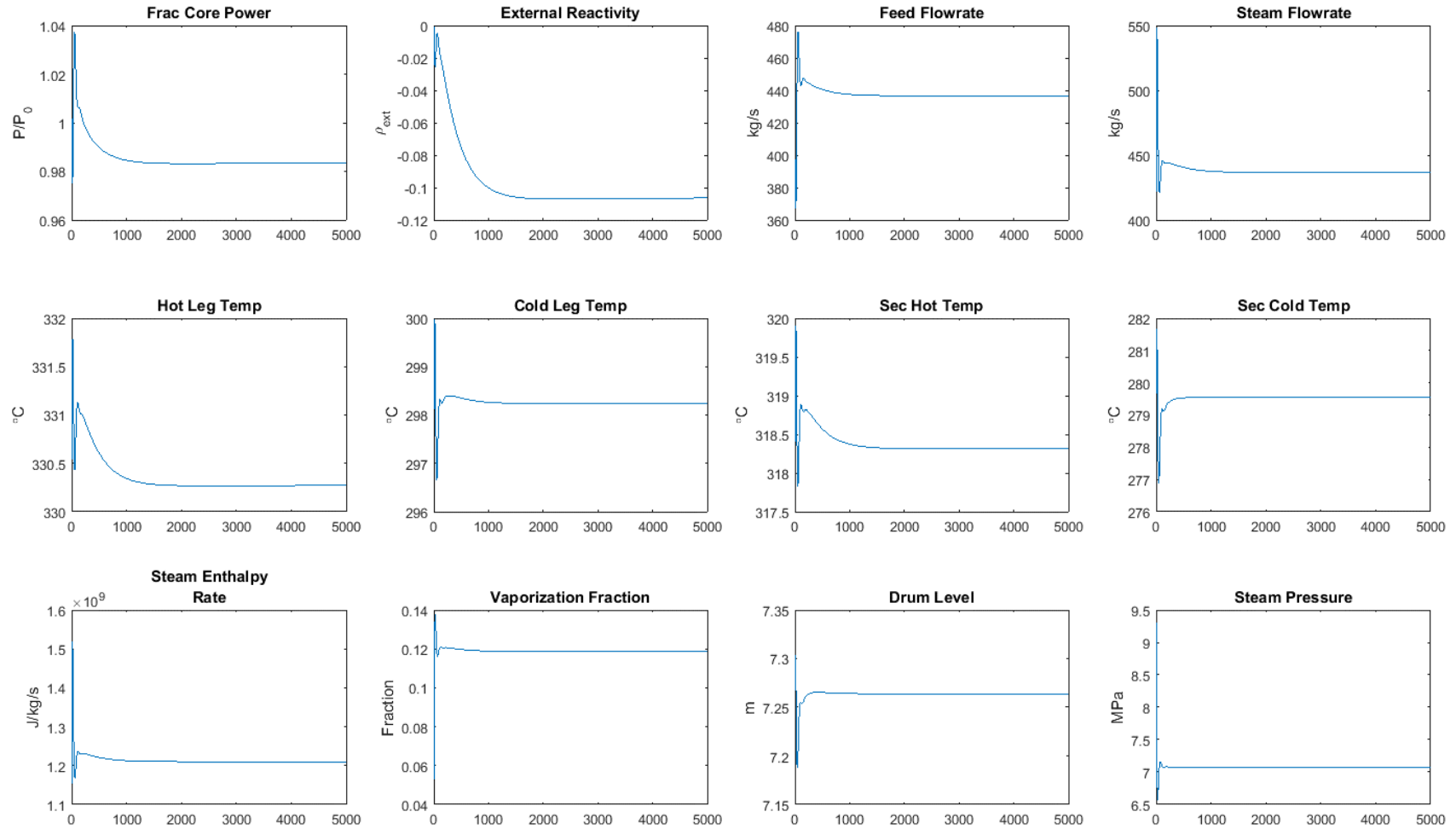


Figure 4-7. Control of P^2S -LWR with controllers operating on external reactivity, steam flowrate and feedwater flowrate.

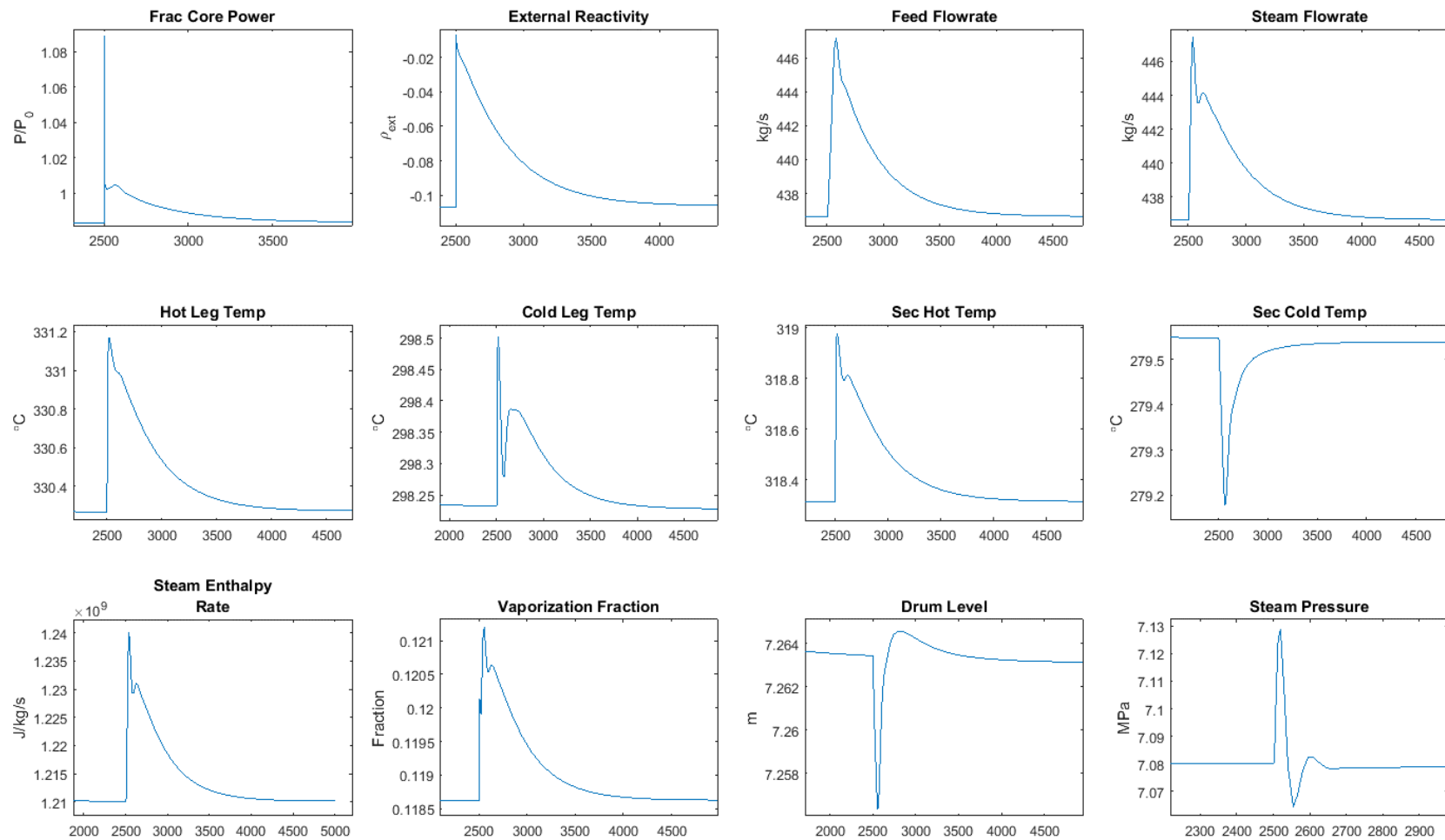


Figure 4-8. Controlled system response to +10-cent reactivity perturbation. System returns to previous condition.

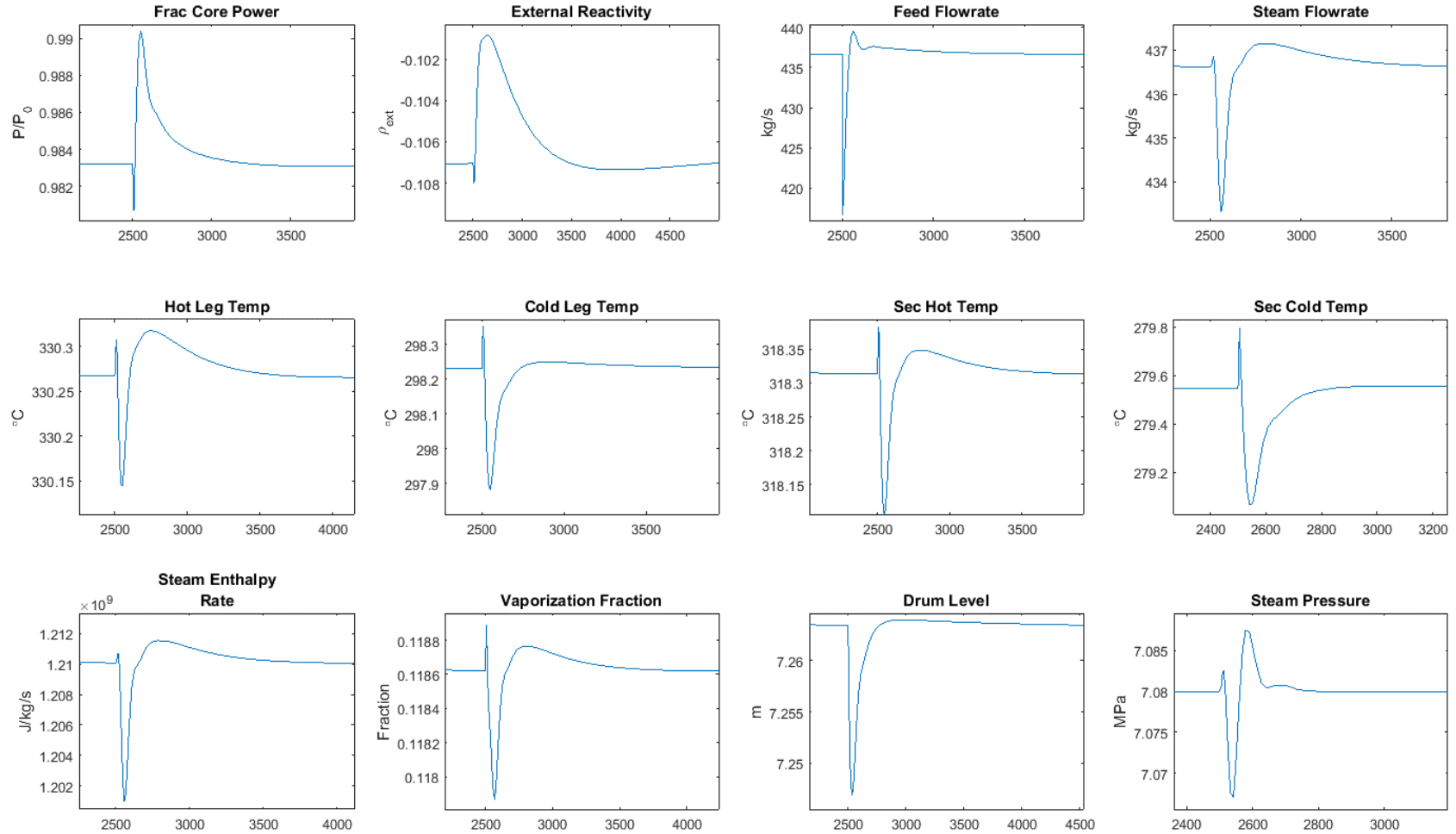


Figure 4-9. Controlled system response to 5% decrease in feedwater flow rate. System returns to previous condition.

4.3 Control during Load Changes

Controlling a nuclear power plant at different power levels is not only necessary for startup and shutdown, but also for accommodating changes in electrical demand. This is especially true of the I²S-LWR, which shows promise for remote deployment as a large singular energy source for multiple purposes. In this section, control strategies for changing reactor power level based upon demand changes are discussed with application to the I²S-LWR system.

4.3.1 Control Strategies for Load Following

In a constant average primary coolant temperature based control system, the primary coolant hot leg, cold leg, and average temperatures vary with power level as shown in Figure 4-10. This is the approach employed in the IRIS design, as well as in Babcock & Wilcox PWRs with once through stream generators producing superheated steam such as Arkansas Nuclear One, Unit 1. Other PWR designs, which relying on U-tube stream generators to boil secondary coolant, such as the CE and WEC PWRs, also use primary coolant average temperature as the controlled variable for reactor power control, but rather than keeping this set point constant over a range of power levels, the set point for average temperature has a different value depending upon the desired power level of the core. This typically results in a nearly constant cold leg temperature, as the average temperature program end points are the full power average temperature at the high end, and the hot startup temperature at the low end.

An alternative control approach is to maintain the average hot leg coolant temperature (T_{hot}) at a fixed value as the controlled parameter for primary reactivity control rather than overall average coolant temperature (T_{avg}). This approach, illustrated in Figure 4-11 and described in detail in a patent application [Malloy and Bingham, 2012], utilizes feedwater flow rate as the principal control action, rather than reactivity adjustment via control rods. This relies on the change in coolant temperature and consequent change in moderator efficacy for reactivity adjustment. Average temperature falls as power increases, increasing the effectiveness of moderator, and rises as power decreases, reducing the effectiveness of moderator, giving this approach the advantage of automatically aiding in safe shutdown.

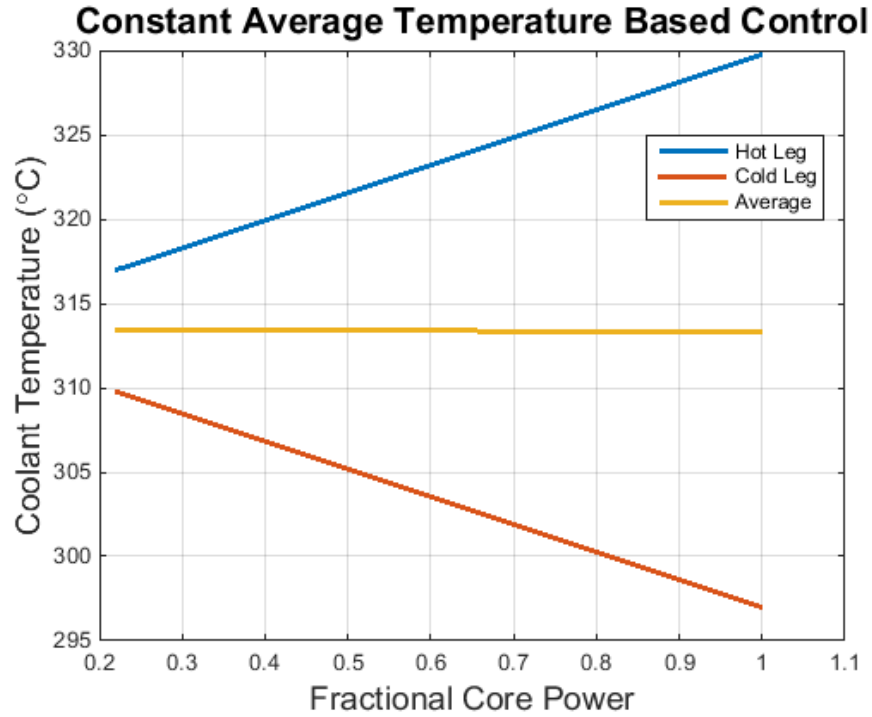


Figure 4-10. Coolant temperature variation with power level for constant average primary coolant temperature based control.

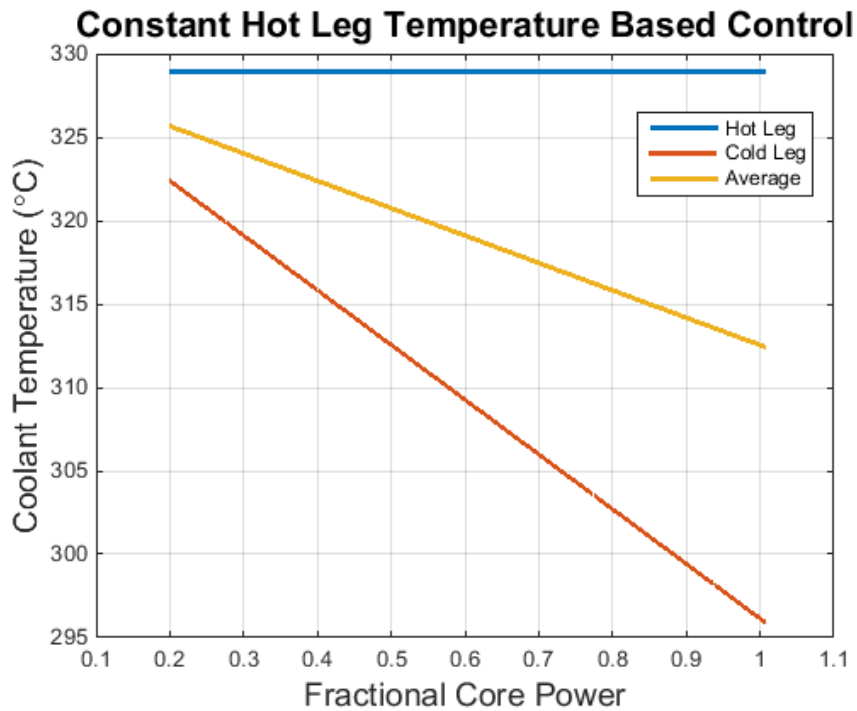


Figure 4-11. Coolant temperature variation with power level for constant primary coolant hot leg temperature based control.

This approach is presented with a variable set point controller for the pressurizer level, all performed with the intention of removing the use of soluble neutron poisons, particularly boric acid, from the reactor design. The use of soluble boron decreases the magnitude of moderator temperature coefficient of reactivity, minimizing the volume changes in primary coolant associated with the power level changes. This removes most of the need to control the pressurizer water level during power transients or adjustments in power level. The downsides of using boron poison include adverse water chemistry effects, particularly at elevated temperatures, which pose safety concerns, as well as environmental detriments which complicate waste management. From the work presented in the patent, the use of feedwater flow rate for normal operational reactivity control, in conjunction with T_{hot} based control and variable set point pressurizer level control, but in the absence of soluble neutron poison, provides an alternative to traditional PWR control paradigms.

4.3.2 Simulating and Controlling Load Changes in I²S-LWR

Upon implementation of a programmed moving average primary coolant set point, it was observed that power did not decrease exactly according to the program. Programming the average coolant temperature profile is generally done by assuming the cold leg temperature will not change very much as the power level is changed, and therefore the average temperature expected at a given power level is half the change in temperature across the core for that power level, added to the nominal cold leg temperature, as shown in the equation below. This works because of how u-tube steam generators (UTSGs) work. In a UTSG, the primary coolant is transferring heat to a larger mass of subcooled and boiling water in which the water at the bottom, interacting first and last with the primary water, stays about the same temperature regardless of power level, because it's the feedwater temperature, the coldest temperature of any water in the UTSG. This allows for reliable primary and secondary control using feedwater flow rate to maintain UTSG level and either constant average, programmed average, or constant hot leg primary coolant temperature as the controlled variable.

$$T_{avg}(P) = \Delta T(P) + T_{cold} \quad \text{Eq. (27)}$$

The significant differences in the I²S-LWR systems are that heat exchange takes place between equal masses of primary and secondary coolant, and that the secondary coolant entering the primary heat exchangers is not necessarily a consistent temperature at different power levels. The feedwater in the I²S-LWR must mix with the recirculating flow from the steam flashing drum before it enters the micro-channel primary heat exchangers. If drum pressure is properly maintained, the recirculation flow will be consistent at different power levels, but the relative contribution of recirculation flow and feedwater flow varies with power level. If feedwater temperature is constant, the secondary coolant entering the MCHX will vary in temperature with power level, namely getting hotter as power level decreases. Furthermore, the secondary hot leg falls at a greater rate than the primary hot leg, because the change in temperature on the secondary side is roughly 22% greater than the change in temperature on the primary side. This causes the primary cold leg temperature to fall, rather than staying constant, during load following. Additionally, the power level achieved at a given average coolant temperature set point is greater than predicted by the control program. The system was programmed to decrease to 20% power before, maintaining this level, then increasing to 80% power for the remainder of the simulation. Instead, it only fell to approximately 30%, and finally settled near 90% power. Results of this simulation are shown in Figure 4-12.

Since both coolants should, at zero power, have the same temperature, in order for any one coolant to maintain a constant temperature throughout operation, all the other coolant temperatures must converge on that value at zero power. With constant feedwater temperature, the convergence point would be dictated by the temperature of the secondary coolant when no feedwater is needed to make up the difference between drum recirculation flow and the prescribed flow rate for secondary coolant through the heat exchanger. Thus the zero power coolant temperature will be the saturation temperature (286.6°C) of the drum at operating pressure, (7.08 MPa). To achieve a constant primary cold leg temperature in the I²S-LWR system, the feedwater temperature must be programmed to increase with power, such that the zero power temperature of the feedwater is sufficient to bring the secondary coolant up to the primary cold leg temperature, 298°C.

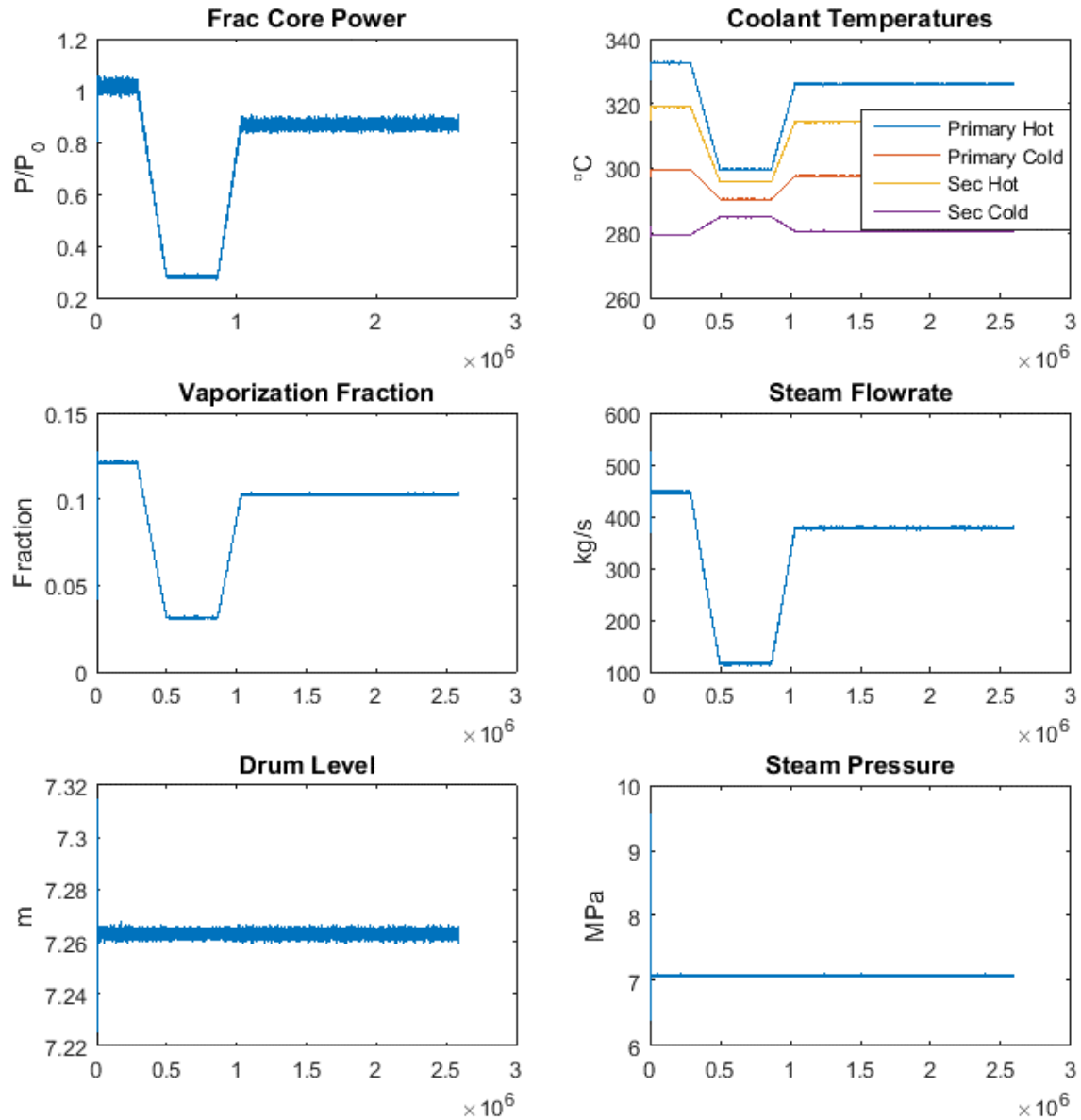


Figure 4-12. Selected variables under load following conditions performed by programmed average primary coolant temperature reactivity control. Controlled parameters of the flashing drum are maintained. Note behavior of coolant temperatures. Rather than maintaining a constant primary cold leg temperature, constant feedwater temperature causes all coolant temperatures to converge at lower value than primary cold leg temperature.

Of course, feedwater reheating is achieved by diverting steam from the turbines and passing it over heat exchangers. Increasing feedwater temperature in this manner while decreasing reactor power decreases plant efficiency, which is unacceptable. The operating parameters of the flashing drum, and thus the secondary coolant, are carefully optimized to maximize the overall efficiency of the Rankine cycle and the multi-stage turbine energy conversion system. Changing these conditions, and thus negatively affecting plant performance is a poor trade simply to achieve a well-recognized primary coolant temperature profile during load following.

Instead, if the average primary coolant temperature program is modified to vary linearly between the average temperature at full power (114.25°C) and the drum operating temperature, accurate power profiles between 100% and 20% power are achievable, as shown in Figure 4-13.

Excellent load following performance using programmed average primary coolant as the primary system control variable is achieved if all four principal coolant temperatures are made to vary with power level. Constant average primary coolant temperature is not feasible for the I²S-LWR because the secondary and primary coolants cannot converge at the full power average temperature of primary coolant (314.25°C) when the reactor is at zero power condition.

4.4 Resilient Control Considerations for the I²S-LWR

Digital control systems have taken over every critical infrastructure system except nuclear power, supplanting analog as the standard in instrumentation and control. Automation has served to improve performance, reliability, and safety in a variety of industries. In the interest of bringing these advantages to the future of the nuclear power industry, it is worthwhile to take a wide point of view with regard to resilient control systems in the I²S-LWR. A resilient control system has been broadly defined as:

“... [a system] that maintains state awareness and an accepted level of normalcy in response to disturbances, including threats of an unexpected and malicious nature.” [Reiger, et al, 2009].

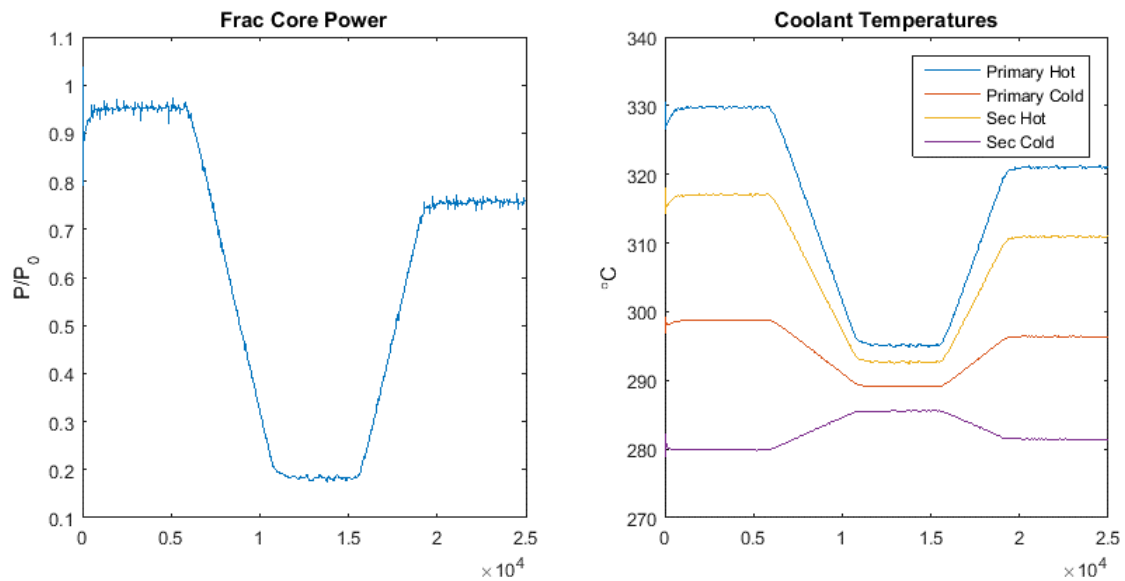


Figure 4-13. Reactor control by average primary coolant temperature program ranging from average temperature at full power (114.25 $^{\circ}\text{C}$) to flashing drum operating temperature (286.6 $^{\circ}\text{C}$). Power is varied between full power and 20% of full power at a rate of 1% per minute.

While this is a general definition not particular to the nuclear power industry, it is useful to describe the landscape of what we want to achieve in advanced I&C for future nuclear power plants. State awareness is a complete operational picture of the power plant, including the ability to detect and diagnose any anomalous condition, whether malicious or otherwise. The ability to maintain a particular level of normal operation involves the pre-planned, and ideally automated, response to the detection of an anomalous condition. Digital I&C and automated response actions pose risks and questions as to the vulnerability of such an integrated system to cyber-attacks. When the consequence of a catastrophic failure is extremely high, as it is in a nuclear power plant, the safeguards must be robust enough to drive the frequency of such failures to arbitrarily small values. Part of how this is achieved is by isolating the RPS and all safety related instrumentation, control, and actuation equipment from the systems which will respond automatically. This isolation is intended to ensure that no matter what happens to the automated systems, the safety systems ensure safe shutdown of the plant in the event that the operational margins, or trip points, of the plant are exceeded. If that can be achieved, then the improvements to anomaly detection, isolation, and automated response, which make up a resilient control system, operate fully within the realm of performance and reliability, rather than safety. This is the intention of the application of resilient control strategies to the I²S-LWR.

In 2012, Idaho National Laboratory (INL) published a report on design bases for achieving fault tolerance and resilience [Quinn, et al, 2012] in which they analyzed NRC licensee event reports for reactor scram events in which a better designed system may have prevented the scram. Their selection criteria were events occurring between January 1, 2007 and July 1, 2012, attributed to the following:

- *“Maintenance or testing was in progress on any sort of control system that caused the reactor scram.*
- *Operators took manual control of a normally automatically controlled system and were unable to adequately control the system which resulted in the scram.*
- *An automatically controlled system failed causing a reactor scram, but sufficient equipment remained in service that it may have been possible to remain online if the system could handle the perturbation.”*

For the events which met the criteria, the causes of the scrams are reported in Table 4-1. The two most frequent causes of trips were failure of electronic components and human error by operator or technician. This shows considerable room for improvement in areas of electronic redundancy and personnel training.

Table 4-1: Total reactor scrams fitting criteria by cause [Quinn, et al, 2012].

Cause	Total	Air	Design	Electronic	Error	Hyd	Motor	Proc	Pump	Relay	Valve
Trips	99	8	3	43	19	4	2	8	5	4	3

Key: **Air:** A component in the air supply failed. **Design:** A design failure was the direct cause of the trip. **Electronic:** An electronic component failed that caused the trip. **Error:** An error on the part of a technician or operator caused the trip. **Hyd:** A component in the hydraulic supply failed. **Motor:** A motor failed. **Procedure:** An error in a procedure directly resulted in a trip. **Pump:** A pump or component integral to the pump failed. **Relay:** A relay failed. **Valve:** A valve failed.

From a detailed analysis of the data, found in the INL report, the authors of the report recommended the following list of opportunities to reduce the frequency of reactor trips in operating commercial power plants. It follows that this experience gained from analyzing systems responsible for common failures in operating reactors should be considered when designing the systems in new reactors. Hence, it is recommended that the incorporation of these approaches into the I²S-LWR design concept:

“Redundant feedwater controls, automated response to a feedwater or condensate pump trip, rapidly reducing power to avoid a reactor trip, and elimination of air operators for the feedwater control valves or providing redundant air supplies for these valves.”

One mechanism of integrating more capability and automation into the control system is to have multiple modes of control which are implemented based upon the state of the plant. Under normal conditions, the plant will operate under a robust control paradigm, designed to maximize performance and accommodate normal operational transients, etc. When the plant enters an abnormal state, a different control paradigm could be used, one optimized to minimize the impact of an adverse condition, potentially keeping the plant in operation rather than initiating a scram. Further, resilient control could be designed to sacrifice performance or components to minimize the probability of core damage,

achieving a safer transition to the new steady state. It is important to note that regardless of the control paradigm employed, all automated control actions would take place within the state space protected by the reactor protection system. It is not proposed to exceed any safety trip point without tripping the reactor protection system. Jin, Ray, and Edwards [Jin, et al, 2010] propose a combination of robust and resilient control which toggles between the two paradigms based upon detection of a sufficiently anomalous condition.

To test their integrated robust and resilient control paradigm, Jin, et al. simulated a 50% LOFA in a simulator of the IRIS. The results of simulation indicate that the resilient controller recovers from the accident with a fast response, while the characteristics of standard robust control are maintained during normal operation. Physically, this is achieved with a combination of reactivity insertion via control rods as well as predictive adjustment of the feedwater flow rate. As soon as the fault is detected, the controller switches to resilient control, and the set points for output power and feedwater flow rate are reduced by half. During the transition from the robust controller to the resilient controller, a transfer function is used to smooth the controller outputs so as not to introduce instability into the system. Consequently, while the new set point of the feedwater controller and reactor power controller is half of the nominal value, the actual control action is to increase the feedwater flow rate by 10%, while reducing the rod reactivity by nearly 80%, over approximately 300 seconds. The net effect is to bring the reactor to 50% power over approximately 400 seconds.

The approaches of combined control systems, increased electrical component redundancy, and automated response to trips and transients should be included in the I²S-LWR design in order to maximize the goals of inherent safety while also paving the way for the best performance and reliability in future nuclear power plants.

5 ANOMALY DETECTION AND ISOLATION

5.1 Auto-Associative Kernel Regression Data Based Modeling

Fault detection and isolation by data-based modeling and statistical decision making requires good data. The I²S-LWR has plenty of sensors to provide that data. In this work, simulated plant data from the dynamic models previously described will be used, as real data do not exist for a hypothetical plant. These data, real or simulated, are used to develop auto-associative kernel regression (AAKR) models, which are a subset of locally weighted regression models. Auto-associative models seek to capture what the normal relationships are between signals so that the predicted value of each signal is consistent with the measured signal under normal conditions. The goal is for the model to predict accurate values even if the input data from the plant contain errors. This discrepancy between prediction and sensor reading is the basis of fault detection.

Locally weighted regression is a modeling technique in which values within the training data are given relative importance in the model prediction based upon the proximity of the data points to the input query point. Data that are nearby will have a greater influence on the model prediction. Data that are far away will have little or no influence on the model prediction. Proximity is calculated as the Euclidean distance between the data points in n -dimensional space, where n is the number of signals being modeled. The kernel function is responsible for calculating the importance, or contribution, of each point in the training data to the prediction value. The kernel function used in this research is of the Gaussian form. This kernel function is shown in the equation below. In the equation, d is the Euclidean distance, h is the model bandwidth, and w_i is the weight applied. The kernel function is tuned by the bandwidth of the function, which essentially determines the second statistical moment, or variance, of the function.

$$w_i = K(d) = e^{-\left(\frac{d^2}{h^2}\right)} \quad \text{Eq. (28)}$$

The optimal bandwidth is determined by a bootstrap method. First, a range is defined within which the bandwidth is reasonably expected to be. This is based upon expertise, prior knowledge of the systems, or trial and error. Then this range is divided into 10 or 20

equal size bandwidth steps. An AAKR model is then built for each of the various bandwidths and evaluated against the data. The bandwidth with the lowest root-mean-square error (RMSE) is the optimal bandwidth. This bandwidth is then surrounded and ten more models are made in smaller bandwidth increments. This process repeats until the RMSE is small enough and is acceptable. Acceptability is based upon engineering judgement for the application, or trial and error application of the model on representative data. Real signals often contain measurement noise, and not all of this noise can be filtered out with signal processing techniques. Consequently, it is important to check that the bandwidth has not been made so small as to over-fit the data. Over-fitting occurs when the model settles on a bandwidth which minimizes the RMSE of the training data, but which is not representative of the dynamics of the data, but rather the noise in the data.

To optimize the model, normal data are split into three subsets: training data, testing data, and validation data. Training data is the largest set representing all the states the model should to handle. Training data is used to build the model. Testing data is used to optimize the model. Validation data is used to evaluate the model performance, characterizing the variance of the noise in the system. The model can further be characterized by a Monte-Carlo based uncertainty estimation which characterizes the variance and bias in the predictions of an arbitrary number of different models built on the same data. From the noise variance, prediction variance, and bias, confidence intervals and prediction intervals can be calculated for each variable in the model.

5.2 Sequential Probability Ratio Test

Once the kernel function bandwidth has been established and the resulting model has been characterized, the model can be used as part of a fault detection regime. To do this, an AAKR model is constructed around each query data point, or data from the plant computer we wish to check for consistency with the data based model. Using the query data and the kernel function, the model calculates predicted values of the plant variables. If the regression model is good, then the outputs of the model will be very close to the outputs of the normal plant.

As each new data vector is processed by the fault detection regime, the difference between the query values and the values predicted by the AAKR model are concatenated

into a matrix. These difference values are called residuals. Statistical decision making compares the statistics of the query residuals to the statistics of the validation data residuals to determine if there is an anomaly in each of the signals. The statistical decision making method employed here is sequential probability ratio testing (SPRT). It is sequential because the test statistic is computed for the entire set of data at each observation, using a larger set of data points at each step of the test. The test statistic used in SPRT is the ratio of likelihood functions, typically employed as the natural logarithm of the likelihood function for efficiency of use with multiple variables. The likelihood of a set of parameters, (observed data) given an outcome, (fault or no fault) is equal to the probability of the outcome, given the data. In the likelihood ratio, the numerator is the maximum of the likelihood function for the null hypothesis outcome (no fault scenario) and the given set of parameters (data), while the denominator is the maximum of likelihood function for the null hypothesis outcome while varying the parameters of the entire space of values. Large values of the likelihood ratio indicate that the evaluated set of parameters are likely to have occurred under the null hypothesis, while small values of the ratio indicate it is more likely that the set of parameters occurred under an alternate hypothesis (fault scenario).

SPRT computes the likelihood ratio at each observation and adds this value to the running sum of likelihood ratios. When the running sum of ratios crosses either an upper or lower threshold, the test reports the appropriate conclusion of confirming or rejecting the null hypothesis, resets the running sum to zero, and begins again. In the implementation used in this work, each observation for which the test has not made a decision is recorded as the null hypothesis because the reporting is binary.

In order to calculate the probabilities in the likelihood ratio, the probability density functions of the residuals for the normal and faulted hypothesis must be established. The implementation used in this work assumes the probability density functions to be Gaussian, thus describable by mean and variance. The mean and variance of the normal distribution of residuals are calculated from the normal data used to train the kernel regression model. The mean and variance for the faulted distribution must be provided by the user based upon engineering judgement and prior knowledge or data of the fault pathway being monitored. If the distributions of residuals in the normal data and faulty data overlap, then in this area, SPRT is prone to type one and type two errors. When this happens, the result is a lot of

fault hypothesis observations mixed with a lot of no-fault hypothesis observations. In the graphical plotting of the results, this appears as a continuous line of both faulted and non-faulted observations.

The implementation of the AAKR modeling and SPRT fault detection is performed using the Process and Equipment Monitoring Toolbox for Matlab, which is developed, maintained, and copyrighted by researchers in the Department of Nuclear Engineering at the University of Tennessee [Hines and Garvey, 2005].

5.3 Simulated Anomalies

Three different types of anomalous conditions within the plant are simulated. Sensor drift, coolant flow rate reduction, and heat exchanger fouling. Normal data used to create data based models is plant simulation data, typically over a range of power levels so that the model is built using data which contains dynamic behavior and encompasses a range of operating states, ensuring that the operating states present in the simulated anomaly data are represented by the model. All of the simulations contain process noise added to the system as core reactivity. For all of these scenarios, the false alarm and missed alarm probabilities (type I and type II errors, respectively) must be specified to the algorithm. In these analysis, a false alarm probability of 0.01 and a missed alarm probability of 0.1 are used. For a slowly developing fault, a missed alarm is not a high consequence scenario, as the fault will continue developing until it is detected. Conversely, a false alarm carries a high penalty because it may cause unnecessary shutdown and maintenance activity. This is the justification for the large difference between the error probabilities.

5.3.1 Sensor Drift

5.3.1.1 Sensors Affecting Control

Sensors which are used by the control systems to regulate the plant have an increased impact on operation and safety when they malfunction. To evaluate this the hot leg signal which feeds the average primary coolant temperature based reactivity controller information about the primary coolant hot leg temperature, is subject to a simulated drift. The drift simulation here is accelerated for the purposes of demonstration and computational efficiency. A positive drift of 10°C occurs over one hour, beginning at 100 seconds into the steady state full power simulation. Signals for reactor power, coolant

temperatures, and coolant flow rates are used to develop the AAKR models and makeup the faulty data set. Normal data for this model consists of load following data for the plant. Figure 5-1 shows the plotted residuals, or differences between regression model output and measured signal, for all the signals in the drifting data set, as well as the overall fault hypothesis for the presence of a fault in the query data set. Figure 5-2 shows the individual fault hypothesis from the SPRT of each variable in the data set. These variables are, in order: reactor power, primary coolant hot leg temperature, primary coolant cold leg temperature, secondary coolant hot leg temperature, secondary coolant cold leg temperature, secondary coolant flow rate, and primary coolant flow rate. The impact of the sensor drift on the other variables, via the control system is evident in the SPRT's inability to decide if the individual signals are faulted, as they are all showing increasing residuals as the sensor drift simulation progresses. However, it can be seen that the second variable, corresponding to hot leg temperature, is the first sensor to be continuously hypothesized as faulted.

5.3.1.2 Redundant Sensors

Distinguishing drifting sensors from among multiple redundant sensors is important for taking accurate readings and removing faulty sensors from control logic. In this scenario, four redundant hot leg sensors are monitored against each other. A drift rate of 1% per month is simulated. Measurement noise is added by adding white Gaussian noise with a specified signal-to-noise ratio (SNR) of 50. This is an excellent SNR for signals acquisition, but still represents a significant amount of noise to leave unfiltered in the data for robust evaluation of the AAKR and SPRT algorithms. Further, the diagnostic result is filtered by adjusting the fault hypothesis to only return a fault if two out of three, or three out of four, consecutive data points met the faulty hypothesis test of the SPRT. This greatly improves fault isolation. These results are shown in Figure 5-3 through Figure 5-6.

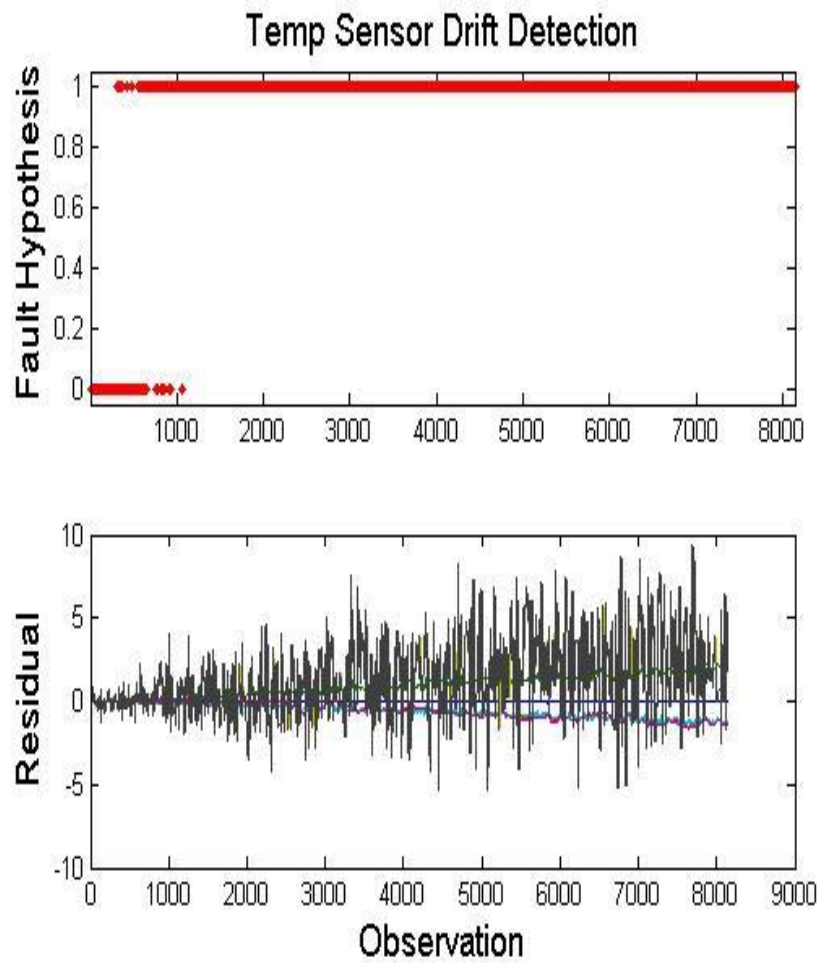


Figure 5-1. SPRT decision-making of the existence of a fault in the hot leg sensor drift data.

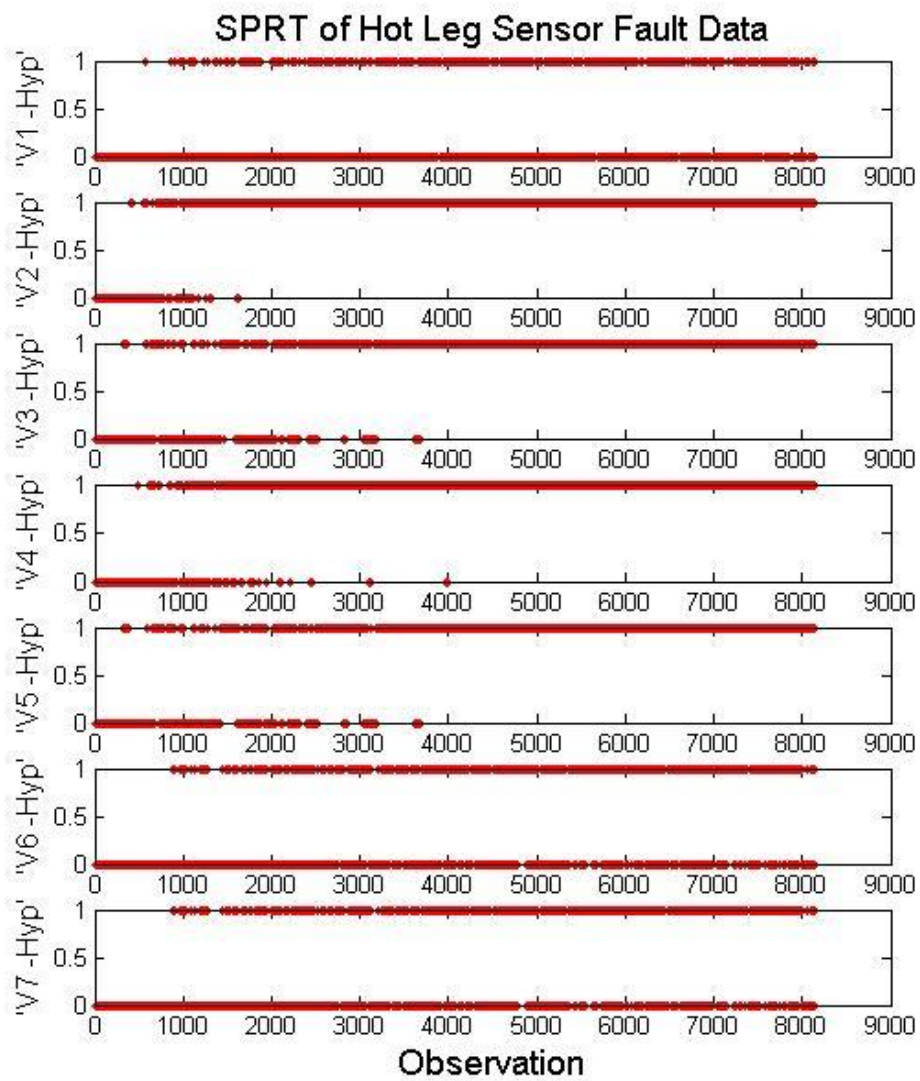


Figure 5-2. Fault isolation by comparison of SPRT results for each variable in sensor fault data set.

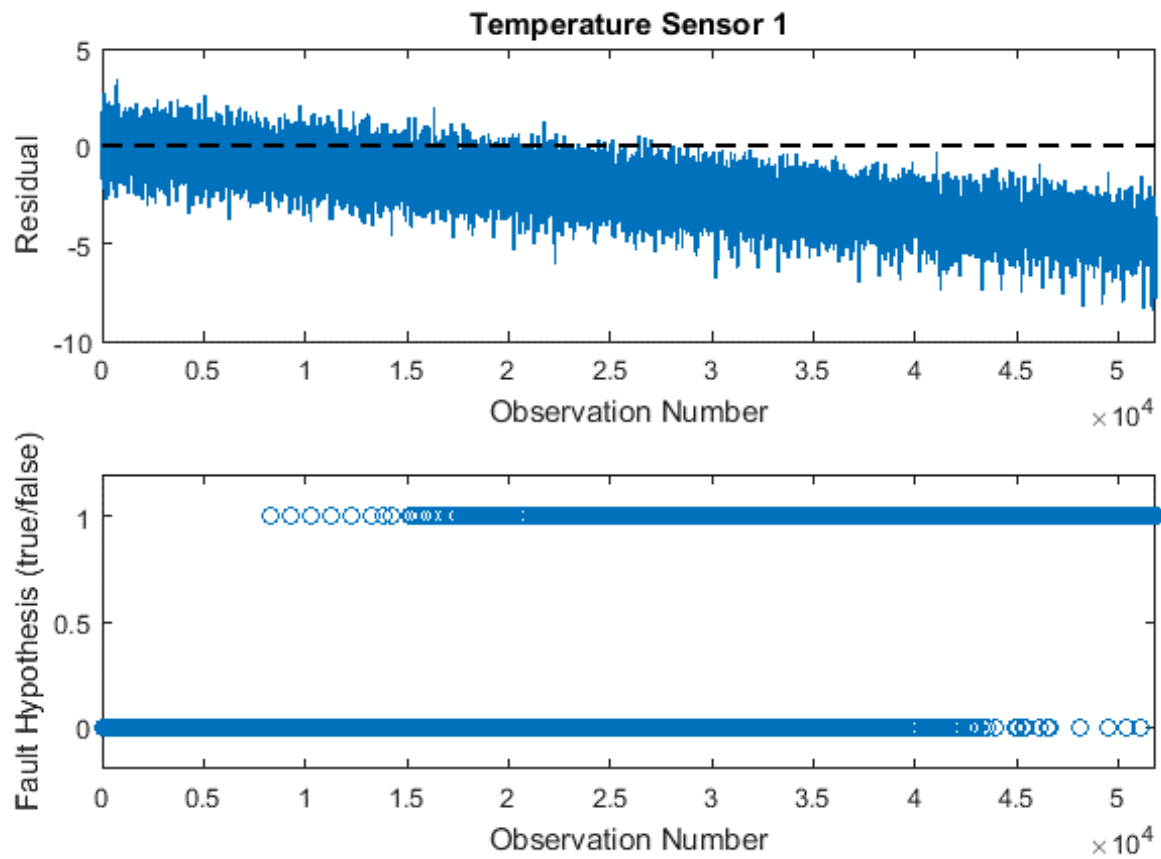


Figure 5-3. Fault hypothesis of drifting sensor among four redundant sensors. At a drift rate of 1%, or 3.3°C per month, the SPRT flags the error by about 17 days into the test, or about 1.9°C of drift.

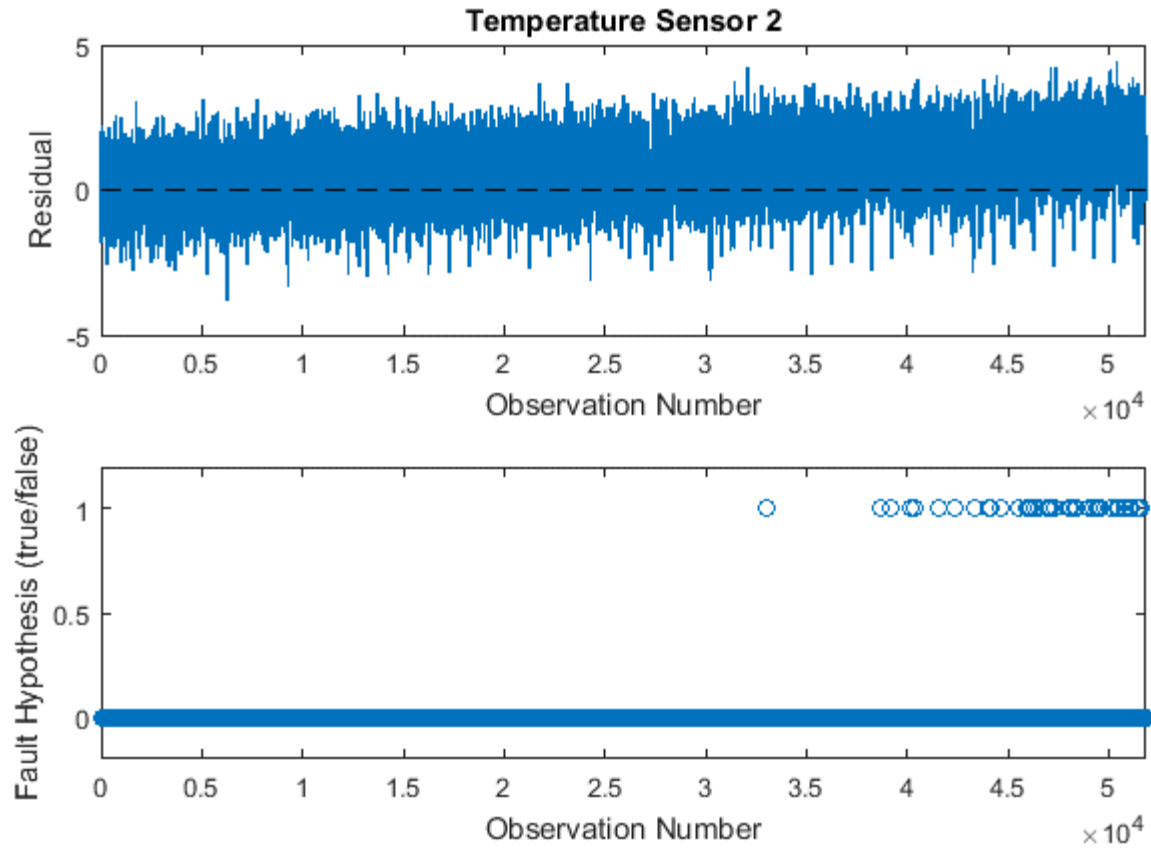


Figure 5-4. Fault hypothesis of non-drifting sensor number 2. If the test persists long enough, without the removal of the drifting sensor from the model, the SPRT eventually determines that the stable sensors are also erroneous. In practice, a drifting sensor is removed from the AAKR model when the drift is detected, allowing for continued, but less robust, monitoring of the remaining sensors.

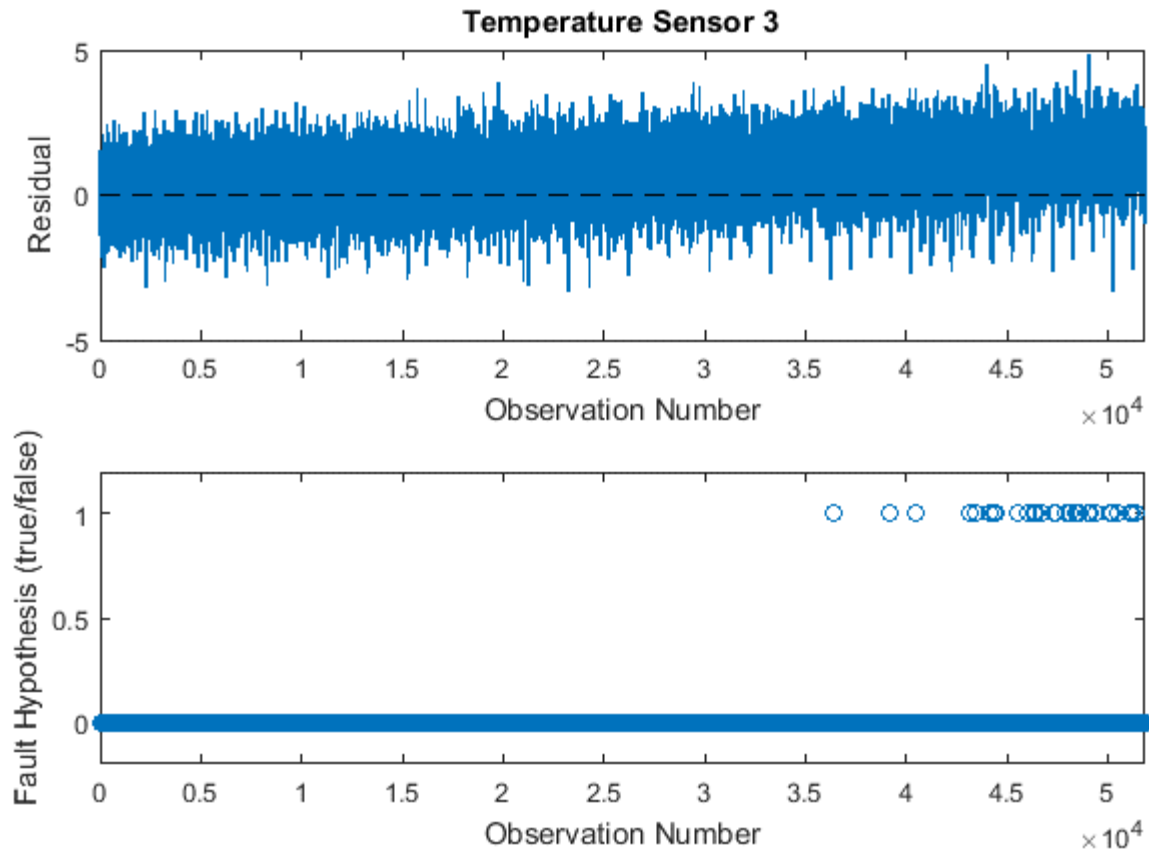


Figure 5-5. Fault hypothesis of non-drifting sensor number 3. If the test persists long enough, without the removal of the drifting sensor from the model, the SPRT eventually determines that the stable sensors are also erroneous. In practice, a drifting sensor is removed from the AAKR model when the drift is detected, allowing for continued, but less robust, monitoring of the remaining sensors.

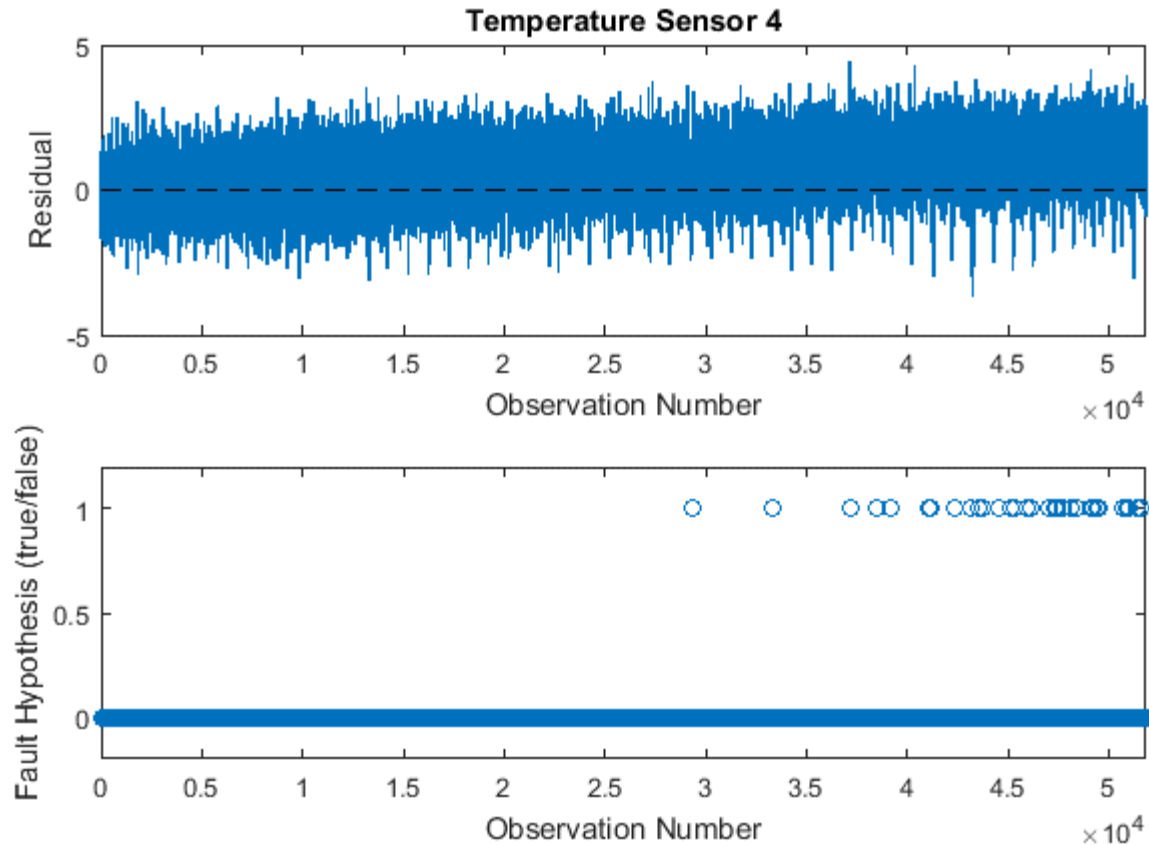


Figure 5-6. Fault hypothesis of non-drifting sensor number 4. If the test persists long enough, without the removal of the drifting sensor from the model, the SPRT eventually determines that the stable sensors are also erroneous. In practice, a drifting sensor is removed from the AAKR model when the drift is detected, allowing for continued, but less robust, monitoring of the remaining sensors.

5.3.2 Coolant Flow Rate Reduction

To simulate pump degradation, malfunction or flow channel obstruction not inside a heat exchanger, the secondary flow rate through the heat exchangers was simulated to decrease by 10% over an hour in order to evaluate how quickly the fault could be detected. In this scenario, the same training data and variables are used for data based modeling and fault detection as were used for the temperature control signal drift analysis. The rapid and obvious deviation of the regression model residuals is evident in Figure 5-7, as is the general SPRT conclusion of the presence of a faulted condition in the system. Analysis of the separate SPRTs of each signal in Figure 5-8 shows that the sixth variable, corresponding to the secondary coolant flow rate, is the first variable to be continuously hypothesized as faulty by the statistical decision making implementation.

5.3.3 Heat Exchanger Fouling

Heat exchanger fouling is simulated as a decrease in the overall heat transfer coefficient for primary to secondary coolant in the MCHX (U_{PS}). U_{PS} is linearly ramped downward at a rate of 1% per day. While this rate is not representative of a realistic fouling scenario, it is useful to examine how quickly, in terms of total fouling, the diagnostic algorithm resolves a fault hypothesis in various plant signals. The signals used for modeling and diagnostics in this scenario are reactor power and primary and secondary coolant temperatures.

The normal data used in this experiment is load following data with process noise. The experimental data is for steady state at full power operation with the heat exchanger fouling implemented as a ramp function. Figure 5-9 through Figure 5-13 show the results of SPRT analysis of each of the signals included in the AAKR model used to monitor for this fault scenario. Reactor power, in Figure 5-9, becomes sufficiently divergent from the model expected value by about 8000 observations, corresponding to nearly 6% fouling of the heat exchanger. For the hot leg temperature, shown in Figure 5-10, the fouling has to reach over 22% before the residuals are large enough for the fault hypothesis to settle on the faulted condition. This is likely due to the minimization of the effect the heat exchanger degradation has on the primary coolant after it has passed through the reactor core, where so much energy is added to it.

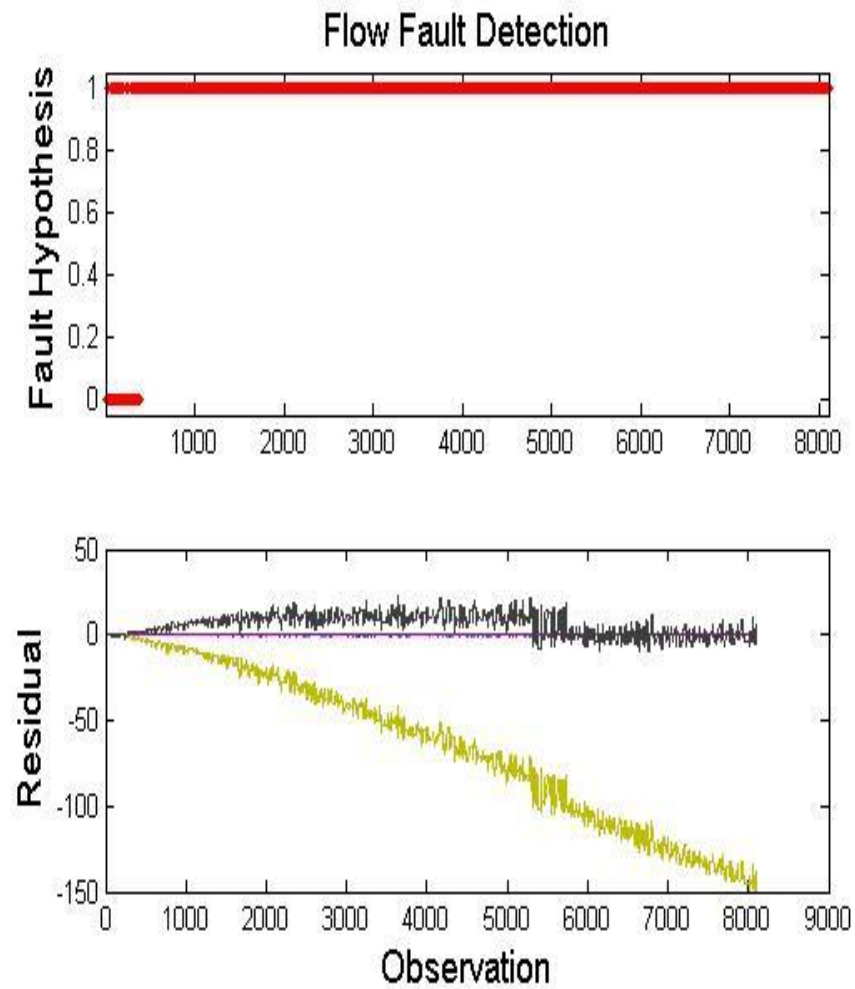


Figure 5-7. SPRT decision-making of the existence of a fault in the pump (motor) malfunction flow fault data.

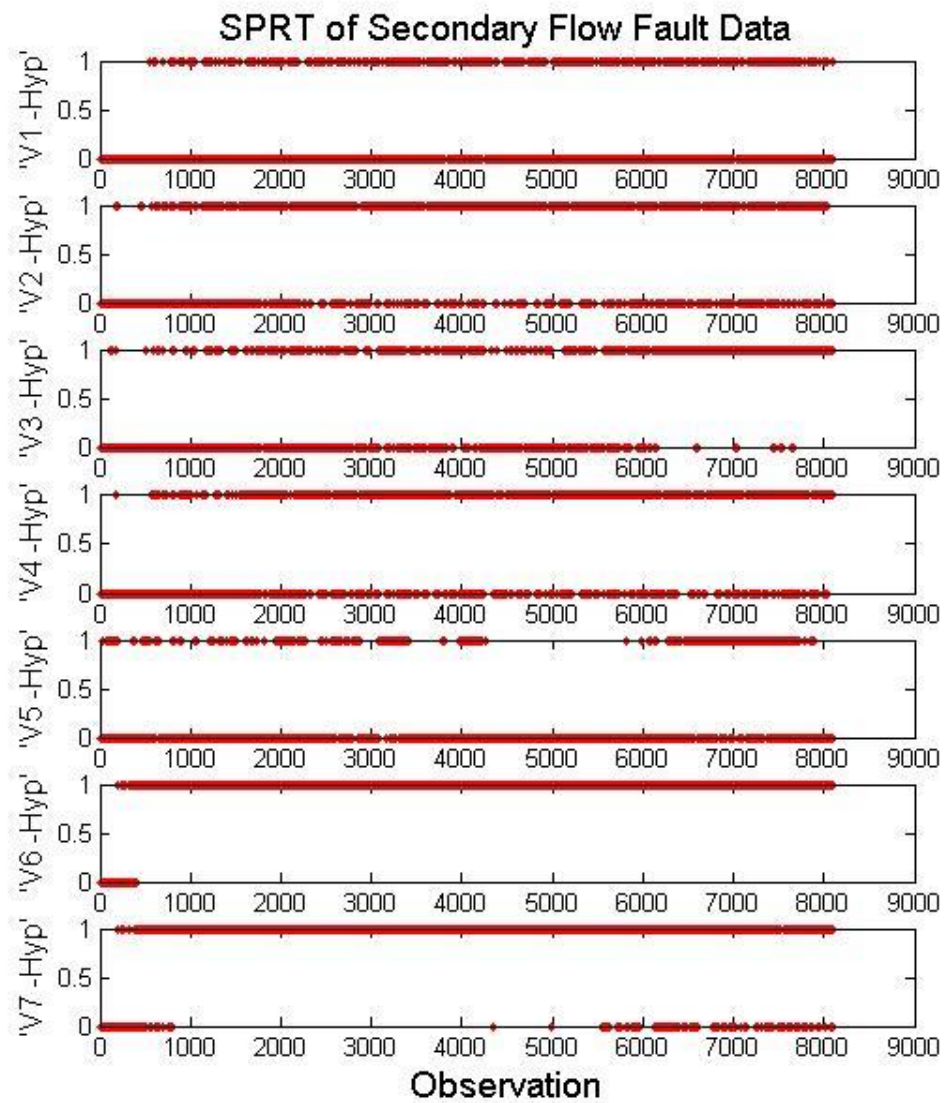


Figure 5-8. Fault isolation by comparison of SPRT results for each variable in flow fault.

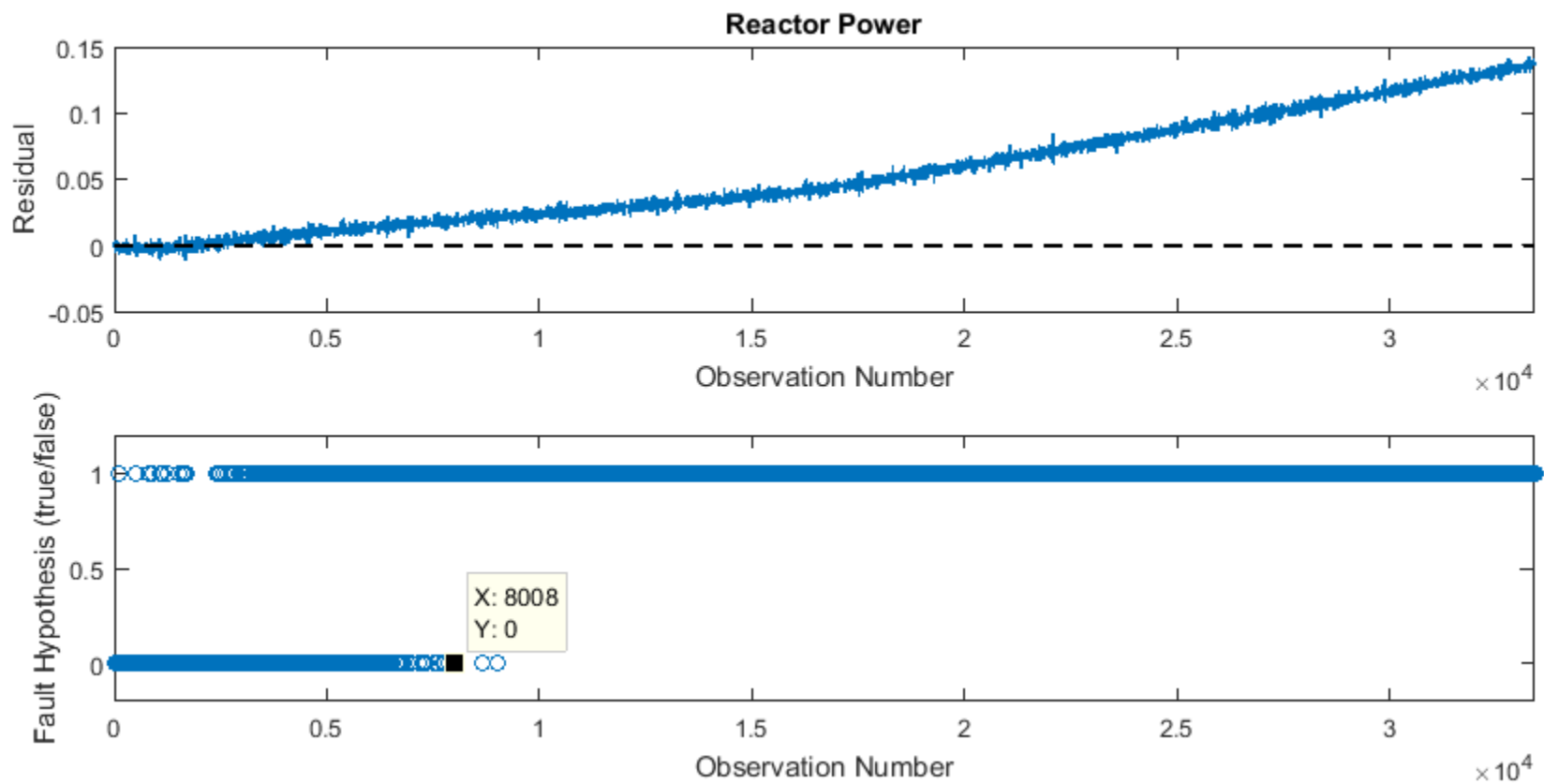


Figure 5-9. Anomaly diagnosis of presence of fault in the fractional reactor core power signal by SPRT under a simulated heat exchanger fouling scenario. After 8,008 observations, corresponding to 5.97% fouling, the ratio test settles on the faulted hypothesis.

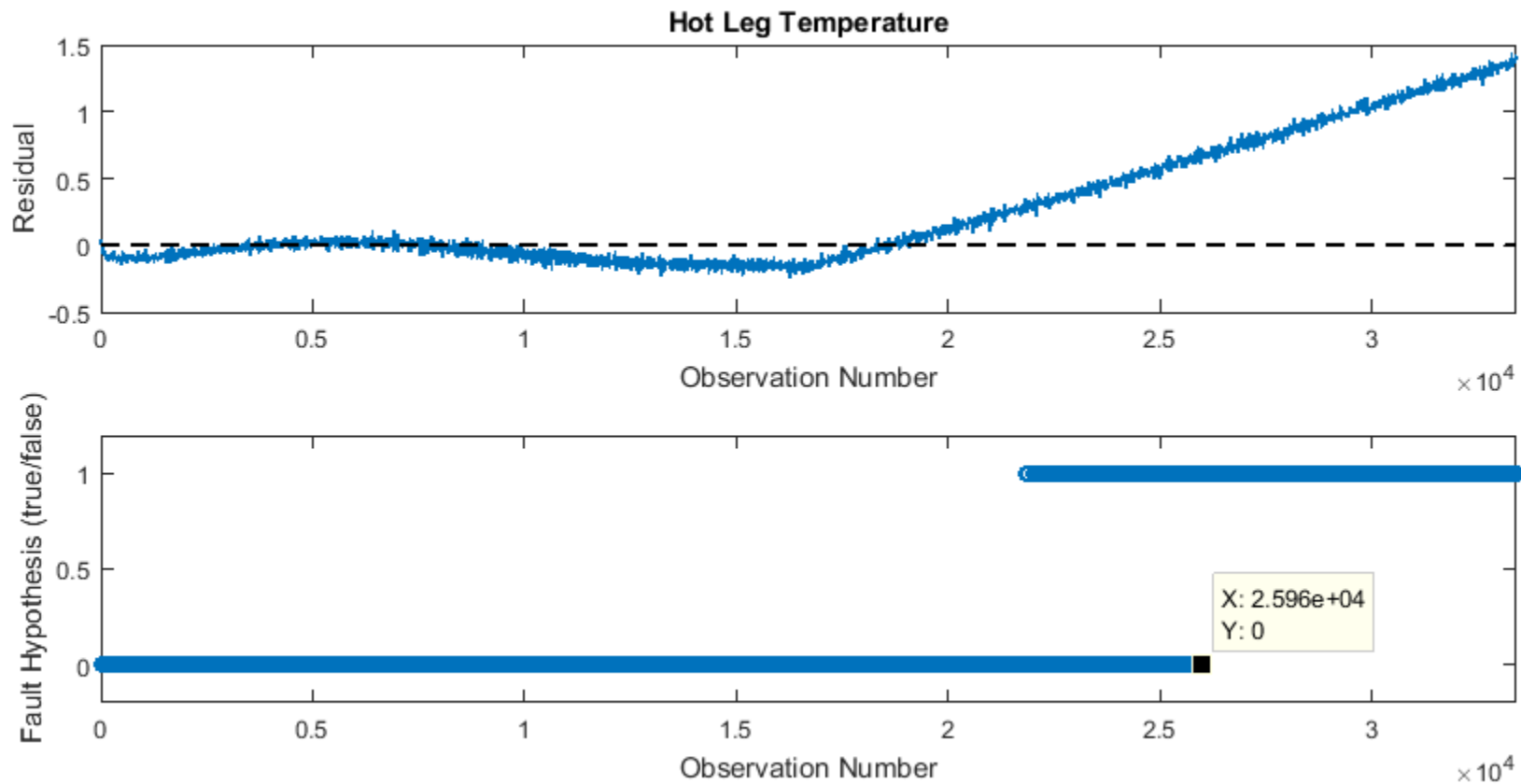


Figure 5-10. Anomaly diagnosis of presence of fault in the hot leg temperature signal by SPRT under a simulated heat exchanger fouling scenario. After 25,960 observations, corresponding to 22.16% fouling, the ratio test settles on the faulted hypothesis. This makes sense when it is considered that the effect of the heat exchanger fouling on hot leg temperature is minimized by the coolant passing through the core, where it picks up a lot of energy.

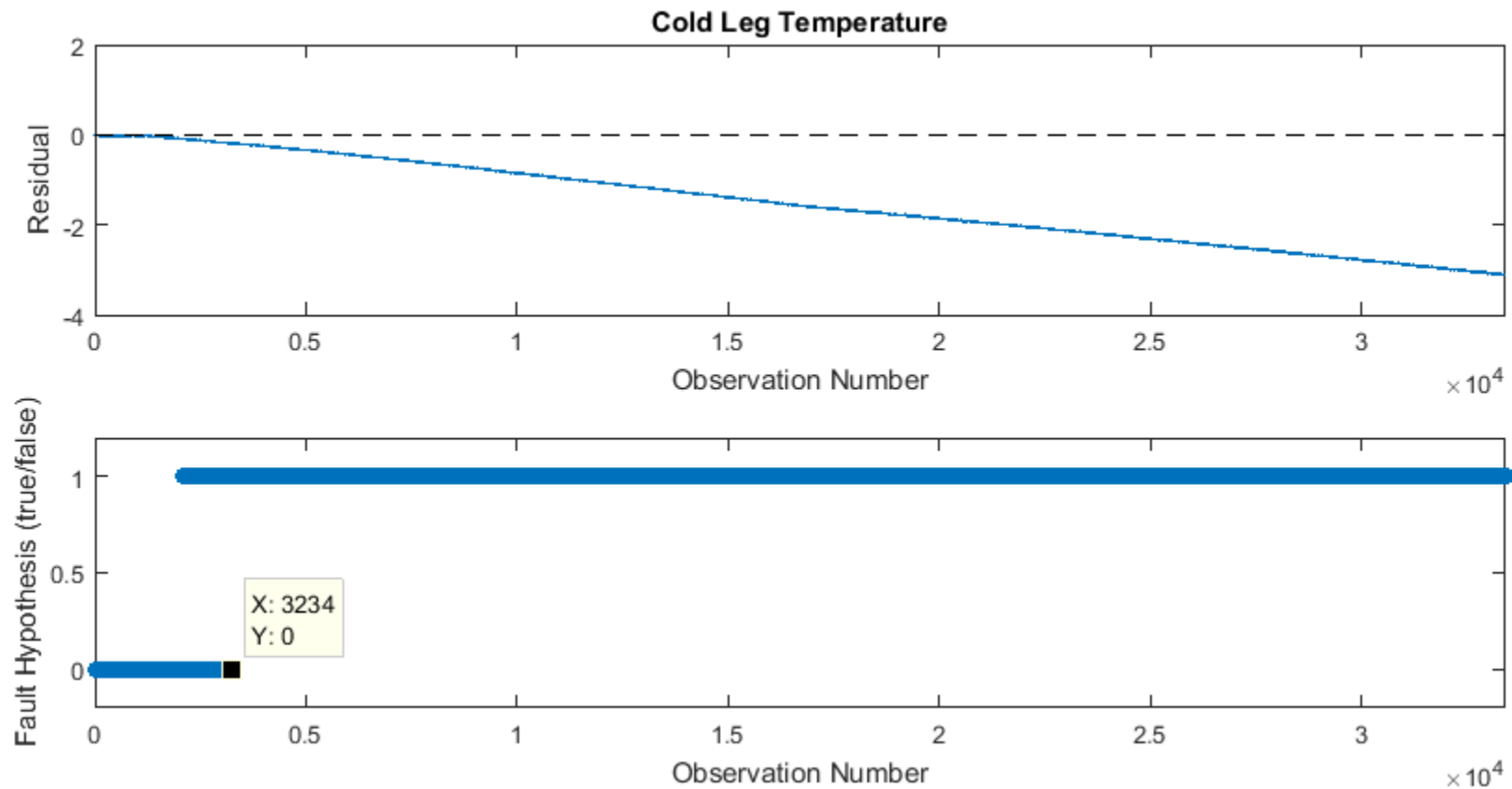


Figure 5-11. Anomaly diagnosis of presence of fault in the cold leg temperature signal by SPRT under a simulated heat exchanger fouling scenario. After 3,234 observations, corresponding to 1.78% fouling, the ratio test settles on the faulted hypothesis. This makes sense when it is considered that the effect of the heat exchanger fouling is most immediately reflected in less energy lost by the primary coolant, increasing the temperature of the secondary coolant as compared to the training data. This shows that the cold leg temperature signal is an important signal to monitor for heat exchanger performance.

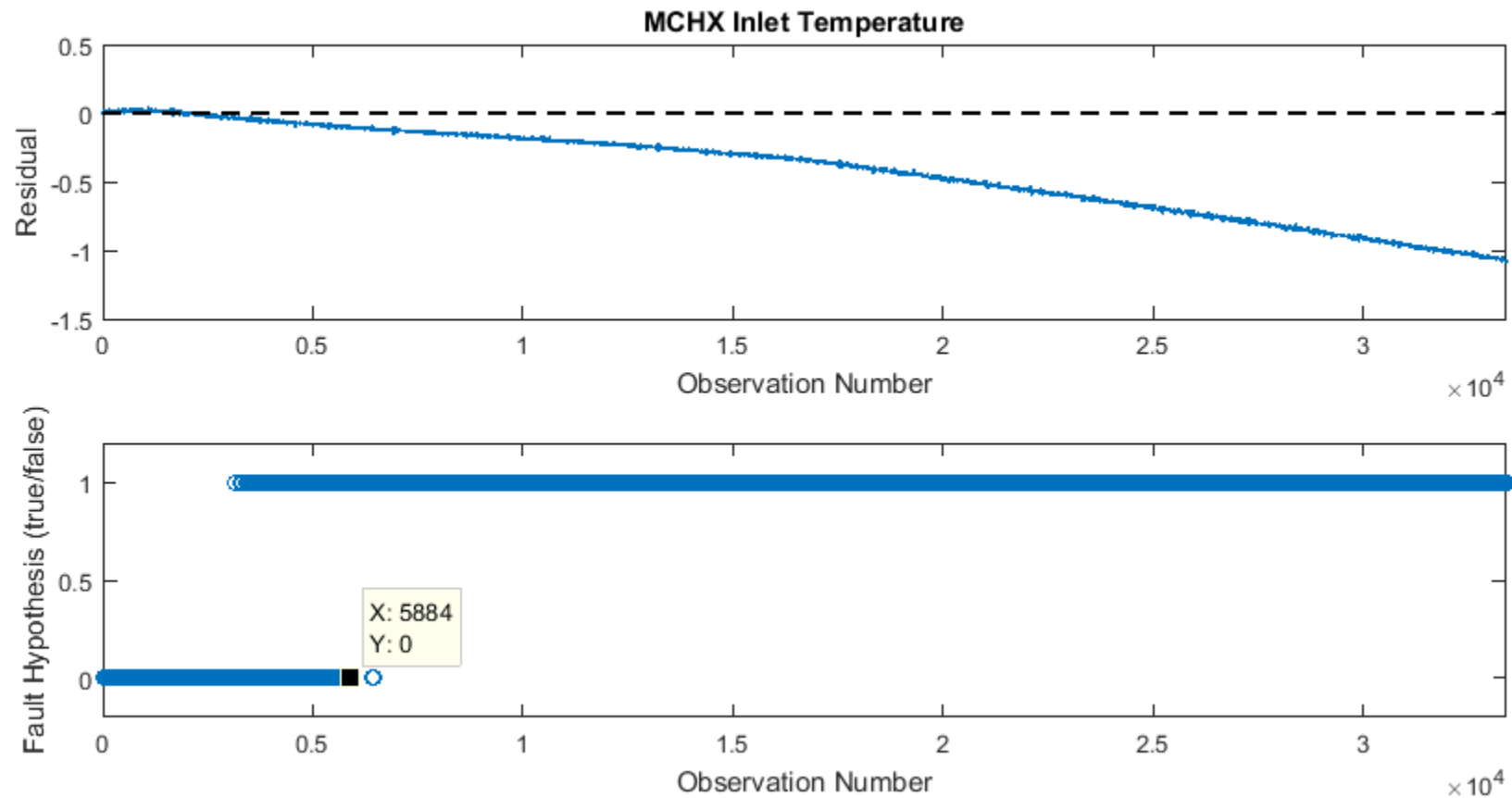


Figure 5-12. Anomaly diagnosis of presence of fault in the MCHX inlet temperature signal by SPRT under a simulated heat exchanger fouling scenario. After 5,884 observations, corresponding to 4.07% fouling, the ratio test settles on the faulted hypothesis.

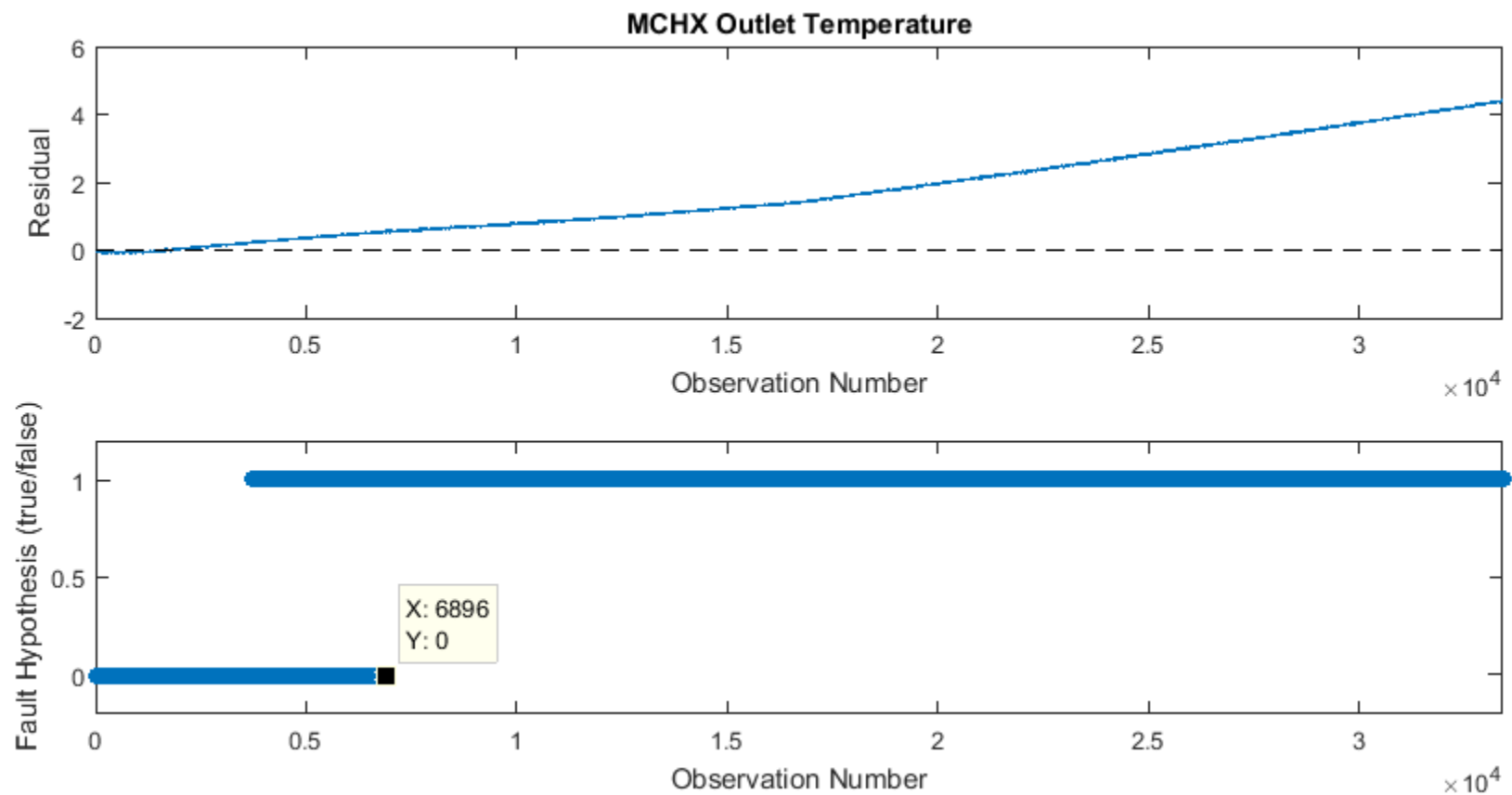


Figure 5-13. Anomaly diagnosis of presence of fault in the MCHX outlet temperature signal by SPRT under a simulated heat exchanger fouling scenario. After 6,896 observations, corresponding to 5.01% fouling, the ratio test settles on the faulted hypothesis.

The primary coolant cold leg and secondary coolant temperatures show fairly rapid detection of the fault condition. The primary cold leg signal, Figure 5-11, shows this degraded pathway the fastest, after 1.78% of the heat exchanger performance has been lost due to fouling. Secondary coolant temperatures reflected the faulted state conclusively at about 4% and 5% for the MCHX inlet (Figure 5-12) and outlet (Figure 5-13) temperature signals respectively. Based upon these results, the primary and secondary heat exchanger outlet temperatures are the best candidates to monitor for heat exchanger fouling. Further, algebraic energy balance across the heat exchanger can be calculated to monitor the heat exchanger. The technique shown here operates solely on existing signals.

6 SUMMARY, CONCLUSIONS, AND RECOMMENDATIONS FOR FUTURE WORK

6.1 Summary

The purpose of the Integral Inherently Safe Light Water Reactor is to make as many incremental technological improvements as are feasibly achievable in a next generation LWR in order to produce a near term deployable power plant that capitalizes on the many reactor years of operational experience and wisdom of LWR, presenting an economically competitive reactor with a demonstrably safer design. Nuclear power in the United States reigns as the safest form of electricity on the planet, bar none, in terms of deaths per unit of energy production [Gordelier and Cameron, 2010]. This is due in large part to the safety culture and strict regulatory burden. This regulatory burden also adds costs. One additional benefit of the I²S-LWR approach is the reduction of regulatory burden that can be achieved by eliminating accident scenarios. This dissertation focuses on the instrumentation and control of the I²S-LWR, particularly the challenges which this design concept poses for I&C. However, the dissertation also seeks to advance the premise of the design project in the I&C area, namely to propose an I&C approach for a near term deployable, economically competitive, safer reactor to carry the burden of nuclear base load generation, while providing the flexibility for future applications of nuclear power, such as co-generation with water desalination. Much of the domestic nuclear fleet will reach the end of its operational lifetime by 2050, and something has to take its place. The I²S-LWR could be a suitable candidate for that role, as well as other roles for future nuclear power generation.

Pursuant to the I&C goals for the I²S-LWR, this dissertation has evaluated the process measurements that need to be taken to safely and efficiently operate the plant, proposed means of taking those measurements, proposed strategies for controlling the operation of the nuclear steam supply system side of the plant based upon those measurements, and proposed means of monitoring the plant for anomalous conditions using established techniques in the field of fault detection and diagnosis. In support of these accomplishments, the dissertation also presents the low fidelity dynamic modeling of the component systems for generating energy from nuclear fission and transporting that energy to a steam turbine for electricity generation. This modeling is necessary to examine how

the different systems interact with one another in transient states and as the power output level of the plant changes, allowing for the examination of different approaches to controlling the plant. The models have further served to simulate scenarios of equipment degradation, reducing component performance. The simulated data have been used to develop and demonstrate approaches for monitoring the condition of these components and detecting and diagnosing these components when they degrade. This kind of automated approach will be critical in future nuclear power plants in order to reduce operation and maintenance costs to compete with advancing technology in other power generation sectors. The deployment and demonstration of these techniques may also serve to build a body of evidence which may lead to a reduced regulatory burden on plants operating with such highly sophisticated systems for monitoring plant health and performance.

Significant instrumentation challenges faced by the I²S-LWR involve:

- rapid response time measurement of primary coolant flow rate,
- placement of temperature sensors to accurately measure primary coolant temperature with acceptable signal to noise ratios, despite needing long cable runs to access primary coolant after it has passed through the heat exchangers and mixed,
- measurement of neutron population in the source and intermediate ranges, without having to replace the measurement equipment unacceptably often due to degradation during full power operation.

The dissertation has proposed that the best candidate for measuring flow rate is the use of ultrasonic, reflection mode transit time flow meters mounted outside of the process, on the exterior of the RPV. Work needs to be done to develop this technology for application to large, thick vessels such as are typical for nuclear pressure vessels. Another promising candidate is noise analysis of signals from fixed in-core neutron detectors and core-exit thermocouples. This analysis can produce rapid response time data about the linear flow rate of coolant in various locations in the core, developing a flow profile and a measure of overall core flow rate. Fully submersible resistance temperature detectors, and housings, need to be developed for application to this reactor in order to avoid pressure vessel penetrations in the lower portion of the vessel, where they are prohibited as a design basis of the reactor. Silicon carbide neutron detectors utilizing lithium-six converting layers are

suitable compromise detectors for placement in the downcomer region of the I²S-LWR, outside of the core, for safety related source and intermediate range neutron population monitoring. If placed at an appropriate radius within the downcomer, they achieve both necessary sensitivity and acceptable lifetime.

Dynamic modeling of the reactor systems produced stable, low fidelity simulation models suitable for feasibility studies of control, monitoring, and diagnostics. The models produced operate with stability and produce numerical results for steady states that are in agreement with the design basis operating points of the I²S-LWR. These models have been used to develop and evaluate control strategies for the reactor core, and steam flashing drum. Reactor core reactivity control is based upon a moving set-point for the average primary coolant temperature. This is done with a PID controller. The set-point moves between the average primary coolant temperature at full power and the saturation temperature of the secondary coolant at the drum operating pressure. This is because the drum pressure remains constant throughout operation, by design. Because of this, the temperature of the recirculation coolant in the drum must be the zero power temperature of both reactor coolants. When not producing power, the coolant flowing through the secondary side of the each exchanger, and not exchanging energy with the primary coolant, is at the drum operation temperature. For no exchange of energy to take place, the primary coolant must also be at this temperature. Implementation of this approach was demonstrated successfully for load following operation. Control of the flashing drum is achieved with two controllers. The drum level is maintained by adjusting the feedwater flow rate using a PID controller. The drum pressure, and thereby the steam pressure delivered to the turbine, is controlled by adjusting the steam flow rate using a throttling valve. Together, these two controllers maintain the flashing drum at the optimal condition to maximize the overall efficiency of the power conversion system.

The monitoring and diagnostics work has used data generated by simulating various kinds of equipment degradation in the plant model to demonstrate the applicability of established techniques for fault detection and isolation to the automated condition monitoring of the I²S-LWR. Detection of sensor drift affecting a control system, sensor drift by one of four redundant sensors, coolant flow reduction, and heat exchanger fouling have all been demonstrated.

6.2 Conclusions

The I²S-LWR can be instrumented, controlled, and autonomously monitored with application and some advancement of existing technology. This work has identified no unsurmountable issues in these areas that would prevent the realization of the design concept. The instrumentation approaches still require additional research and development before the technology can be deployed. These tasks should be able to be completed in order to achieve deployment of the reactor concept before the current fleet of reactors has largely been retired. The same is true of the control approaches. Established techniques for controlling process systems will serve to control the I²S-LWR. Advances in control approaches can only serve to improve the performance and economic competitiveness of the reactor system. Advanced monitoring and diagnostics can be implemented to improve plant reliability, increase plant performance, and reduce operations and maintenance costs by providing the information for intelligent planning of maintenance activities.

6.3 Recommendation for Future Work

There is plenty of work to be done in several discrete areas to continue the research and development of the I&C for the I²S-LWR. There are future directions for work in instrumentation, modeling, control design, and holistic integration and implementation of plant monitoring techniques.

In the area of instrumentation, a thorough evaluation of the flow characteristics of coolant within the primary loop of the reactor is needed in order to validate the number and location of temperature sensors that are required to accurately monitor primary hot leg and cold leg coolant temperatures. Ultrasonic technology needs to be scaled, advanced, and tested for use operating on large vessels through 10 in (25.4 cm) of steel, as well as tested to determine the best location, azimuthally and axially to place the meters for accurate flow measurement. The number of sensors needed to monitor the overall flow rate also needs to be determined. Cross correlation of in-core neutron detectors and core exit thermocouples is another candidate for estimating flow transit time, however the body of evidence for this approach is too small. This area need further study to characterize the accuracy and uncertainty, and response time of the approach.

The next step in the modeling and control system design is high fidelity modeling. The models used to design specific control actions, controller parameters, and determine instrument and actuator performance requirements must accurately portray the temporal evolution of mass and energy around the plant. Instruments, actuators, and control hardware must be included in the modeling. This work only demonstrated the most rudimentary of monitoring and diagnostic implementations. Integrated monitoring systems connected to data from all the plant sensors are far more powerful than the simple systems demonstrated here. Implementation of thoroughly developed systems, along with remaining useful life estimation techniques has great potential to reduce maintenance costs and improve plant performance and reliability.

REFERENCES

Anderegg, W.R.L., "Expert Credibility in Climate Change," *Proceedings of the National Academy of Sciences* Vol. 107 No. 27, 12107-12109 (21 June 2010); DOI: 10.1073/pnas.1003187107.

Arizona Public Service Company, "Palo Verde Final Safety Analysis Report", Rev. 14, Tonopah, Arizona, June 2007.

Arkansas Power & Light Company, *ANO-Unit 2 FSAR*, Arkansas Power & Light Company, Doc. No. 50-368, 1978.

Bisconti Research, Inc. "Public Favorability of Nuclear Energy Climbs for Today's Reactors, Future U.S. Development and Global Leadership," 17 March 2015. www.bisconti.com

Bisconti Research, Inc. "6th Biennial Survey of U.S. Nuclear Power Plant Neighbors: Broad and Deep Support For Nuclear Energy and the Nearby Plant Continues," Summer 2015. www.bisconti.com

Caldon, Caldon Experience in Nuclear Feedwater Flow Measurement, Publication No. MLI62, Rev. 2, Cameron International, Houston, TX, 2006.

Cook, J., et al, "Consensus on consensus: a synthesis of consensus estimates on human-caused global warming," *Environmental Research Letters* Vol. 11 No. 4, (13 April 2016); DOI:10.1088/1748-9326/11/4/048002.

Cook, J., et al, "Quantifying the consensus on anthropogenic global warming in the scientific literature," *Environmental Research Letters* Vol. 8 No. 2, (15 May 2013); DOI:10.1088/1748-9326/8/2/024024.

Doran, P.T., and Zimmerman, M.K., "Examining the Scientific Consensus on Climate Change," *Eos Transactions American Geophysical Union* Vol. 90 Issue 3 (2009), 22; DOI: 10.1029/2009EO030002.

Ferroni, P., *Private Communication*, Westinghouse Electric Company, 30 Apr 2015.

FLEXIM, Technical Specification WaveInjector, [Internet], Berlin, Germany, 2013 [cited 2015 Feb 4] Available from: <http://www.flexim.com/us/waveinjector>.

Garimella, S., Colin, S., Dongqing, L., and King, M.R., "Single-Phase Liquid Flow in Minichannels and Microchannels." *Heat Transfer and Fluid Flow in Minichannels and Microchannels*. (Ed) S. G. Kandlikar. Amsterdam, Netherlands: 2005.

Goncalves, F.M., et al., "Dynamic Simulation of Flash Drums Using Rigorous Physical Property Calculations," *Brazilian Journal of Chemical Engineering*, Vol. 24, No. 02, pp. 277-286, April-June 2007.

Gordelier, S., and Cameron, R., "Comparing Nuclear Accident Risks to Those from Other Energy Sources," Nuclear Energy Agency, Organisation for Economic Co-operation and Development. 2010. ISBN: 978-92-64-99122-4

Heibel, M., and Kistler, D., "Core Power Distribution Measurements Using Long-Lived Vanadium Incore Detectors in the AP1000TM," Presentation at the 17th International Conference on Nuclear Engineering, July 2009, Brussels, Belgium.

Hines, J.W., and Garvey, D., "The development of a process and equipment monitoring (PEM) toolbox and its application to sensor calibration monitoring." *Fourth International Conference on Quality and Reliability (ICQR4)*. 2005.

IAPWS, International Association for the Properties of Water and Steam, Revised Release on the IAPWS Formulation 1995 for the Thermodynamic Properties of Ordinary

Water Substance for General and Scientific Use, IAPWS, Doorwerth, The Netherlands, September 2009.

IEEE Standard 497-2002, *IEEE Standard Criteria for Accident Monitoring Instrumentation for Nuclear Power Generating Stations*, Institute of Electrical and Electronics Engineers (IEEE), (<http://www.ieee.org>), 2002.

International Atomic Energy Agency, “Instrumentation and Control Systems Important to Safety in Nuclear Power Plants” No. NS-G-1.3, Austria, March 2002.

International Water Management Institute, 2000. www.iwmi.cgiar.org

Jin, X., *et al.*, “Integrated robust and resilient control of nuclear power plants for operational safety and high performance,” *IEEE Transactions on Nuclear Science*, Vol. 57, No. 2, 2010.

Kromer, D., *et al.*, “I²S-LWR Microchannel Heat Exchanger Design and Experimental Validation” *Annals of Nuclear Energy Special Issue on I²S-LWR*, 2016 (submitted).

Lima, E.R.A.. *et al.*, Differential-Algebraic Approach to Dynamic Simulations of Flash Drums with Rigorous Evaluation of Physical Properties, *Oil and Gas Science and Technology*. 2008.

Lombardi, C., Padovani, E., Cammi, A., Bucholz, J.A., Santoro, R.T., Ingersoll, D.T. Petrovic, B., Carelli, M., “Internal Shield Design in the IRIS Reactor and its Implications on Maintenance and D&D Activities,” *Proc. 4th Intl. Conf. on Nuclear Option in Countries with Small and Medium Electricity Grids*, June 16-20, 2002, Dubrovnik, Croatia.

Malloy, J.D., and Bingham, B.E., “Control system and method for pressurized water reactor (PWR) and PWR systems including same,” U.S. Patent Application 12/970,067, published 21 June, 2012.

Memmott, M., Marchese, M., and Petrovic, B., "Integral Inherently Safe Light Water Reactor (I2S-LWR) Concept: Integral Vessel Layout," Proc. 2014 Intl. Congress on Advances in Nuclear Power Plants (ICAPP 2014), Charlotte, NC, Paper 14313, pp. 86-94, 2014.

Michelsen, M.L., State Function Based Flash Specifications, *Fluid Phase Equilibria*, 158-160, 617. 1999.

OECD, The Organisation for Economic Co-operation and Development
www.oecd.org/about/

Oreskes, N., "Beyond the Ivory Tower: The Scientific Consensus on Climate Change," *Science* Vol. 306 no. 5702, p. 1686 (3 December 2004); DOI: 10.1126/science.1103618.

ORNL, "Development of Advanced Instrumentation and Control for an Integrated Primary System Reactor," ORNL, Westinghouse Electric Company, and IPEN, Brazil, I-NERI Project Summary Report, December 2005.

Papadakis, E.P., Ultrasonic Instruments and Devices, New Holland Publishing, New Holland, PA, 1999.

Petrovic, B., Ruddy, and Lombard, C., "Optimum Strategy for Ex-Core Dosimeters/Monitors in the IRIS Reactor," in Reactor Dosimetry in the 21st Century: Proceedings of the 11th International Symposium on Reactor Dosimetry: Brussels, Belgium, 18-23 August 2002, 2003, p. 43.

Petrovic, B., "Integral Inherently Safe Light Water Reactor (I2S-LWR) Concept – Promoting Safety and Economics," *Nuclear Engineering International*, pp 26-29 (March 2014).

Petrovic, B., and Flaspoebler, T., “Feasibility of Ex-Core In-Vessel Nuclear Instrumentation for Integral Inherently Safe Light Water Reactor (I2S-LWR),” 2015 International Conference on Applications of Nuclear Techniques, Crete, Greece, 2015.

Quinn, T., *et al.*, “Design to achieve fault tolerance and resilience,” INL/EXT-12-27205, September, 2012.

Reiger, C.G., *et al.*, “Resilient control systems: next generation design research,” Proceedings of HIS, Catania, Italy, May 2009.

Rosemount, “Rosemount 1153 Series D Alphaline Nuclear Pressure Transmitter,” Reference Manual 00809-0100-4388 Rev. BA. January 2008.

Shankar, R., “Measuring Feedwater Flow with Ultrasonic Flow Meters,” Electric Power Research Institute (EPRI), Publication No. 1004582, EPRI, Palo Alto, CA, 2001.

Sweeney, F.J., Upadhyaya, B.R., and Shieh, D.J., “In-Core Coolant Flow Monitoring of Pressurized Water Reactors Using Temperature and Neutron Noise,” Progress in Nuclear Energy, Vol 15, pp. 201-208, 1985.

Thorade, M., Saadat, A. (2013): Partial derivatives of thermodynamic state properties for dynamic simulation. - *Environmental Earth Sciences*, 70, 8, 3497-3503.

Ultra Electronics, “Nuclear Qualified Weed Model N9004 Fast Time Response RTD,” USA. Pub. 0015-002-1005. February 2014.

UNEP, United Nations Environmental Program, Division of Early Warning and Assessment, Accessed: 1 April 2016. <http://www.unep.org/dewa/vitalwater/jpg/0400-waterstress-EN.jpg>

Upadhyaya, B.R., Kitamura, M., and Kerlin, T.W., “Multivariate Signal Analysis Algorithms for Process Monitoring and Parameter Estimation in Nuclear Reactors,” *Annals of Nuclear Energy*, Vol. 7, pp. 1-11, 1980.

Upadhyaya, B.R., “Survey of In-core Instrumentation in Operating Pressurized Water Reactors,” AMS-BRU8301R0, Analysis and Measurement Services Corporation, Knoxville, TN, 1984.

Upadhyaya, B.R., and Li, F., “Advanced Instrumentation and Control Methods for Small and Medium Reactors with IRIS Demonstration, Vol. 4: Dynamic Modeling, Sensor Placement Design, and Fault Diagnosis of Nuclear Desalination Systems,” *Final Report prepared for the U.S. Department of Energy*, University of Tennessee. Report No. DE-FG07-07ID14895/UTNE/2011-6, May 2011.

Upadhyaya, B.R., and Perillo, S.R.P., “Advanced Instrumentation and Control Methods for Small and Medium Reactors with IRIS Demonstration, Vol. 5: Multi-modular Integral Pressurized Water Reactor Control and Operational Reconfiguration for a Flow Control Loop.” *Final Report prepared for the U.S. Department of Energy*, University of Tennessee. Report No. DE-FG07-07ID14895/UTNE/2011-7, May 2011.

Upadhyaya, B.R., et al., “In-situ Condition Monitoring of Components in Small Modular Reactors Using Process and Electrical Signature Analysis,” Annual Report, NEUP-3212-Y1Q4-2012, University of Tennessee, October 2012.

Upadhyaya, B.R., Mehta, C., Lollar, V.B., Hines, J.W., and de Wet, D., “Approaches to Process Monitoring in Small Modular Reactors,” Proceedings of the ASME 2014 SMR Symposium, ASME, Washington, D.C, 2014.

Upadhyaya, B.R., Lish, M.R., Hines, J.W., and Tarver, R.A., “Instrumentation and Control Strategies for an Integral Pressurized Water Reactor,” *Nuclear Engineering and Technology*, Vol. 47, Issue 2, pp. 148-156, 2015.

U.S. Energy Information Agency. International Energy Outlook 2013. www.eia.gov

U.S. NRC “Regulatory Guide 1.97, Revision 3, Instrumentation for Light-Water-Cooled Nuclear Power Plants to Assess Plant and Environs Conditions During and Following an Accident,” May, 1983.

U.S. NRC “Regulatory Guide 1.97, Revision 4, Criteria for Accident Monitoring Instrumentation for Nuclear Power Plants,” June, 2006.

U.S. NRC, “Standard Review Plan,” NUREG-800 Chapter 7, May 2010.

WEC, “AP1000 Final Safety Evaluation Report,” Westinghouse Electric Company, Cranberry Township, PA, 2004, Ch. 7.5.7.

WEC, “The Westinghouse Pressurized Water Reactor Nuclear Power Plant,” Westinghouse Electric Company, Cranberry Township, PA, 1984, page 106.

WHO, World Health Organization and UNICEF, Joint Monitoring Programme (JMP). “Progress on Drinking Water and Sanitation, 2015 Update and MDG Assessment,” 2015. http://www.who.int/water_sanitation_health/monitoring/jmp-2015-update/en/

Wood, R.T., *et al.*, “Emerging Technologies in Instrumentation and Controls,” Report Number NUREG/CR-ORNL/TM-2003, 2003.

World Nuclear Association, “The Economics of Nuclear Power,” Updated March 2016, accessed 1 April 2016. <http://www.world-nuclear.org/information-library/economic-aspects/economics-of-nuclear-power.aspx>

VITA

Matthew Lish was born in December, 1986. He was raised in Chapel Hill, North Carolina, by a neuroscientist and a surfer, who also practiced medicine. Matthew developed his love of science from one and his love of adventure from the other. He graduated Cardinal Gibbons High School in 2005, before attending The University of North Carolina at Chapel Hill for undergraduate studies, where he earned a Bachelor of Science in Chemistry with a second major in Spanish, graduating in 2010. In the autumn of 2011, Matthew moved to Knoxville, Tennessee to embark on his graduate studies in the Department of Nuclear Engineering at the University of Tennessee, where he has concentrated in system dynamics, modeling, instrumentation, and control in the pursuit of his Doctor of Philosophy. His goals in life are to learn as much as he can, contribute to a sustainable life-cycle between our species and our planet, and walk around in deep space. He'll settle for low earth orbit.